

# Feasibility of Bridge Structural Health Monitoring Using Short Term Data Acquisition System

Final Report  
January 2015

**Paul Barr**  
Professor  
Utah State University  
Logan UT 84332

**Raimondo Betti**  
Professor  
Columbia University  
New York NY 10027

**Tommy Cousins**  
Professor  
Virginia Tech  
Blacksburg VA 24061

**Paul Dyreng**  
Graduate Student  
Virginia Tech  
Blacksburg VA 24061

**Robert W. Fausett**  
Graduate Student  
Utah State University  
Logan UT 84332

**Marv W. Halling**  
Professor  
Utah State University  
Logan UT 84332

**Carin Roberts-Wollmann**  
Professor  
Virginia Tech  
Blacksburg VA 24061

External Project Manager  
Michael Brown  
Virginia Department of Transportation

In cooperation with  
Rutgers, The State University of New Jersey  
And  
State of Utah  
Department of Transportation  
And  
U.S. Department of Transportation  
Federal Highway Administration

## **Disclaimer Statement**

The contents of this report reflect the views of the authors, who are responsible for the facts and the accuracy of the information presented herein. This document is disseminated under the sponsorship of the Department of Transportation, University Transportation Centers Program, in the interest of information exchange. The U.S. Government assumes no liability for the contents or use thereof.

TECHNICAL REPORT STANDARD TITLE PAGE

1. Report No. CAIT-UTC-024	2. Government Accession No.	3. Recipient's Catalog No.	
4. Title and Subtitle  Feasibility of Bridge Structural Health Monitoring Using Short Term Data Acquisition System		5. Report Date January 2015	
		6. Performing Organization Code CAIT/Utah State University	
7. Author(s) Paul J. Barr, Raimondo Betti, Tommy Cousins, Paul Dyreng, Robert Fausett, Marv W. Halling, Carin Roberts-Wollmann		8. Performing Organization Report No. CAIT-UTC-024	
9. Performing Organization, Name and Address Utah State University 4110 Old Main Hill Logan, UT 84332		10. Work Unit No.	
		11. Contract or Grant No.  DTRT12-G-UTC16	
12. Sponsoring Agency Name and Address Center for Advanced Infrastructure and Transportation Rutgers, The State University of New Jersey 100 Brett Road Piscataway, NJ 08854		13. Type of Report and Period Covered Final Report 2/01/13 - 8/30/2014	
		14. Sponsoring Agency Code	
15. Supplementary Notes U.S Department of Transportation/Research and Innovative Technology Administration 1200 New Jersey Avenue, SE Washington, DC 20590-0001			
16. Abstract Long-term testing of bridges can expensive and result in a large amount of data that is difficult to manage and analyze. The purpose of this study was to investigate the feasibility of a short-term data acquisition system that used a minimal number of gauges to quantify a bridges behavior. As a result, a system was developed that could use up to eight sensors and could be utilized in the field for up to two weeks on two marine batteries. Once the system was developed, it was installed on a bridge near Perry, Utah. This particular bridge had a permanent data acquisition system installed so a direct comparison could be performed as well as with data that was recorded during a live-load test. In general, the short-term data acquisition system performed well. It was determined that two marine batteries did not supply enough power to operate the system for the desired two week period. Future work will investigate a sleep mode that should conserve additional energy and prolong the operating life of the system. The measured results were similar to those recorded with the permanently installed system as well as the live-load data. While the testing of the system was successful, additional work needs to be performed prior to implementation. Specifically, the battery issue needs to be resolved to prolong the viable operation time of the system. Additionally, improvements to the software in terms of post processing and capabilities could be improved to make it more useful to the user.			
17. Key Words Structural Health Monitoring, Bridges, Equipment, Short-Term Monitoring		18 Distributional Statement	
19. Security Classification Unclassified	20. Security Classification (of this page) Unclassified	21. No. of Pages 127	22. Price

## Table of Contents

Chapter 1: Literature Review .....	6
Live-Load Distribution Factors in Prestressed Concrete Girder Bridges (Barr 2001).....	6
Live-Load Analysis of Posttensioned Box-Girder Bridges (Hodson 2012) .....	7
Live Load Distribution Formulas for Single-Span Prestressed Concrete Integral Abutment Bridge Girders (Dicleli and Erhan 2009) .....	8
Deck Slab Stresses in Integral-abutment Bridges (Mourad and Tabsh 1999) .....	9
New Technologies in Short Span Bridges: A Study of Three Innovative Systems (Lahovich 2012).....	10
Load Testing and Modeling of Two Integral Abutment Bridges in Vermont, US (Kalayci 2011).....	12
Chapter 2: Bridge Description .....	13
Chapter 3: Long-term Monitoring & Instrumentation .....	17
Weigh-in-Motion (WIM) .....	17
Traffic Camera .....	20
Weather Station .....	20
Strain Gauges .....	21
Velocity Transducers (Seismometer) .....	21
Deck Water Saline Content .....	22
Tilt Meters .....	22
Thermocouples .....	23
Chapter 4: Long-term Instrumentation Installation .....	25
Chapter 5: Black Box Instrumentation Description.....	36
Chapter 6: Live-Load Instrumentation Plan & Testing .....	41
Instrumentation.....	41
Live Load Paths.....	46
Data Analysis .....	54
Static vs. Dynamic Comparison .....	56
Chapter 7: Black Box Instrumentation Plan & Testing .....	59
Chapter 8: Black Box Comparison .....	62

Chapter 9: Research Conclusions .....	71
Chapter 10: Bridge Instrumentation & Diagnostics Using STS4 & STS Live Testing System...	72
Introduction .....	72
Proof of Concept Testing .....	73
Bridge Selection.....	74
Instrumentation .....	76
Test Procedure .....	79
Data Organization .....	82
Results.....	83
User Operation of STS4 .....	92
System Hardware .....	93
System Software – STS Live .....	95
Attempted System Validation .....	107
Current Test Setup .....	107
Deployment of STS4 for comparison .....	109
Results.....	112
Conclusions and Recommendations.....	121
Appendix .....	122
Speed Calculation Algorithm.....	122
AutoZero Function Algorithm (Developed by Rene Hamer of Bridge Diagnostics Inc.)..	123
Calculation for Expected Strains in Kerrs Creek Bridge .....	124
Instructions for Using TDMS Files in Excel .....	125
Updating STS Live and the Remote Core.....	125
Statistical Difference of Calculated vs. Observed speeds.....	126
Chapter 11: References .....	127

## **Chapter 1: Literature Review**

In order to document previous bridge studies from other researchers, a literature review was conducted. The review focused on the types of tests that have been conducted in the past on bridges similar to the bridge at Perry, Utah. The goal of the literature review was to document the type of data, equipment, and results that would need to be developed through the proposed development of the short-term equipment. Six of the articles reviewed have been summarized in the following sections.

### **Live-Load Distribution Factors in Prestressed Concrete Girder Bridges (Barr 2001)**

The research presented in this article focused on determining flexural live-load distribution factors for three-span, prestressed concrete girder bridges. The study used the results from a live-load test on a bridge in Washington in order to calibrate twenty-four finite-element models which then were used to obtain Live Load Distribution Factors (LLDFs). The moments calculated from the recorded strain values of the actual bridge, as compared to the moments computed from the finite-element model, differed by a maximum of less than 6% showing a good correlation.

Changes in LLDFs due to lifts, intermediate diaphragms, end diaphragms, continuity, skew angle, and load types were determined by comparing the finite-element model of the Washington Bridge to alternative models with adjusted characteristics. The study also compared the acquired LLDFs to those calculated in accordance to the American Association of State Highway and Transportation Officials (AASHTO) Load and Resistance Factor Design (LRFD) Specifications. When making this comparison, the study found that the AASHTO LRFD procedures were up to 28% larger than the calculated LLDFs from the finite-element models,

meaning the AASHTO LRFD specifications are relatively conservative. However, this large percentage difference occurred when comparing the alternative bridge models such as imposing lifts and different skew angles. When comparing the models that most closely followed the configuration that was considered in developing the LRFD specifications to the LRFD specifications, the distribution factors varied by a maximum of 6%.

The final conclusions of the paper indicate that distribution factors decrease with an increase in skew, distribution factors calculated for lane loading are lower than those calculated for truck loading, and finally, if the Washington Bridge used in the study had been designed using finite-element model analysis, the required release strength could have been reduced by 1000 psi (6.9 MPA) or the bridge could have been designed for a 39% higher live-load.

### **Live-Load Analysis of Posttensioned Box-Girder Bridges (Hodson 2012)**

This study focused on the determination of flexural live-load distribution factors for cast-in-place, box-girder bridges. The bridge used for this research was a two-span, cast-in-place, prestressed, continuous box-girder bridge with a skew of 8°. This bridge was instrumented with 42 uniaxial strain transducers (strain gauges), 10 vertical deflection sensors (displacement transducers), and one uniaxial rotation sensor (tilt sensor). A live-load test was conducted by driving two heavily loaded trucks along predetermined load paths of the bridge. The data collected from the live-load test was then used to calibrate a finite-element model of the bridge. Once calibrated, the finite-element model was then used to determine the actual live-load distribution factors and load ratings for the bridge. These values were compared to the distribution factors and ratings in accordance to the AASHTO LRFD Specifications. In addition,

the finite-element model was used to investigate the various bridge parameters affecting the distribution of vehicle loads for this type of bridge.

The parameters evaluated included span length, girder spacing, parapets, skew, and deck thickness. This study concluded that the procedures to calculate the distribution factors from the AASHTO LRFD Specifications are conservative as compared to the finite element model distribution factors for the interior girder. Additionally, the AASHTO LRFD Specifications are non-conservative for the exterior girder distribution factors. In response to these findings, and through the use of the relationships obtained through the parametric study, a new equation for calculating exterior girder distribution factors was proposed to ensure a more conservative approach.

### **Live Load Distribution Formulas for Single-Span Prestressed Concrete Integral Abutment Bridge Girders (Diceli and Erhan 2009)**

The research presented in this article focused on determining formulas for live-load distribution factors for the girders of a single-span integral abutment bridge. To accomplish this objective, the researchers developed two and three dimensional finite-element models of multiple different integral abutment bridge types. The study used a variation of the bridge model's superstructure in order to improve the current understanding of integral abutment bridges. The bridge properties that were varied included span length, number of design lanes, prestressed concrete girder size and spacing, and slab thickness.

Live-load distribution factors (LLDFs) were determined using the different models and then these values were compared to the LLDFs calculated in accordance with the American Association of State Highway and Transportation Officials (AASHTO) Specifications for simply

supported bridges. In comparison to the AASHTO Specifications, the determined formulas for the interior girder shear differed by as much as 10%, but were generally between 3-6%. For the girder moments and outside girder shear, the results varied greatly. Some comparisons provided nearly exact matches between the models and AASHTO Specifications while other results varied by as much as 87%. Generally these results were conservative, however, there were cases where the comparisons were up to 13% non-conservative.

The results of this study led the researchers to conclude that the AASHTO Specifications for simply supported bridges could be used for interior girder shear but was inaccurate for girder moments or outside girder shear due to the large variations. Modifications were provided by the authors for the AASHTO LLDF Specifications which, the authors state, will provide more accurate LLDFs for IABs. In addition to those modifications, other equations were provided and determined to provide good results independent of the AASHTO LLDF Specifications.

### **Deck Slab Stresses in Integral-abutment Bridges (Mourad and Tabsh 1999)**

The research presented in this article involved using finite-element models to evaluate the behavior of integral-abutment bridges with concrete deck slabs on composite steel beams. The results of these models were then compared to the American Association of State Highway and Transportation Officials (AASHTO) Specifications. This study was performed in response to integral-abutment bridges being built using the design specifications provided by AASHTO for jointed bridges without regard to the different behavior of the integral-abutments.

Two integral-abutment bridges were modeled in this study differing in slab thickness, beam cross sections, and the number of spacing piles. The load for the models consisted of two HS20 trucks placed side-by-side in accordance with the 1996 AASHTO Load Factor Design

provisions. The moments provided from the models were then compared to simply supported bridges of equal size and similar properties. In addition, the stresses presented by the model were compared to the stresses calculated using the AASHTO Specifications for bridges.

When comparing the moments, the researchers determined that the maximum positive moment in the deck slabs was 10-30% lower for the integral-abutment bridges as compared to the simply-supported bridges. The differences nearly doubled for the case of negative moments with the integral-abutment bridges being 20-70% lower than the simply-supported bridges.

When comparing the stresses from the finite-element models to the AASHTO Specifications, the study concludes that the integral-abutment bridges are conservative by 40%.

### **New Technologies in Short Span Bridges: A Study of Three Innovative Systems (Lahovich 2012)**

The research presented in this paper involved studying the behavior of three separate types of short span bridges: integral abutment bridges, “bridge-in-a-backpack”, and the folded plate girder bridge. The “bridge-in-a-backpack” and folded plate girder bridges were studies performed on actual bridges. These bridges were instrumented throughout construction and live-load tests were conducted on them upon their completion. The author concluded that the largest strains for both bridges were experienced during the construction of the bridges. The bridges were continually monitored for long-term effects until the end of 2011, and the study ended due to issues with the data acquisition system.

The author created detailed finite-element models for different theoretical integral abutment bridges. This analytical study was performed by varying the span lengths, skew angles, and beginning or not beginning the live-load analysis from the stiffness of the deformed shape under active soil pressure and dead load. This study also included the analysis of simply

supported bridge models with similar characteristics, and then determined the live-load distribution factors for the integral abutment bridge models. These LLDFs were then compared to the distribution factors calculated in accordance to the procedure in the AASHTO LRFD specifications to determine whether or not the design of integral abutment bridges using common practices is conservative.

The conclusions obtained from this study were that the midspan moments for the integral abutment bridge models were between 35-50% less than those from the model with the simply supported models. The author concludes that if an engineer designs for the simply-supported structure, that moment could be up to 50% greater than the moment actually experienced in an integral abutment bridge.

When comparing the live-load distribution factors to the AASHTO LRFD equations, the author determined that the LLDFs increased as the skew angle was increased, while the AASHTO LRFD skew correction factor reduces the LLDFs under the same conditions. Similar to the finite element comparison, the author concluded that the design of integral abutment bridges was conservative when designed assuming simply supported conditions.

The effect of initiating the analysis from the stiffness, based on the deformed shape under active earth pressure and dead load, was determined to have the largest effect for long spans with higher skews. The author concluded that a maximum increase of less than 5% for the LLDFs for the midspan moment, a maximum decrease in the LLDFs of the endspan moments of 10%, and no effect for the shear LLDFs occurred when beginning the analysis based on the deformed shape, rather than the undeformed shape.

## **Load Testing and Modeling of Two Integral Abutment Bridges in Vermont, US (Kalayci 2011)**

The research presented in this article focused on comparing two integral abutment bridges (IABs), located in Vermont, US, with two finite-element models (FEMs) and live-load test data. Both bridges were designed using composite steel I-girders with reinforced concrete decking, HP piles, wing walls, and abutments. The two bridges spanned 43 m (141 ft) and 37 m (121 ft) long. For the live-load test, each bridge was instrumented with displacement transducers, tilt meters, earth pressure cells, strain gauges, and inclinometers. These gauges measured changes in the overall movement, earth pressure against the abutment, the strain of the girders, as well as the strain and angle of the piles. In addition, each gauge was equipped with a thermistor to record the temperature at the gauge location. For the live-load test, each bridge was loaded with either two or three loaded dump trucks stationed at 13 various positions across the bridges.

After the live-load test of each bridge, the data was analyzed and it was determined that temperature corrections were required for the measured data in order to determine accurate neutral axis locations for the girder cross sections. Finite-element models were created in order to replicate each of the bridges. Once created, these FEMs were calibrated to more accurately represent each of the bridges. The research concluded that the superstructure of the two IABs had a 20% higher negative moment at the ends, when taken as an absolute value, as compared with the positive bending moment at the midspan. The researchers also concluded that the substructure displacements were minimal for both bridges and the backfill pressures were negligible due to winter month temperatures. Overall, the researchers suggest that temperature induced stress is a problem and should be taken into account, and that live-load distribution factors would provide more beneficial information.

## Chapter 2: Bridge Description

The Utah Test Bridge (structure number 1F 205), as shown in Figure 2.1, was selected as the test bridge for the proposed equipment trial test as it is also part of a larger study of bridge performance for the Long-term Bridge Performance Project (LTBP). The research conducted was performed by Utah State University. The bridge structure, constructed in 1976, is a single span, five girder, pre-stressed concrete bridge built with integral abutments. It is located 80.5 km (50 miles) north of Salt Lake City, UT. The bridge carries two lanes of northbound traffic, as part of Interstate 15/84 traveling over Cannery Road in the town of Perry, UT. The exact location is  $41^{\circ} 27' 25.92''$  latitude and  $112^{\circ} 03' 18.72''$  longitude. The bridge has a clear span length of 24.4 m (80 ft) and an overall length of 25.1 m (82.5 ft). The height from the road below is 4.68 m (15.3 ft). Figure 2.2 shows a cross section of the bridge. The bridge incurs an average daily traffic (ADT) of approximately 22,000 vehicles, 29 percent of which are large trucks. There is no skew associated with this bridge. A superelevation of 2% was built into the bridge.

The width of the deck is 13.5 m (44.4 ft) wide measured from the outside of the barriers, and 12.3 m (40.5 ft) wide measured from the inside of the barriers. The deck is comprised of 203 mm (8 in.) thick of reinforced concrete with a 152 to 203 mm (6 to 8 in.) asphalt overlay that had accumulated over years of maintenance. The concrete had a specified compressive strength of 24.1 MPa (3500 psi) and was reinforced with Grade 60 billet-steel, no. 5 bars with at least a 50.8 mm (2 in.) cover. A cross section of the deck is shown in Figure 2.3. The barriers were cast with a cold joint and have a height of 1.07 m (3.5 ft) running along either side of the bridge. The barriers are reinforced with no. 4 bars of Grade 60 steel with a cover of at least 38.1 mm (1.5 in.).



*Figure 2.1 Utah Perry Bridge (structure number IF 205) side view*

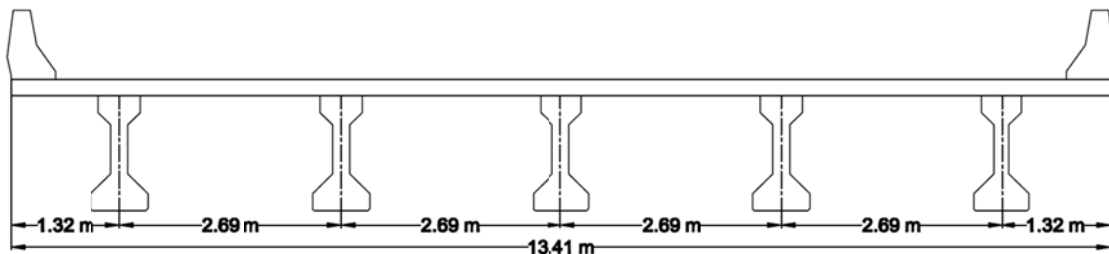


*Figure 2.2 Utah Perry Bridge cross section*

The girders supporting the deck are precast AASHTO Type IV bridge girders and are 25.1 m (82.5 ft) long, 1.37 m (4.5 ft) tall, and made of precast concrete. A cross section of the girder is shown in Figure 2.4. The specified compressive strength of the concrete is 34.5 MPa (5000 psi) and is reinforced with Grade 60 steel. The girder was prestressed prior to shipping to the job site using a harped strand profile. The harping points are located 9.75 m (32 ft) from the ends of the girder on either side and the centroid of the strands at the harping point is 103 mm

(4.06 in.) as measured from the bottom of the girder. At the girder ends, the centroid of the strands is located at 340 mm (13.4 in.) from the bottom of the girder. The final prestressing force for each girder, after losses, was calculated to be 3367 kN (757 kips). The girders were designed using a center-to-center spacing of 2.68 m (8.8 ft).

The support of the Utah Perry Bridge superstructure is comprised of integral abutments that are 0.76 m (2.5 ft) thick and 3.20 m (10.5 ft) tall and span the width of the bridge. Within the abutment, each girder rests on a 12.7 mm (0.5 in.) elastomeric bearing pad. These pads are above 76.2 mm (3 in.) tall concrete pedestals which transfer the load from the girders to five concrete drilled piles which each have a maximum allowable load of 356 kN (80 kips). Wing walls were cast adjacent to both abutment ends and are positioned parallel to the bridge with a total length of 4.72 m (15.5 ft), a width of 0.30 m (1 ft), a height of 2.90 m (9.5 ft) near the abutment, and a height of 0.61 m (2 ft) near the center of the bridge.

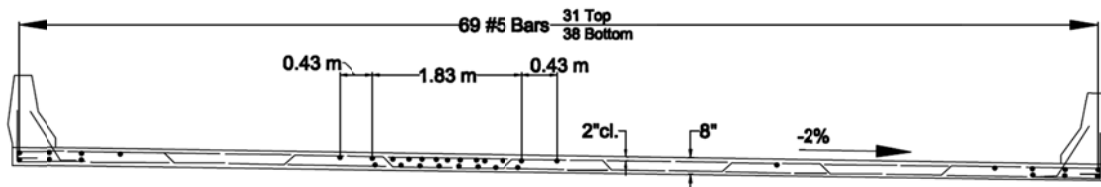


*Figure 2.3 Utah Perry Bridge deck cross section*

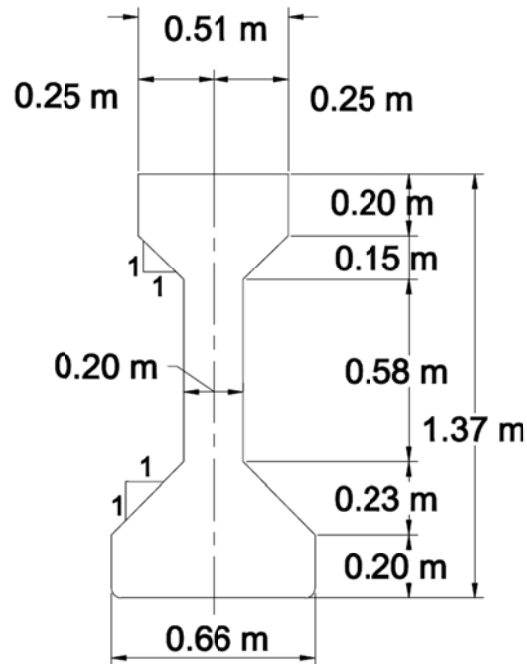


*Figure 2.4 Utah Perry bridge girder cross section*

Inspections and repairs have occurred periodically for this bridge throughout its service life. In September of 1982, an inspection report for the bridge mentioned severe wear and dilapidation. In September of 1991, the deck surface and parapets were repaired due to findings in the 1982 report. An inspection taking place in 1995 reported that the repairs were complete and looked good. In 1997, the inspection report made mention of minor cracking with efflorescence at the south end of the bridge. In 2005, a new asphalt overlay was placed on the deck after reports that the cracking had gotten much worse since the 2003 inspection report. The 2005 inspection also recorded spalling in the parapets along with full transverse cracking with efflorescence every 1.52 to 2.13 m (5 to 7 ft). Finally, a report in 2010, despite giving the bridge a 95.1 sufficiency rating, recommended the replacement of the bridge due to substandard load carrying capacity or inadequate bridge roadway geometry. This replacement had an estimated cost of \$515,000.

## **Chapter 3: Long-term Monitoring & Instrumentation**

As part of another research program, the Perry Bridge was permanently instrumented with various instrumentation. To provide a comprehensive long-term monitoring system that was capable of continuously monitoring data from all possible bridge characteristic parameters, many different instruments were selected and installed. The type of instruments selected and a brief description of each is provided in the following sections.

### **Weigh-in-Motion (WIM)**

The WIM sensor preferred for the Utah Perry Bridge is a quartz piezoelectric sensor. This sensor was chosen, among all possible WIM sensors, because it is capable of measuring vehicle weights at freeway speeds, 75 mph. A graphical representation of a Quartz WIM sensor is given in Figure 3.1. A WIM sensor is capable of recording traffic counts to inform researchers of the number of vehicles that use the bridge each day, as well as the percentage of the daily flow that is attributed to trucks.

Initially researchers planned to purchase and install this instrument. Further investigation found that a quartz piezoelectric sensor is installed near the Utah Perry Bridge. A Port of Entry is located approximately one mile south of the Utah Perry Bridge. It currently operates four WIM sensors, two for the southbound and two for the northbound traffic. Each direction of traffic has one WIM on the freeway, where vehicles travel at the posted freeway speed limit, and one along the lane leading to the port of entry where trucks travel at a speed much less than freeway speeds. Figure 3.2 shows the WIM sensor installed along the lane leading to the port of entry; showing sensors in parallel and an inductive loop. The WIM that is located along the lane is owned by the Utah Department of Transportation (UDOT) Motor Carrier Division (MCD). The

WIM that is located on the interstate is owned by a private company, Pre-Pass. Figure 3.2 and Figure 3.3 show the instrument as installed in the roadway for the Perry, Utah Port of Entry.

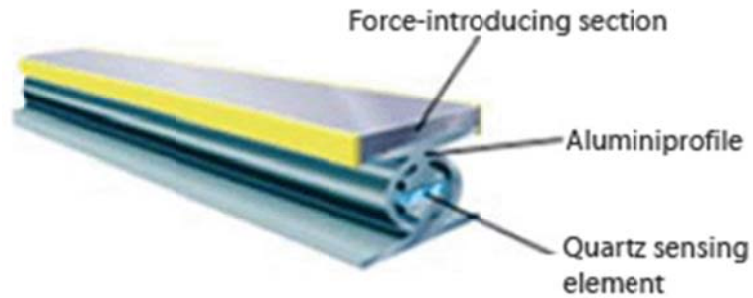


*Figure 3.1 WIM sensor, [www.judico.co.kr](http://www.judico.co.kr)*



*Figure 3.2 Quartz based WIM installed in lane leading to Perry Utah Port of Entry*

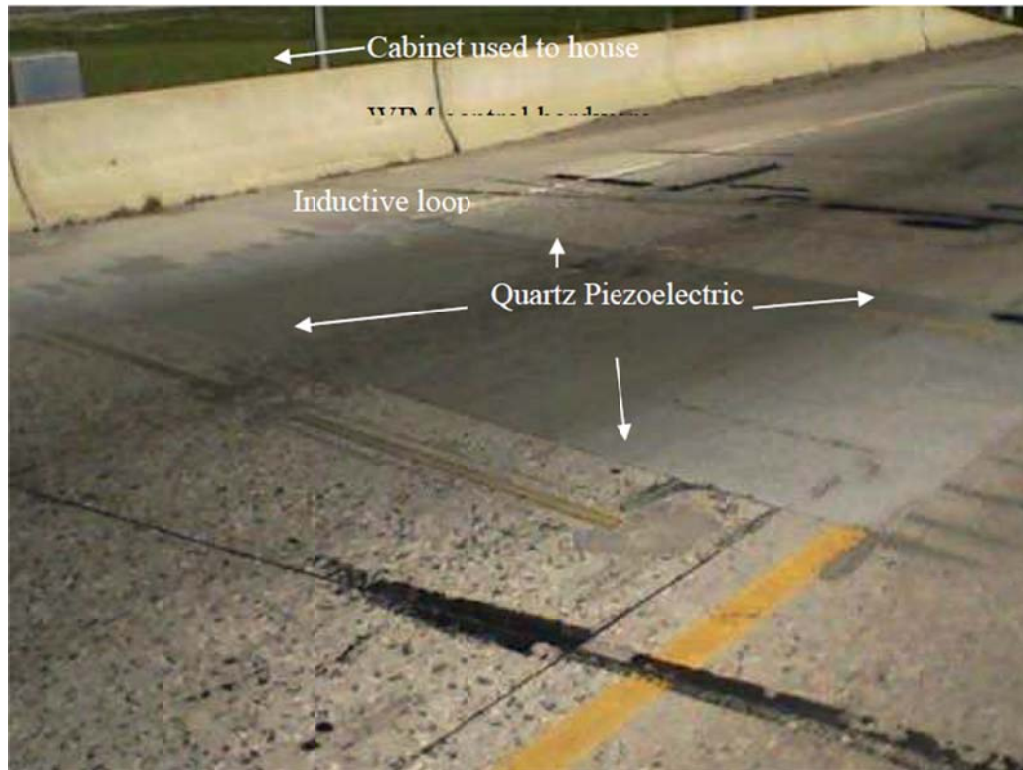


*Figure 3.3 WIM installed in lane leading to Perry, Utah Weigh Station*

As part of the study, researchers from USU were given a tour of the weigh station and shown how the WIM sensors work and record data. The WIM owned by UDOT is calibrated automatically every 100 trucks with comparison to the static scale. The computer algorithm knows when the 100<sup>th</sup> truck crosses and subsequently directs that truck to the static scales. A calibration is made from the static scale measurement to the WIM sensor so that the WIM sensor maintains a high level of accuracy.

Data from the WIM location in the northbound direction are available to the USU research team through an agreement between USU and the UDOT Motor Carrier Division. WIM sensor data is monitored continuously and catalogued in a rain-fall histogram.

The WIM sensor is important to obtain vehicle weights that lead to strain and deflection measurements. This aids researchers gathering data for the following list of LTBP Study Topics. performance of bridge deck treatments (2), performance, maintenance and repair of bridge joints

(3), performance of bare/coated concrete super and sub-structures (5), performance of embedded pre-stressing wires and tendons (7), performance of bridge bearings (8), performance of precast reinforced concrete deck systems (9), risk and reliability evaluation for structural safety performance (15), performance of pre-stressed concrete girders (17), performance of structure foundation types (19), and criteria for classification of functional performance (20).

## **Traffic Camera**

A traffic camera with the basic capability of a low resolution streaming video is necessary to understand traffic flows during significant events. When coupled with a WIM, a streaming video camera will provide supplemental data to understand the cause of a certain event. Since the WIM setup for the Utah Perry Bridge is not capable of providing an accurate trigger of an event because of the varying times for trucks in and out of the port of entry, a streaming video feed will facilitate in capturing traffic events.

## **Weather Station**

Environmental effects ranging from expansion and contraction of materials through heating and cooling cycles due to daily temperature variations to the more extreme freeze-thaw conditions of seasons are important for determining bridge health. Seasonal temperature changes can cause joint movement, bearing movement and local strain variations. All of these parameters require attention. Knowing the response of the bridge to environmental conditions helps in understanding changes in stress and strain.

The weather station includes instruments to record the following data: precipitation, wind direction, wind speed, radiation, humidity, and ambient air temperature. All equipment for a weather station is securely fastened to a pole located near the bridge. The location was selected

based on approval from FHWA and UDOT according to standards, installation requirements and UDOT permission.

## **Strain Gauges**

The Utah Perry Bridge has two permanently installed, vibrating wire strain gauges from the long-term data system placed on the girders. The high accuracy and longevity of the vibrating wire strain gauges provides a precise comparison of the structural response of the bridge over time and through deterioration. The slow sampling rate of the vibrating wire strain gauges is recorded on a set time interval. There are an additional six foil strain gauges placed on the bridge. They aid in understanding the bridge response to excitation/loading scenarios. The data is recorded on a much faster time interval than the vibrating wire strain gauges and only on triggered events. Collected data from the foil strain gauges is stored following a triggered event. Foil strain gauges have a tendency to “drift” over time, which will require periodic zeroing and eventual replacement to maintain data quality.

## **Velocity Transducers (Seismometer)**

Three velocity transducers are placed on the bridge to record dynamic responses due to excitation from vehicles passing over, as well as any possible seismic activity. In addition to vehicle loading, Utah is in a seismically active location and any seismicity will affect the bridges. It is important to know how the Utah Perry Bridge responds to dynamic loading. Long-term dynamic analysis will provide for an opportunity to see the change in bridge mode shapes, modal frequency and damping ratio through daily and seasonal changes, as well as changes due to any deterioration or rehabilitation efforts.

## **Deck Water Saline Content**

The Utah Perry Bridge experiences repeated freeze-thaw conditions with heavy snow fall during the winter season. It is well documented that bridge decks freeze before soil supported roadway surfaces. UDOT applies varying amounts of de-icing agents on roadways to provide for safe driving conditions with extra de-icing agents applied to bridge decks to keep the water from freezing. The most common de-icing agent used in Utah is salt. The chlorides in salt can result in differing levels of corrosion to the bridge superstructure.

It is of interest to determine the quantity of salt placed on the Utah Perry Bridge in order to understand the effects that chloride application has on the deterioration of the superstructure. Two IRS21 Lufft Intelligent Road Sensors are installed on the deck of the bridge to measure the saline content of the water on the bridge deck.

## **Tilt Meters**

Four total tilt meters are used on the bridge to monitor the effects of an integral abutment behavior. To compare the change of abutment rotation to girder rotation, one tiltmeter was placed on the abutment while a second tiltmeter was placed a few feet off the abutment on the girder, as seen in Figure 3.4. A primary reason that the Utah Perry Bridge was selected was because it is constructed with integral abutments. For this reason, monitoring of the abutment and near-abutment girder behavior is accomplished through the use of four tilt-meters.

The tilt meters are located on the first interior girder on the east side, which also correspond to the right or truck travel lane. A pair of tilt meters is installed at the north and south ends of the bridge. At each location, one tilt meters is placed on the abutment wall between the east exterior girder and the first interior girder from the east side, while the additional tilt meter is

placed on the first interior girder from the east side; approximately two feet from the abutment wall.

These sensors will address the performance of bridge bearings, risk and reliability evaluation for structural safety performance, unknown foundation types, performance of structure foundation types, and criteria for classification of functional performance.



*Figure 3.4 Showing two tiltmeters installed one on girder and one on abutment*

## **Thermocouples**

Temperature sensors are installed on the bridge with the intention of measuring the temperature of the girders and abutments at select locations. Localized knowledge of thermal gradients will allow researchers to understand joint movements, bearing movements, and local strain ranges as a result of the differential temperature reading across a girder.

A thermocouple is placed in the same protective housing as each of the six foil strain gauges and the three velocity transducers. The vibrating wire strain gauges and tilt-meters have built in thermistors to account for temperature variations so the temperature is known at those locations without the placement of a thermocouple.

## Chapter 4: Long-term Instrumentation Installation

Data processing of the long-term instrumentation was conducted by the Utah State University Research Team during the same time as the short-term instrumentation. A datalogger, capable of connecting to the internet or communication with a modem, collects, delivers, and records raw data to a secure site for further analysis. Integration with the communication service and the datalogger allows for constant real-time updating of data. This constant communication connection removes the need for time consuming visits to the bridge site for data retrieval. This instrumentation also provides a direct comparison with the short-term instrumentation.

While this study will focus on a comparison of the two data acquisition systems, one drawback of the long-term instrumentation is the large amount of collected data and installation effort. A large amount of raw data has been, and will be, collected through the project life of the Utah Perry Bridge with the permanent equipment. Because of this large volume, the data is stored at Utah State University on a large server for comparison and analysis purposes.

Installation was divided into two phases due to time and resource constraints. The first phase consisted of the site preparation which included the installation of the instrument pad, instrument tower, instrument cabinet, conduits, junction boxes, and instrument boxes. The second phase included the installation of the sensors. Phase two was carried out over multiple events dictated by arrival of instruments and determination of installation methods. The following two sections describe each phase and the work completed during both.

Installation progressed starting from the instrument pad and working toward the bridge. It was decided that this would ensure quality assembly and placement of all conduit. The instrument pad is the focal point of the installation, so its location was a top priority. The exact

location was selected based on the ease of access for a ride-on trencher to scale the steep slope safely and adequate room for tower maintenance and tower guy wires.

Once the location of the pad was selected, the conduit running from the bridge to the cabinet and tower was placed and the pad was poured and finished. The installation of the cabinet and tower occurred after the concrete had time to set. The finished product is provided in Figure 4.1.

Multiple junction boxes were installed to allow for easy transition of multiple turns and intersections due to the bridge geometry and instrument location. One large junction box was installed on the abutment wing-wall that provides a transition from the underground conduit to the conduit installed on the bridge. Although only one length of conduit was needed to house all instrument cables, an additional three conduit lengths were placed in the trench to allow for growth or troubleshooting in the future without the need for extra trenching. Figure 4.2 shows the four buried conduit pipes entering the junction box on the wing-wall from the top and the single conduit leading to the instruments on the bridge at the bottom of the junction box.

Smaller junction boxes were used near the abutment to provide a transition from the east-west oriented conduit to the north-south oriented conduit. These boxes were modified with coring bits to provide a secure, water-tight connection between box and conduit, as seen in Figure 4.3. These smaller boxes were modified to act as instrumentation protection by cutting the backs. The main supply conduit runs a few inches under the girders with a junction box at each location where an additional line of conduit rises up to the deck level.

The conduit was installed on the deck between the girders to collect as many instruments as possible with the least number of conduits. Additional boxes were used at instrument locations. These boxes allow for the main line of conduit to continue, if needed, while providing

an easy access for each individual sensor cable. Flexible PVC conduit was used to transition from the main feeding line to the individual instrument boxes. The last step in phase one was the installation of the individual sensor boxes and then connecting them via the flexible conduit was.



*Figure 4.1 Instrument pad with installed tower and cabinet after grading*



*Figure 4.2 Junction box located on abutment wing-wall*



*Figure 4.3 Junction boxes showing water-tight fittings*

Phase two involved the installation of the instruments on the bridge, their assemblage into the data acquisition system, verification that all instruments are sampling correctly, and ensuring that data is streaming to the collection center. The first instruments installed were the vibrating wire strain gauges, the full bridge foil strain gauges, thermocouples, and tiltmeters. Cabling was placed for the future installation of the velocity transducers. The installation of the velocity transducers occurred shortly after receiving them.

The weather station, with its respective instruments, was installed once the solar panel system was decided on and received. Since both the solar panels and the weather station instrumentation are installed on the same tower, it was decided that their installation would occur concurrently to ensure the best fit. Also installed on the instrumentation tower is the traffic camera. The instrument tower was the last portion of the instruments to be installed.

The vibrating wire strain gauges are Model 4000 from Geokon. Installation of the vibrating wire strain gauges required the use of groutable anchors for concrete applications. A 1/2" hole is drilled for each of two anchors, as shown in Figure 4.4. The hole is filled with an epoxy and the anchors are set in. To ensure accurate placement of the anchors, a spacing jig (provided by Geokon) was used. This jig provided the exact drill location.

Installation of the foil strain gauges by Hitec required an epoxy purchased from Vishay Microsystems, M-Bond AE-10, that is made for long-term applications. M-Bond AE-10 has a 6-hour cure time, during which time a constant pressure of 5-20 psi is required. In order to apply the needed pressure to the strain gauges, a system of pressure application was devised, as shown in Figure 4.5.

Prior to applying the epoxy, the concrete surface was prepared by sanding the surface with fine sandpaper, degreasing the surface area, conditioning, and then neutralizing the area. All products used for this process were recommended by and purchased from Vishay Microsystems.

The tiltmeters are Geokon Model 6160 MEMS Tiltmeters. Installation on the Model 6160 requires only one bolt mounted into the concrete, and the leveling was accomplished through the zero adjust pins, as shown in Figure 4.6.

Thermocouples were installed in all foil strain gauge boxes for a total of six on the bridge. The thermocouples were placed with the foil strain gauges to allow for any needed temperature compensation for strain. Type T, shielded thermocouple wire was purchased to ensure that the 200 ft distance from the instrumentation box to the thermocouple would not be damaged and to provide the most accurate temperatures possible.

Velocity transducers chosen are model L4 Seismometers, or Geophone, from Sercel. The L4 chosen has a 1000 gram suspended mass with moving dual coil. The instrument operates at 1.0 Hz. A significant reason for choosing this instrument is due to the small size and relatively nonexistent need for maintenance. The overall dimensions of the L4 are 5 1/8 in. tall and 3 in. in diameter, weighing just less than five pounds. Sercel provides the L4 completely sealed, therefore requiring no maintenance. In fact, the manufacture recommends that any maintenance needed be performed at their laboratory.

During the instrumentation development stage, it was determined that the physical location of the L4 along the cross-section of the bridge would be on the underside of the deck, equally spaced between the two girders. To secure the instrument in this location, a holding cradle was designed and manufactured at USU for installation. This cradle has the capability of leveling so that the L4 will produce accurate readings. The solar panel and all weather station

instruments were installed on the instrumentation tower by lowering the tower and installing each instrument individually according to manufacture recommendations. To protect the cable wires from the harsh environment, a combination of rigid and flexible conduit was used. The instrument tower has a conduit that takes cables from the base of the tower to the instrumentation box. This is a separate conduit from the conduit used for the instruments from the bridge.

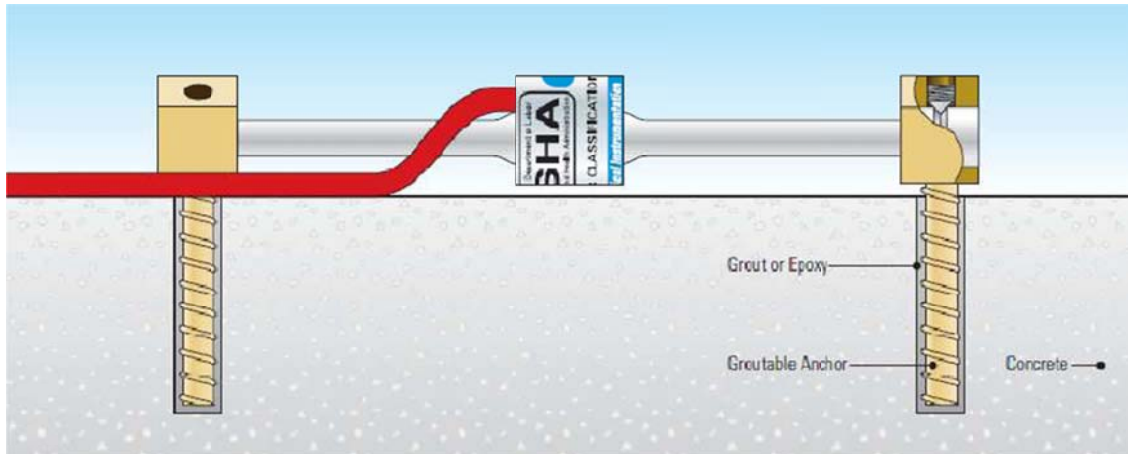


*Figure 4.4 Schematic drawing of vibrating wire strain gauges*



*Figure 4.5 View of installation method for hitec foil strain gauges*

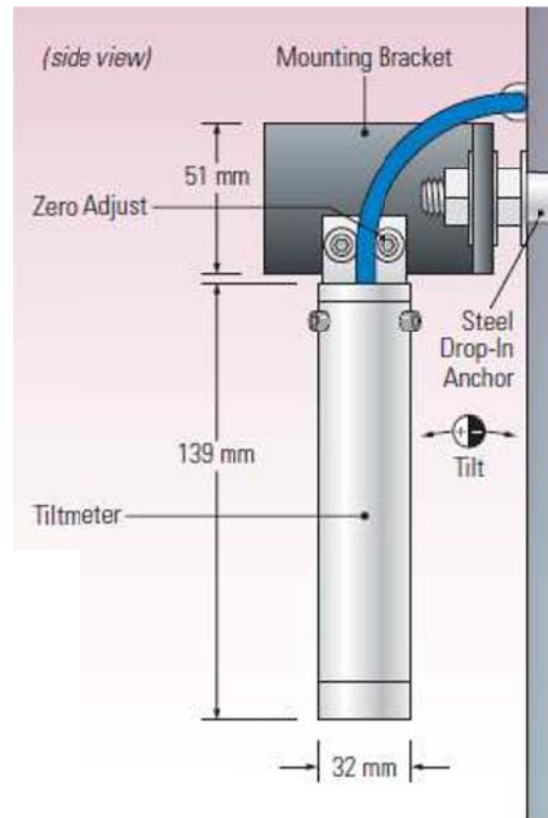


*Figure 4.6 Side view installation of Geokon MEMS 6160 Tiltmeter*

The chosen data acquisition system includes multiple modules purchased from Campbell Scientific as well as additional equipment from various vendors. The core of the data acquisition system is a Campbell Scientific CR5000. This system is capable of supporting almost any instrument and sampling at high rates. Due to the assortment of instruments selected for installation on the Utah Perry Bridge, a data acquisition system capable of sampling data from all types of instruments was necessary. The CR5000 was selected and purchased based off of flexibility and performance.

To expand the number of sensors possible on the bridge, a multiplexer was used to increase the number of channels. The selected multiplexer is a Campbell Scientific AM16/32 Multiplexer. The multiplexer serves as the reading unit for the thermocouples as well as the temperature reading from the Geokon Tiltmeters.

In order to relay information from the bridge site to a storing facility, a wireless CDMA router was selected. The router is a CalAmp LandCell 882-EVDO-VZW router. It is capable of operating at a frequency of 800 Mhz on a cellular bandwidth. With the option of using either a serial or Ethernet connection to the external device, the chosen router allows for direct connection with the CR5000, thus reducing additional modules or instrumentation requirements for a network interface. The router is activated with an account through Verizon Wireless and runs off of 12V DC, supplied through the CR5000.

With the guidance of personnel from Campbell Scientific, a code was developed to sample data through each of the sensors. The detailed, customized code allowed for individual settings on instruments including calibration values, sampling rates, channel location, trigger values, channel selection, recording location, automatic processing, and information delivery.

Upon complete installation of the instruments, as well as the data acquisition system, a check for accuracy was made. Software purchased from Campbell Scientific allowed for real-time viewing of the data at the bridge site with a laptop computer. Verification was made that all sensors were sampling correctly and that they were all zeroed properly.

The majority of all code development was made previous to installing the system, some settings could not be made until everything was set-up on site and data was flowing. For instance, triggers for the foil strain gauges could not be determined until real-time viewing of the data was possible. Strain ranges gathered during the Live-Load test were available, but it was unknown what the range would be based off of typical, everyday traffic. In addition, the trucks crossing the bridge on any given day are much heavier than the trucks used during the Live-Load test. Another area requiring specific attention once the system was complete was the Fast Fourier Transform calculated from the Velocity Transducers.

Monitoring equipment includes: a weather station, a traffic camera, vibrating wire strain gauges, foil strain gauges, velocity transducers, tilt-meters, deck water saline content sensors and thermocouples. Table 4.1 provides a description of instrument location categorized by bridge anatomy. All of these instruments were linked to a datalogger that controls the sampling rate for each instrument. The datalogger is housed in a cabinet located within the right-of-way of the freeway but out of the “clear zone”. The cabinet is securely fastened to a concrete pad. An instrumentation tower houses the weather station instruments as well as a video camera and internet satellite dish. It is located on the same concrete pad as the instrument cabinet.

Each instrument was installed according to manufacture recommendations for proper long-term durability. Cable transmitting data from the instrument to the data acquisition system is protected from the environment through the use of Schedule 40 Gray PVC conduit. This conduit is attached to the girders and abutment with the use of concrete anchors. From the abutment to the instrument cabinet, the conduit is buried for additional protection and safety. At the instrument pad, the conduit enters the cabinet and connects with the data acquisition system.

*Table 4.1 Distribution of instruments*

<b>Tower</b>
Wind Direction/Speed
Temperature/RH Probe
Precipitation Detector
Pyranometer (Radiation)
Traffic Camera
Solar Panel
<b>Deck</b>
Lufft Intelligent Road Sensor
<b>Underside of Super Structure</b>
Vibrating Wire Strain Gauge
Foil Strain Gauge
Tilt Meter
Accelerometer

As is shown, the requirements for a typical long-term, data acquisition system can be very involved. In addition, the costs can be prohibitive. For this particular bridge, the cost of the system was approximately \$89,000. In addition to the high cost, the system is very difficult to transfer from one bridge to another. Due to these restrictions, a desire to develop a low-cost, portable system that can provide suitable results was desired.

## Chapter 5: Black Box Instrumentation Description

The black box system, as shown in Figure 5.1, is a data acquisition system that is designed to be a mobile alternative to a permanently instrumented bridge. The system came with two nodes that can each monitor readings from four instruments, as shown in Figures 5.2-5.4. The sensors that can currently be monitored with the system are strain gauges, accelerometers, tilt meters, LVDTs, or any other BDI sensor. The computer software, as shown in Figure 5.5, is made for easy use and will automatically identify the type of sensor that is plugged into each node. No programming is required of users. Some sensors require the calibration factor to be entered into the program though the system is able to automatically input others. There is a computer within the black box that is called the core computer and it can be connected to an external monitor or it can be connected to a laptop installed with the user interface software to control the computer and set up tests, as shown in Figure 5.1. The entire black box weighs approximately 10 lbs and each node weighs approximately 2 lbs.

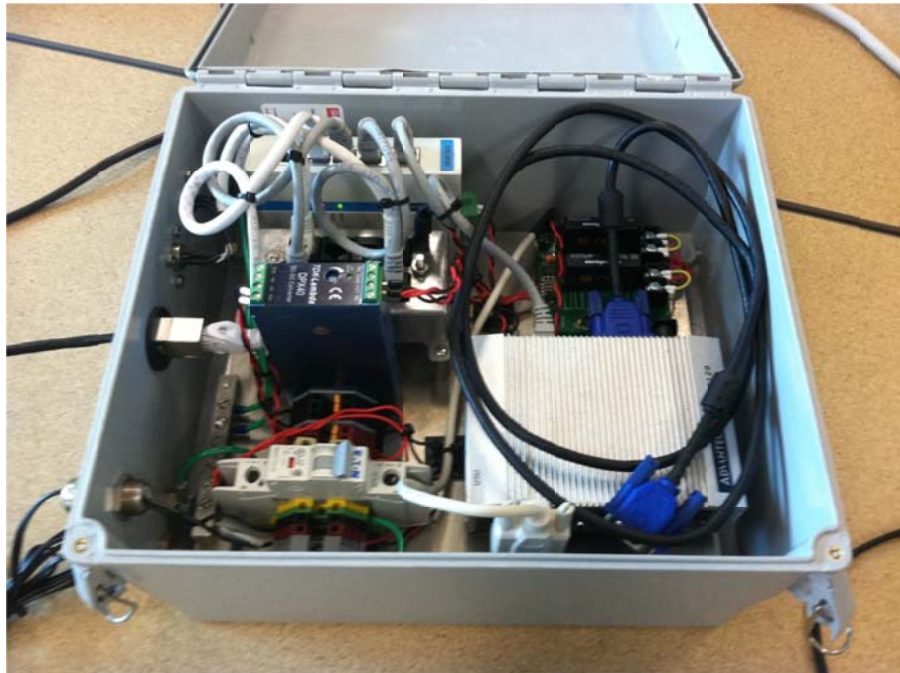


*Figure 5.1 Black Box*



*Figure 5.2 Installation of Sensor Node*

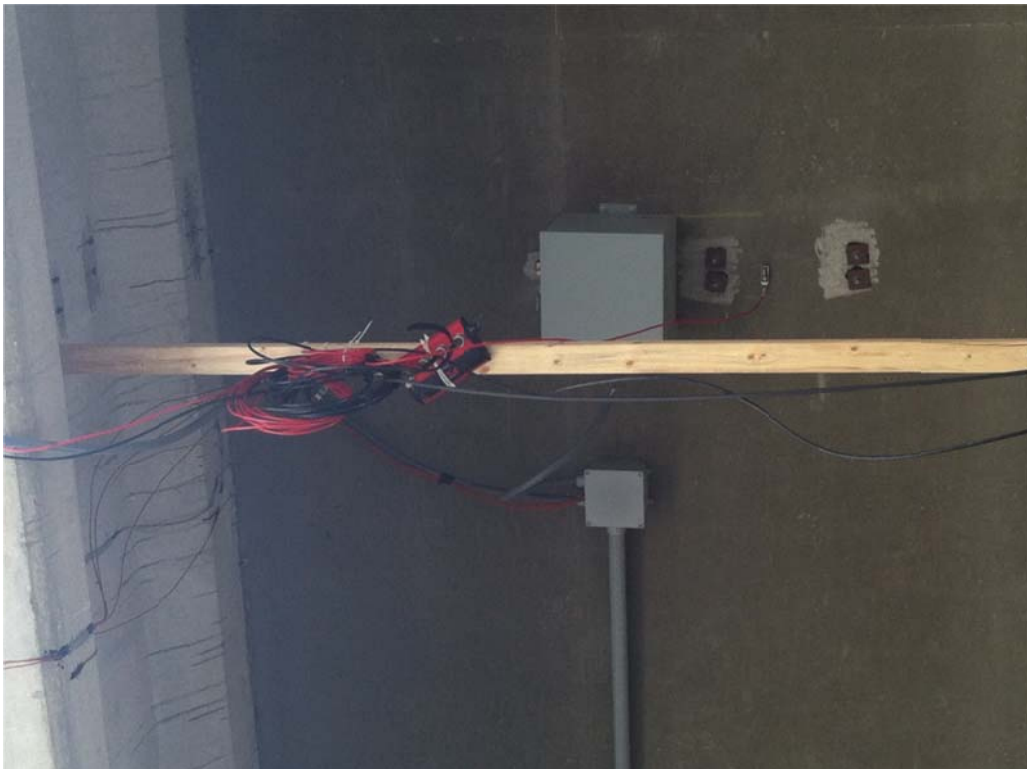


*Figure 5.3 Sensor Node 1*



Figure 5.4 Sensor Node 2 (top right corner)

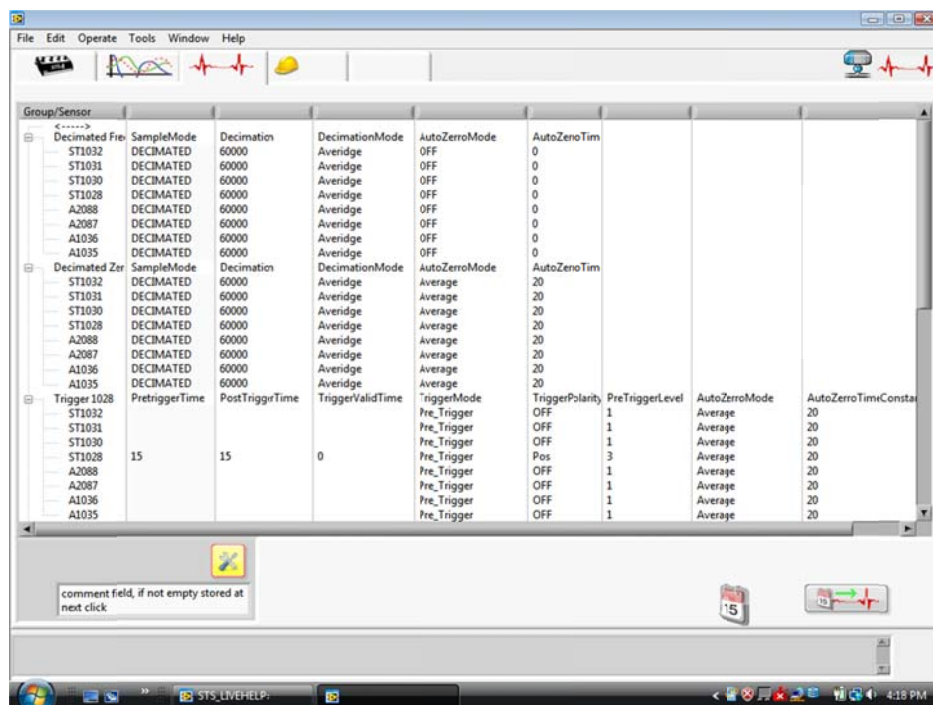


Figure 5.5 Black Box computer interface screen shot

The black box user interface allows you to perform three different types of tests including triggered tests, decimated tests, or calendar based tests. The triggered tests will initiate the data collection based on a sensor exceeding a predefined trigger threshold as specified by the user. The amount of data collected before and after the trigger is also determined by the user. The decimated tests work by collecting all the data at a specified frequency and then decimating the data, either by calculating the average over the selected decimated period, or by the maximum and minimum points of the decimated period. Finally, the calendar option allows the user to specify certain times of the day, or certain days of the week, for collection periods (i.e. collect for five minutes every three hours on Monday, Wednesday, and Friday). The calendar function is not currently operational though it is expected to be functional with the next software update.

Other positive aspects included with the black box are the grouping function and sleep mode. The grouping function allows you to base each of your tests only on a certain group of sensors. This allows the user to place a trigger for a group of sensors on one part of the bridge and another trigger for a different group of sensors on a separate part of the bridge thereby eliminating lag time. In addition, a user could set up one group of sensors to document how the bridge is affected by temperature changes while another group of sensors is set to document the strain imposed by trucks passing over the bridge. Different sensors can be in multiple groups including being capable of recording both trigger and decimated data simultaneously.

The sleep mode is another essential feature which allows the system to run on only battery power without requiring external charging. Because the requirement of the desired system was to be able to monitor the gauges for a week long period on batteries, lower consumption was an issue. The sleep mode allows the system to continuously collect data while the computer is only using 1 W of power and then wake up to download all of the data recorded

while it was sleeping. The current system is asleep 90% of the time and downloading the recorded data only 10% of the time. In addition to the described features, BDI is currently working to reduce the amount of power required during sleep mode.

## **Chapter 6: Live-Load Instrumentation Plan & Testing**

### **Instrumentation**

An initial comparison of the functionality of the system was performed on a controlled test. A study was conducted on live-load data in order to establish a baseline to evaluate the bridge performance. The live-load test was conducted by driving a truck, or combination of trucks, along a predetermined load path and measuring the strain, displacement, and temperature from live-load sensors that were installed on the bridge. The sensors installed on the structure are positioned in four separate locations longitudinally along the bridge. These sensors include twenty surface mounted strain gauges, as shown in Figure 6.1, and seven deflectometer vertical displacement sensors, as shown in Figure 6.2. Most instruments were mounted using a boom lift though the instruments near the abutment were attached using the embankment underneath the bridge. Researchers used a fast setting adhesive and specially designed mounting tabs in order to fasten the instruments to the concrete. The deflectometers were deflected before the live-load test using a weight located on the ground to hold the deflection.



*Figure 6.1 Surface mounted strain gauge*



*Figure 6.2 Deflection instrument, "deflectometer"*

The live-load strain sensors were placed in two locations horizontally across the bridge; one set at 13.1 m (43 ft) and the other set at 22.9 m (75 ft) as measured from the south end of the bridge. These locations are marked as cross sections BB and DD in Figure 6.3. In theory, the ideal locations for the sensors would be at the abutment and at the mid-span. Due to the harping point and diaphragm at the mid-span, gauge locations were slightly adjusted. In addition, placing a strain gauge right on the abutment would provide for extremely low strain readings. In order to receive accurate and useable data, the gauges were offset by 0.91 m (3 ft) from the mid-span and 1.52 m from the abutment. The strain sensors were also placed at two different locations along the height of the girder. Half of the instruments were placed on the bottom flange of the girders while the other half were placed near the top of the web of the girders. The locations of the sensors at cross sections BB and DD, as well as the sensor identification numbers, are provided in Figure 6.4 and Figure 6.5, respectively.

Like the strain sensors, the deflection sensors were also split between two longitudinal locations, however, for these sensors, five were placed in one longitudinal location while only two were placed in the other location. These two locations are shown as cross sections AA and CC, respectively, in Figure 6.1. Because the harping point and diaphragm would have no effect on the deflectometers, the set of five deflection sensors was put at the exact mid-span of 12.2 m (40 ft). This is cross section AA and can be seen in Figure 6.6. The other two deflectometers were placed at 14.6 m (48 ft) as measured from the south end of the bridge. This point was cross section CC of the bridge and is provided as Figure 6.7. All of the deflectometers were attached on the bottom flange of the girders.

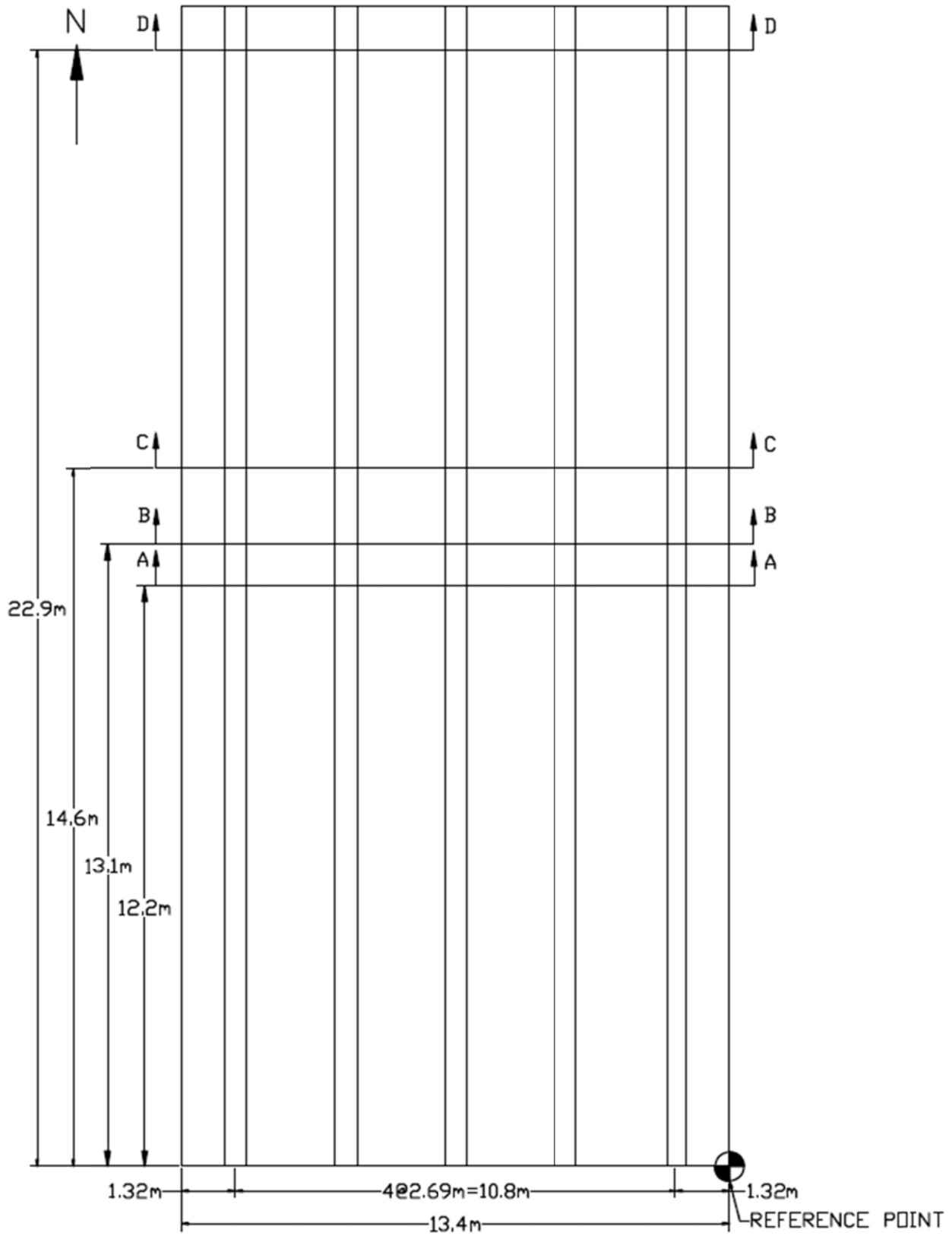


Figure 6.3 Plan view of bridge providing instrumentation locations

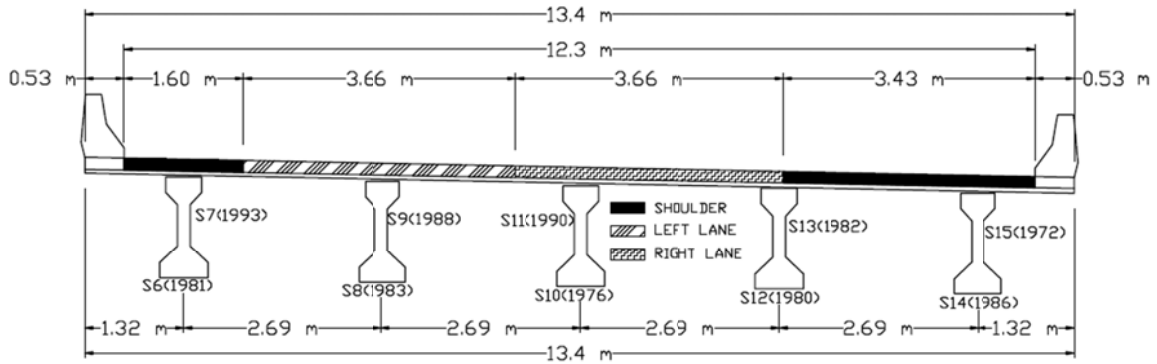


Figure 6.4 Bridge cross-sectional view Section B-B

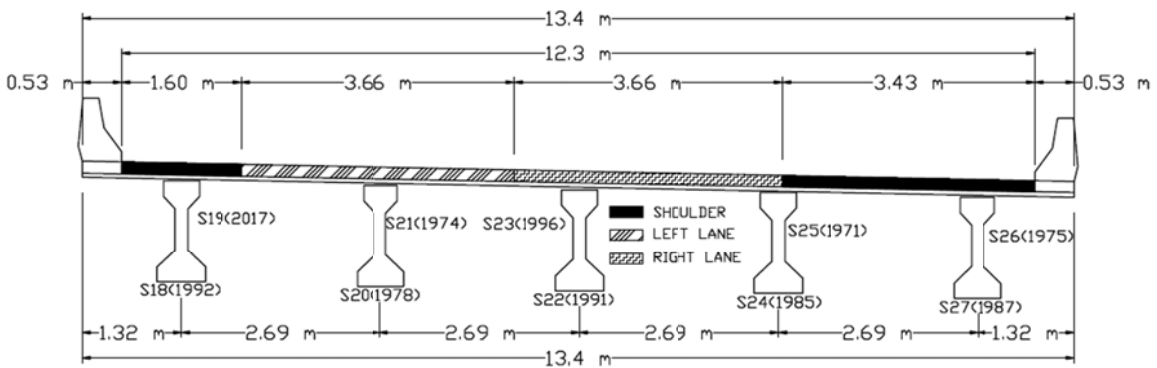


Figure 6.5 Bridge cross-sectional view Section D-D

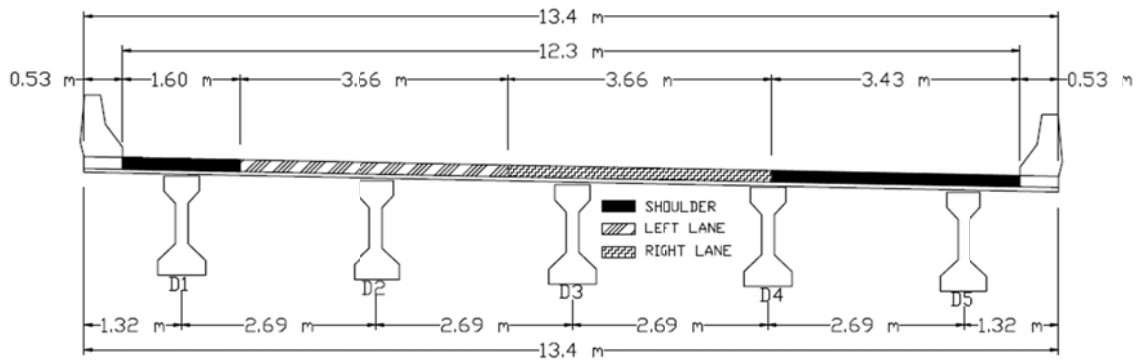


Figure 6.6 Bridge cross-sectional view Section A-A

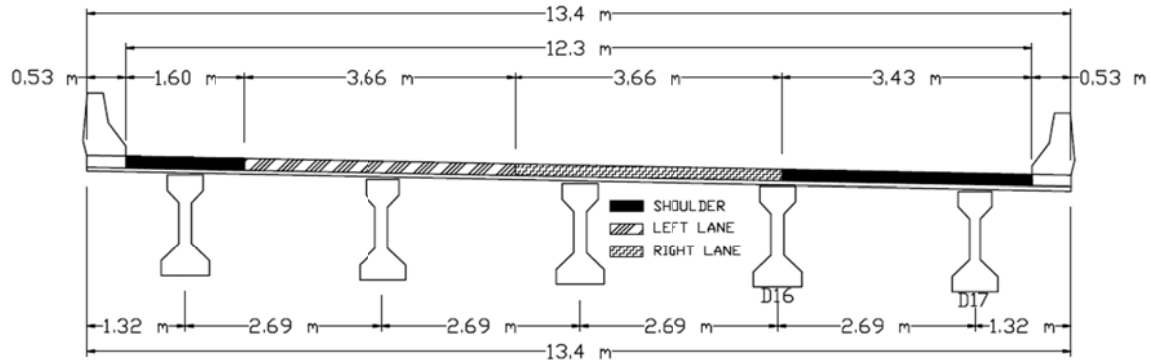


Figure 6.7 Bridge cross-sectional view Section C-C

## Live Load Paths

Multiple live-load tests were performed using a controlled lane closure during a time of low traffic flow. In addition, a moving roadway block was utilized in order to keep all traffic off the bridge during testing. This was accomplished by having a highway patrol car drive down the middle of both lanes of the highway, beginning 3.66 km (2.28 miles) before the bridge, in order to cause a slowdown in traffic, as shown in

Figure 6.8. This slowdown allowed for a window of four to five minutes of uninterrupted testing. In this amount of time, trucks were positioned and one load path was able to be completed.



*Figure 6.8 Police officers causing a slowdown in traffic*

Two heavily loaded UDOT tandem rear axle dump trucks were used to apply the live-load weights. Truck 1 had a Gross Vehicle Weight (GVW) of 223 kN (50,080 lbs) while Truck 2 had a GVW of 229 kN (51,460 lbs). Both trucks are shown in Figure 6.9. All Truck 1 and Truck 2 information is provided in Table 6.1 and Table 6.2, respectively. Figure 6.10 and Figure 6.11 provide dimensions of the footprints of Truck 1 and Truck 2, respectively. Six tests were conducted in all, one high speed test and five pseudo-static tests (truck driving at 5 mph). The strains, displacements, and corresponding truck positions were both recorded at a frequency of 100 Hz for the high speed test and 50 Hz for the pseudo-static tests. The load cases describe the six different tests that occurred during the live-load testing. Table 6.3 provides information for the different load cases. The load paths are the positions the trucks are either placed at or, in the case of the high speed test, the part of the bridge the truck drove over. Information regarding the

load paths can be found in Table 6.4. In order to show details of each of the load cases, Figure 6.12 through Figure 6.15 are provided.



*Figure 6.9 Truck A and Truck B*

*Table 6.1 Truck A Information*

<b>Axle</b>	<b>Spacing (m)</b>	<b>Gauge (m)</b>	<b>Weight (kg)</b>
1	-	2.03	7,756
2	4.11	1.88	7,480
3	1.35	1.88	7,480
		Total	22,716

*Table 6.2 Truck B Information*

<b>Axle</b>	<b>Spacing</b>	<b>Gauge</b>	<b>Weight (kg)</b>
1	-	2.03	7,747
2	4.09	1.88	7,797
3	1.37	1.88	7,797
		Total	23,342

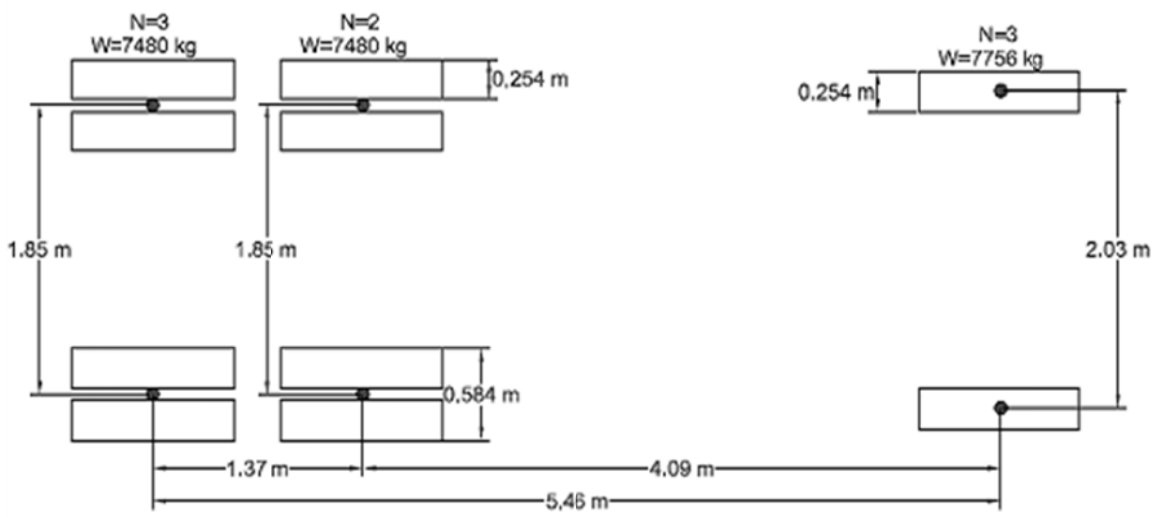


Figure 6.10 Truck A Footprint

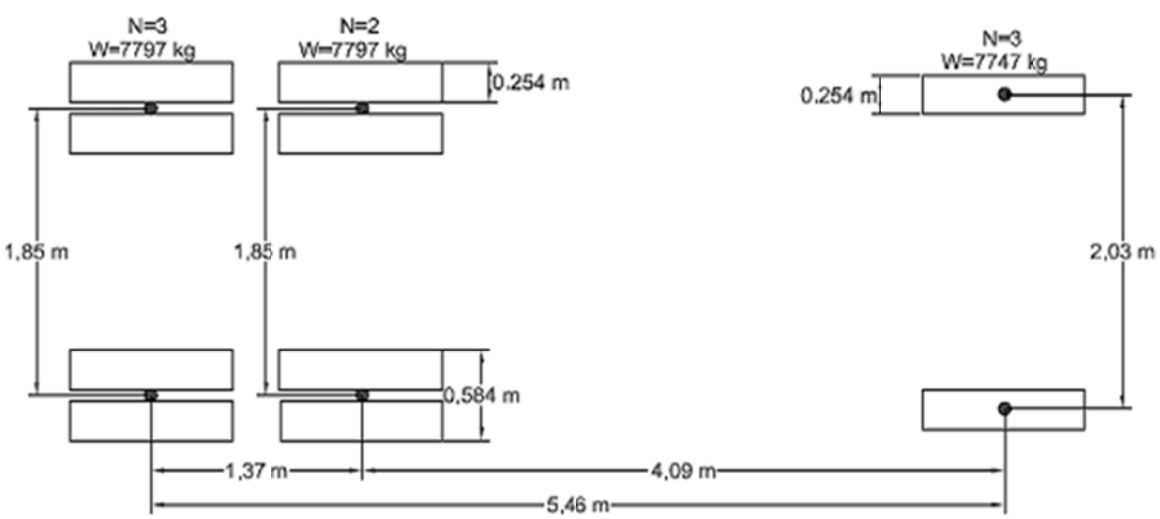


Figure 6.11 Truck B Footprint

*Table 6.3 Load Case Descriptions*

<b>Load Case #</b>	<b>Load Case Description</b>	<b>Truck 1 Load Path</b>	<b>Truck 2 Load Path</b>	<b>Repetitions</b>
1	Maximize Exterior Girder Response (Static)	1	1	3
2	Maximize First Interior Girder (psuedostatic)	1	2	2
3	Place One Truck in Each Travel Lane. Maximize Multiple Presence (psuedostatic)	3	4	3
4	Maximize Exterior Girder Response Truck 2 Following Truck 1 (psuedostatic)	1	1	2
5	Place On White Line of Right Travel Lane (psuedostatic)	5	-	2
6	High Speed	5	-	2

*Table 6.4 Load Path Descriptions*

<b>Load Path #</b>	<b>Load Path Description</b>	<b>Load Path Horizontal Distance (m)</b>	<b>Load Combination Uses</b>
1	East Most Location, 0.61 m off of parapet edge.	3.33	1, 2, 4, 5
2	Places Truck in East of Right Travel Lane	6.27	2
3	Center Truck In Right Travel Lane	6.58	3, 6
4	Center Truck in Left Travel Lane	10.64	3
5	Center Passenger Side Wheel on White Marking Line (over First Interior Girder) in Right Lane.	6.07	5

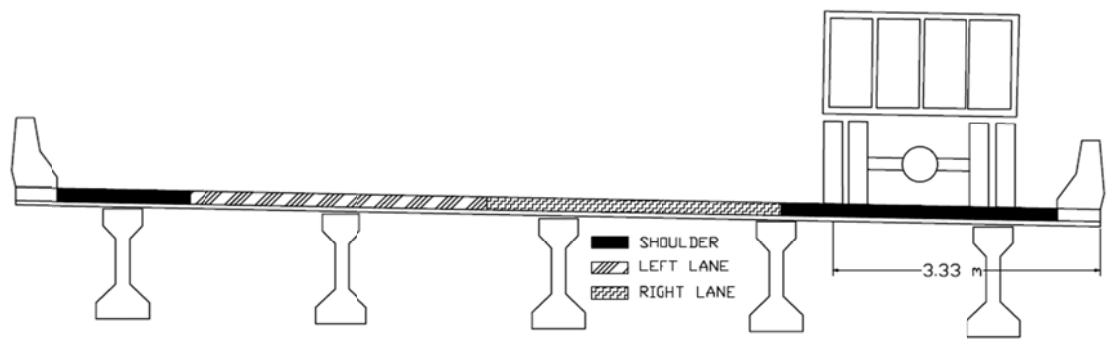


Figure 6.12 Load Case 1, Truck A and Truck B backed toward each other, and Load Case 4, Truck B following Truck A

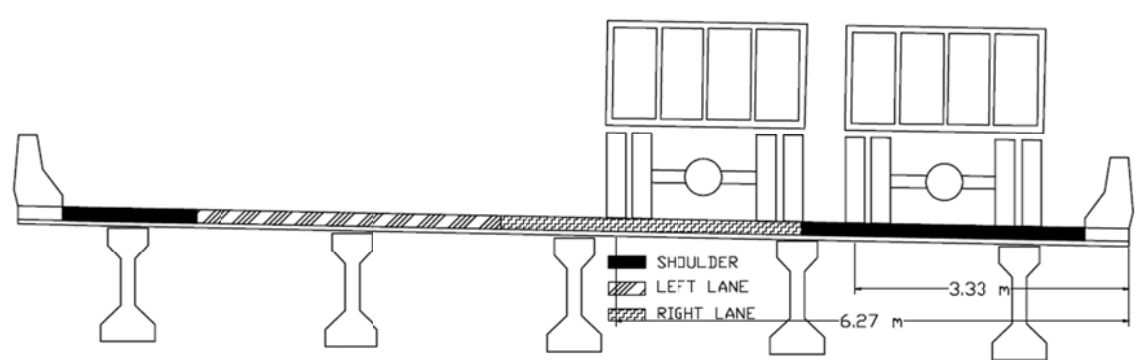


Figure 6.13 Load Case 2, Truck A (right) aside Truck B (left)

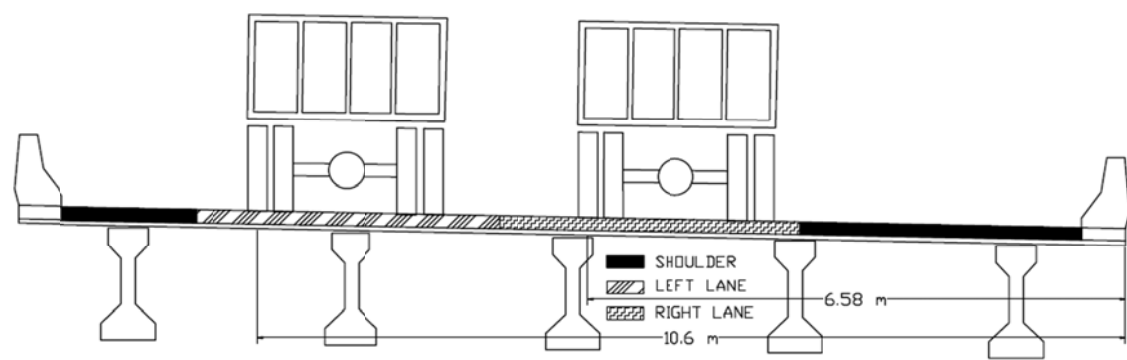
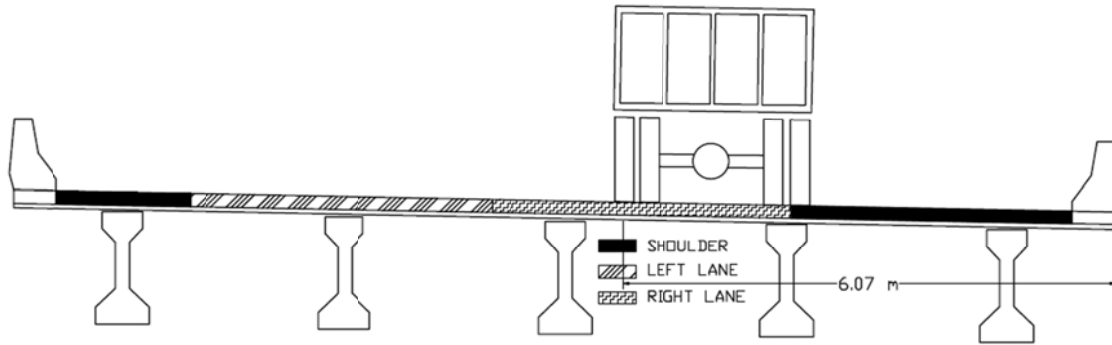


Figure 6.14 Load Case 3, Truck A (right) aside Truck B (left)



*Figure 6.15 Load Case 5, Truck A (psuedostatic), Load Case 6, Truck A (high speed)*

The truck position was monitored for the first five load cases using a device called an “Autoclicker” which was mounted to the driver side tire of Truck 1, as shown in Figure 6.16. At each wheel rotation, the data acquisition system would receive a signal from the device and would subsequently mark the data. Using the data marks and the known circumference of the tire, the exact location of the truck could be determined as it traverses across the bridge. For the high speed test, the autoclicker was removed but the truck was driven along load path 3.



*Figure 6.16 Automated position tracking sensor, "Autoclicker," mounted on left front tire of Truck A*

## **Data Analysis**

Before using the data collected from the live-load test, an analysis was required to determine whether or not the data was acceptable for use. Two analyses were conducted to ensure accurate data. First, multiple trials were run for each load case which allowed for a comparison between two sets of what should be identical data. All cases resulted in accurate data between the multiple runs for each load case. Figure 6.17 provides an example of this comparison. The second analysis that was conducted on the live-load data was a strain vs. deflection analysis for each gauge in order to make sure all of the gauges were reading correctly. This analysis is effective because strain and deflection are inversely proportional. In order to make this comparison, the strain and the deflection (which was multiplied by a negative multiplier) were plotted vs. all five girders for multiple positions. This analysis was completed on Load Case 4 which was found to provide an increasing shape with Girder 1 being the smallest and Girder 5 being the largest as determined by a hand calculation and modeling. Figure 6.18 provides the results for a position of 24.4 m (80 ft) and Figure 6.19 provides the results for a position of 18.3 m (60 ft). As shown by both figures, Girder 3 for deflection and Girder 5 for strain stray from the intended course of increasing. An argument could be made that the strains in Girders 3 and 4, as well as the deflection for Girders 4 and 5 were off though a quick hand calculation disproves this theory.

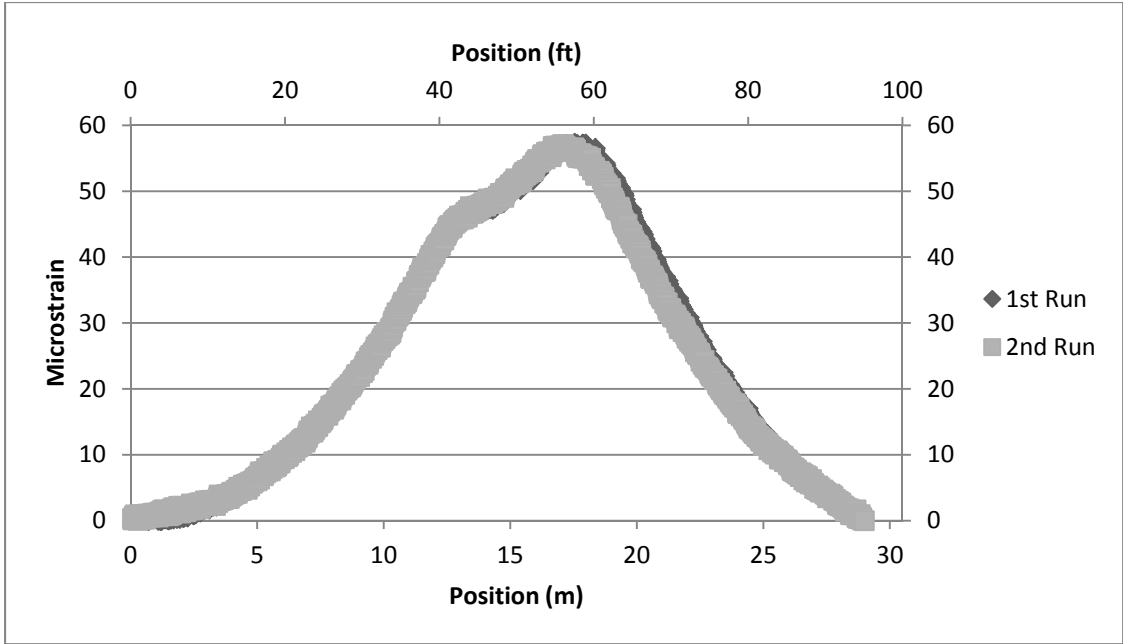


Figure 6.17 Comparison of Load Case 3, 1<sup>st</sup> Run vs. 2<sup>nd</sup> Run

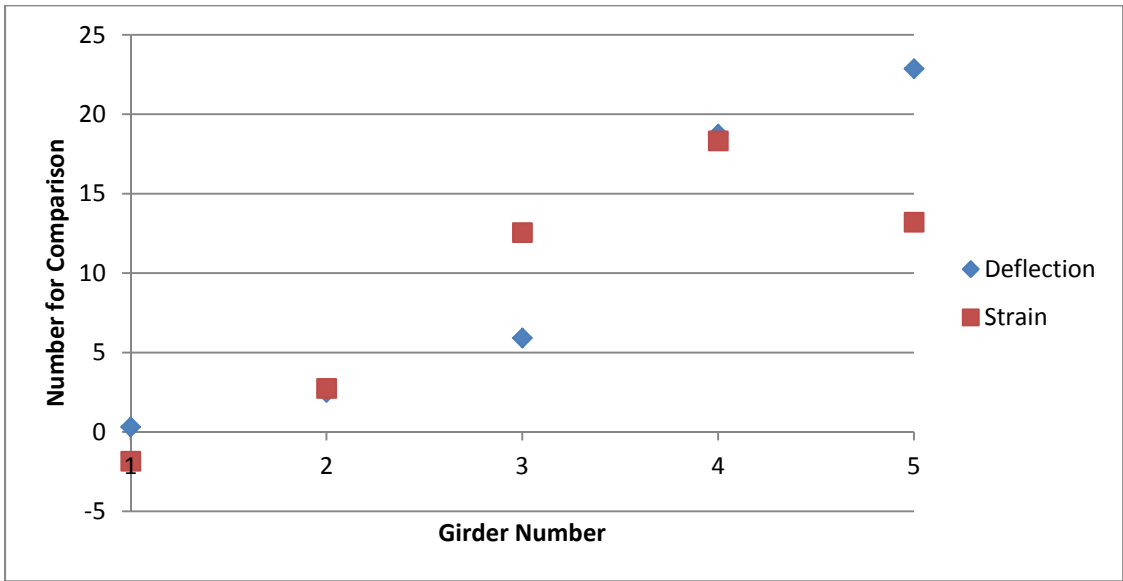


Figure 6.18 Strain vs. Deflection comparison for Load Case 4 at 24.4 m

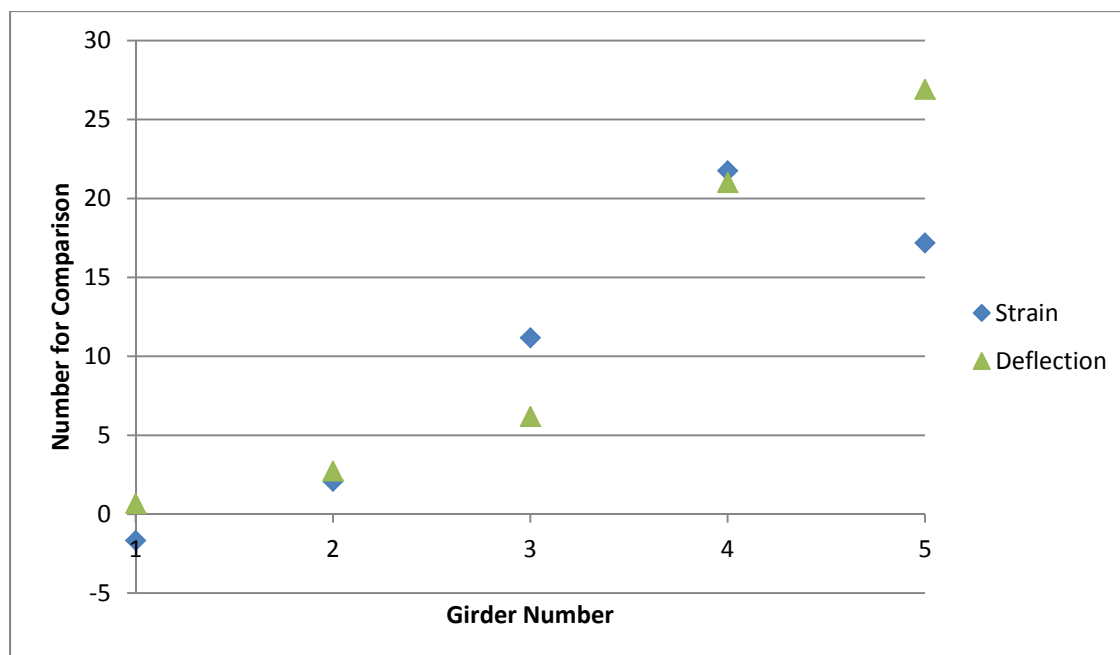


Figure 6.19 Strain vs. Deflection comparison for Load Case 4 at 18.3 m

## **Static vs. Dynamic Comparison**

Dynamic testing was conducted in order to determine the effect of a dynamic loading on the bridges strain and deflection. Dynamic testing was conducted by driving Truck A at both 7.2 m/s (16 mph) and 37.1 m/s following Load Path 5. This was deemed Load Case 6 and these dynamic effects were then compared to Load Case 5 which followed the same path, psuedostatically. Girder 4 was compared in both the strain and deflection cases to allow for consistency. The strain and deflection comparisons are shown in Figure 6.20 and Figure 6.21, respectively. The psuedostatic loading provides the largest maximums for both strain and deflection. In order to ensure this was correct, the order of maximum to minimum was compared for both strain and deflection. In both cases, the psuedostatic condition is the largest, followed by the fastest moving truck, followed by the medium moving truck. Because of this consistency and the fact that all three cases were measured by the same gauge within a short amount of time from each other, the data looks to be correct. The reason this occurred is likely due to the fact

that for the psuedostatic case, it was possible to guide the trucks exactly along the white line while for the high speed tests, the driver was unable to exactly line the right tires of the truck up with the right line. By being slightly off from the line, the strain and deflection in Girder 4 decreased causing the dynamic affects to be less than the psuedostatic affects. In addition, it was odd to not have a larger range from the dynamic tests, however, this is consistent with the gauges reading long-term data.

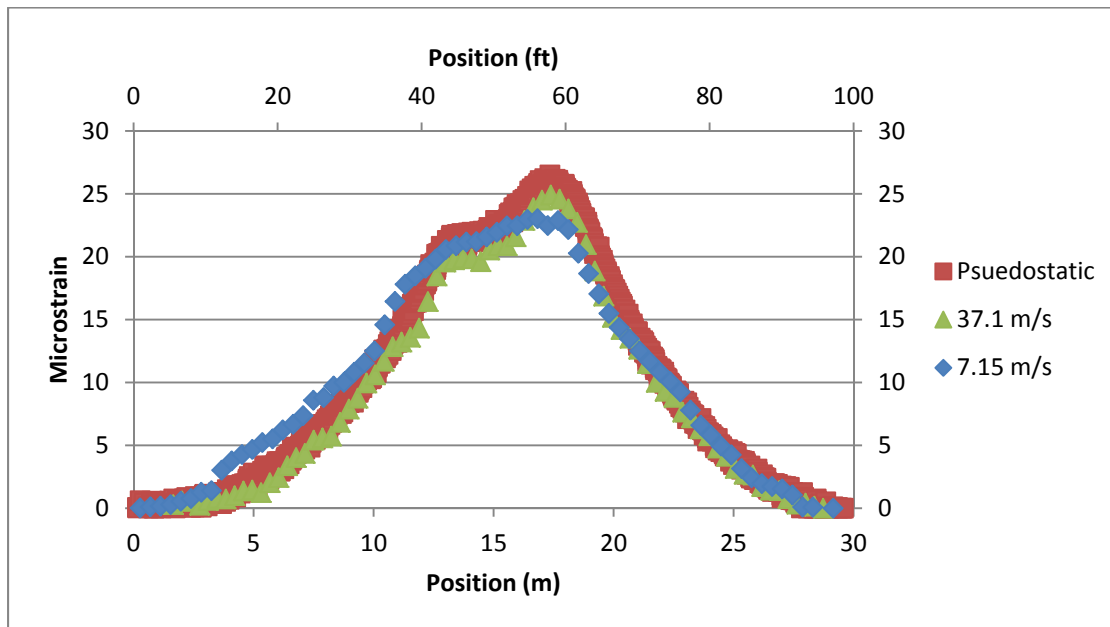


Figure 6.20 Comparison of microstrain for psuedostatic and dynamic cases

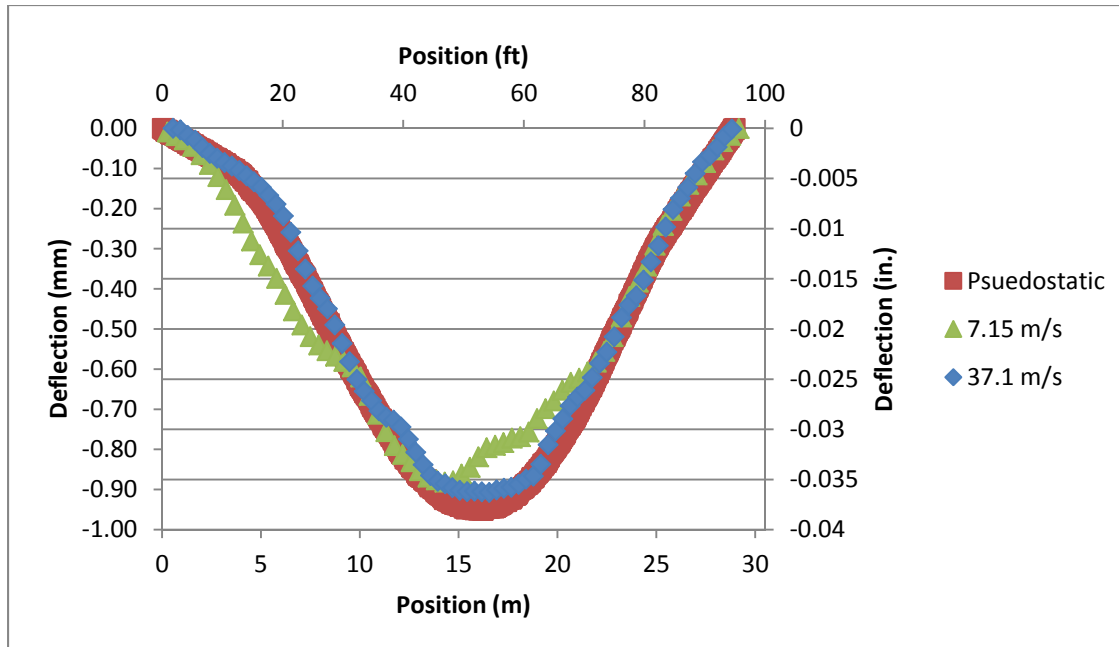
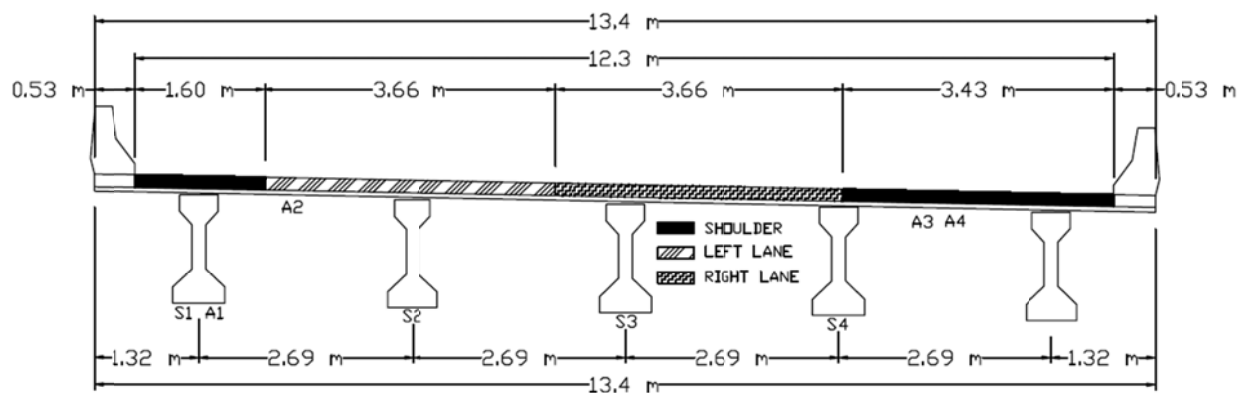


Figure 6.21 Comparison of deflection for pseudostatic and dynamic cases

## Chapter 7: Black Box Instrumentation Plan & Testing

In order to perform baseline testing of the accuracy of the black box system, the bridge was instrumented in a way that would allow for a direct comparison between the black box and long-term data. The eight black box sensors chosen for the comparison were four strain gauges attached transversely across the bottom of Girders 2-5 at 0.6L of the bridge, and four accelerometers attached transversely across the bridge on the bottom of Girder 5, attached on the deck between Girders 4 and 5, and two being attached between Girders 1 and 2. The position of these sensors are shown on a cross sectional view in Figure 7.1. These sensors were mounted using fast setting adhesive and specially designed mounting tabs in order to fasten the instruments to the concrete. Ladders were used to reach the bottom of the girders and deck. All eight sensors were attached to the bridge in less than an hour using two ladder crews.



*Figure 7.1 Sensor position on bridge cross-sectional view*

When running, the computer of the black box uses 10 W. When it is in the sleep mode, it only uses 1 W. After running the system in the lab to estimate the power consumption by the eight sensors, we determined that our two 12V 29DP-DL marine batteries, each with an amp-hour rating of 106Ah, could run the system for four days. To account for any inaccuracies, and

to ensure that the batteries were not over drained, the system was only initially run out in the field for two days, nonstop.

The black box system came with two 200 ft cables that attach the black box to the nodes. In order to prevent someone from being able to cut the cables by placing the system at the ground level, the entire system, including the black box, two nodes, 400 feet of cables, and two marine batteries, was placed in between Girders 3 and 4 as shown in Figure 72.



*Figure 7.2 Black Box system set-up*

The testing of the black box occurred over a constant two day period and two tests were run at the same time. The first test was a decimated test which was set up to run constantly over

the entire two day period at a frequency of 100 Hz. The decimation was set to average every 60000 records into one record which provides an average reading over every ten minute period. This test was intended to evaluate the movement of the sensors with temperature over the two day period. The second test was set up as a triggered event to record the data 15 seconds before and after any of the strain gauges recorded a change exceeding three microstrain. This test was used to provide data for each time a moderate sized vehicle traveled across the bridge. In all, 334 triggered events occurred over the two day test. More triggers were expected but the gauges were found to vary due to temperature causing our triggers to only work during certain periods of the day. The auto zero function is being fixed in the black box software and is expected to solve this problem.

## Chapter 8: Black Box Comparison

After the two day black box test, the data collected from the strain gauges and accelerometers was compared to the data collected over the same time period from the sensors of the long-term instrumentation. Although the black box pilot test was continuously monitored over two days, it was determined that the strain gauges were influenced due to temperature and so during some periods of the day they would not trigger. This issue will be addressed in future progress of the software. In addition, the long-term data is only collected for five minutes every three hours so, of the 334 triggers collected, only 10 sets of data could be compared.

For the strain gauges, a direct comparison could be employed between the two sets of data. In most cases, the two sets of data were highly correlated, as shown in Figure 8.1. However, in some instances, the two sets of data were different in terms of magnitude, as shown in Figure 8.2. This difference could be attributed to a timestamp difference which would indicate that the comparison is between two different groups of vehicles. A comparison of the live-load test data was also compared to the black box data in Figure 8.3 showing a strong correlation. Because the live-load data had been zeroed previously, the data was superimposed on the other two sets of data beginning on the y-axis at -33.5 microstrain. The two sets of data are not comparing the same truck and so an exact replica was not expected but more of a qualitative comparison can be made.

In addition, the decimated test for the strain gauges was compared to the long-term strain gauge data that was collected as one record every 15 minutes as shown in Figure 8.4. This comparison shows that the trend is the same throughout the day though the black box varies more due to temperature than the long-term instrumentation. This could partly be caused by the fact that the black box gauges are all unprotected underneath the bridge while the long-term

instrumentation sensors are all housed in boxes underneath the bridge. A comparison of the long-term strain data, the ambient temperature, and the bridge temperature, as shown in Figure 8.5, shows a strong correlation between the outside temperature and the strain data; with a slight delay from the bridge temperature, as expected. In the figure, the sets of data were zeroed at their means in order to provide for a better comparison. The ambient and bridge temperatures are provided along the y-axis as temperature in Fahrenheit while the strain data is provided along the y-axis as microstrain. All sets of data are averaged and recorded along the x-axis with each record indicating a 15 minute interval.

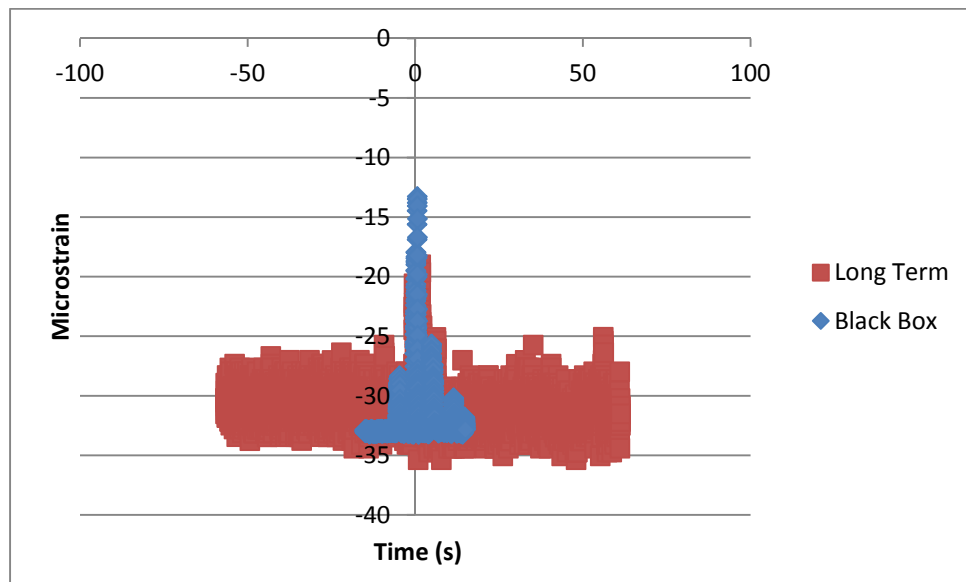


*Figure 8.1 Girder 2 strain for 30 second period*

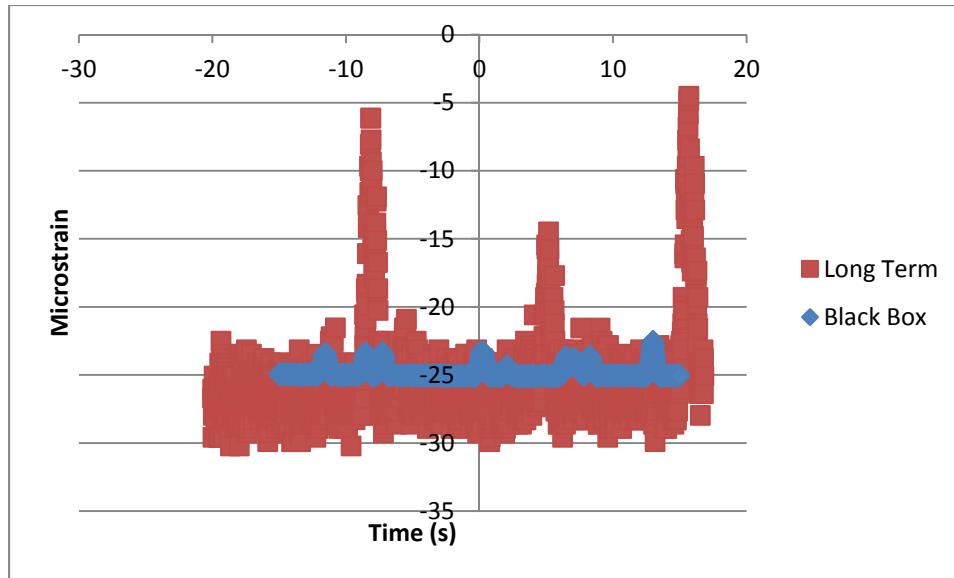


Figure 8.2 Girder 3 strain for 30 second period

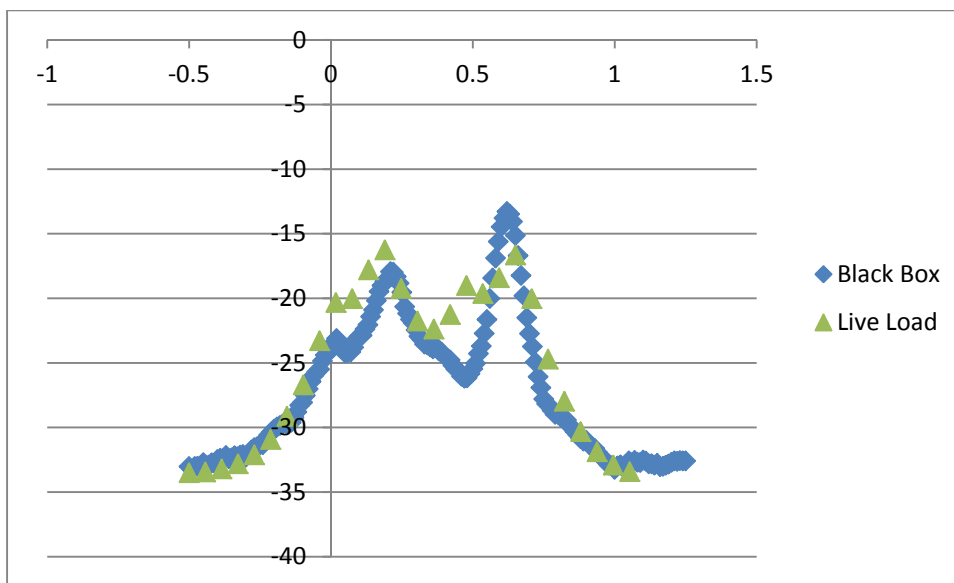


Figure 8.3 Comparison of single truck crossing bridge

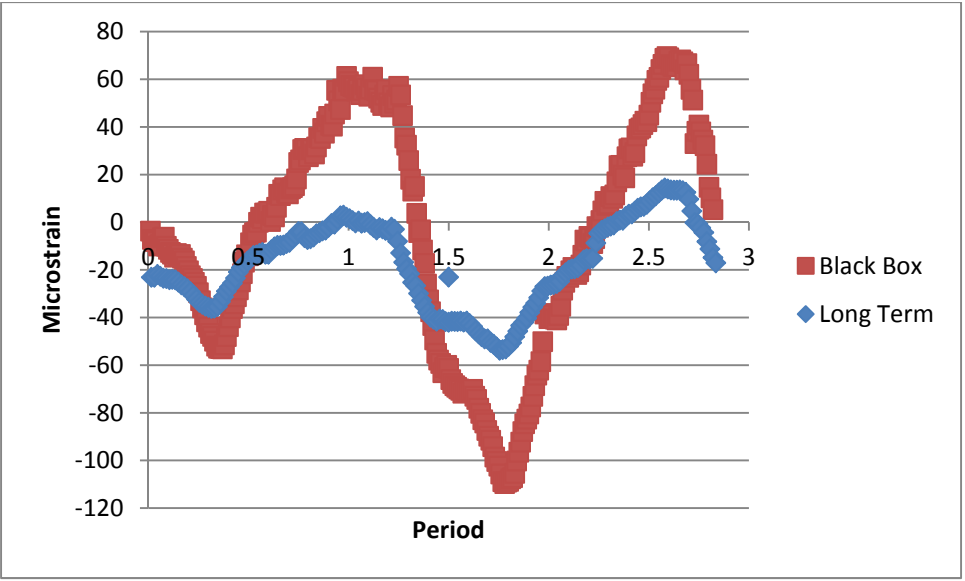


Figure 8.4 Girder 3 strain, two-day period

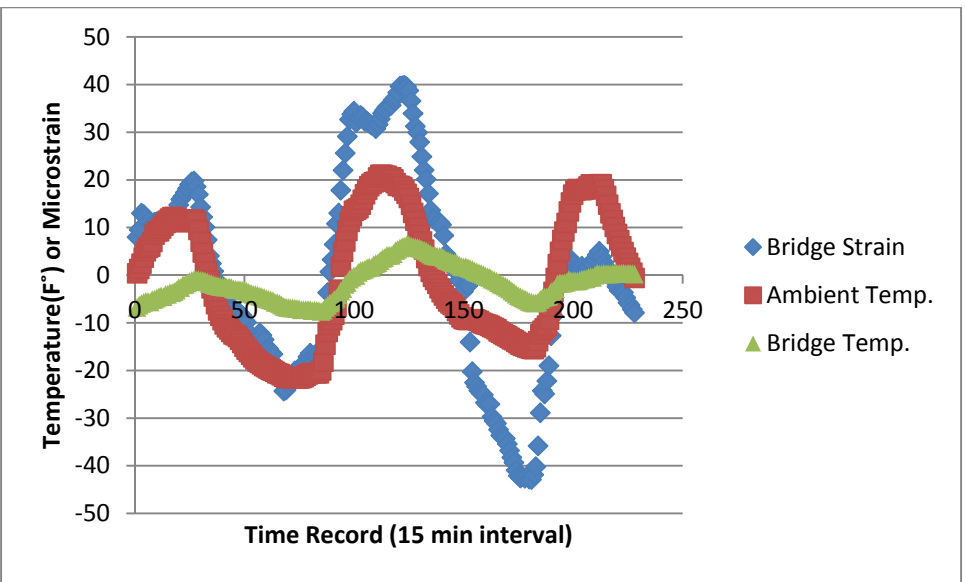
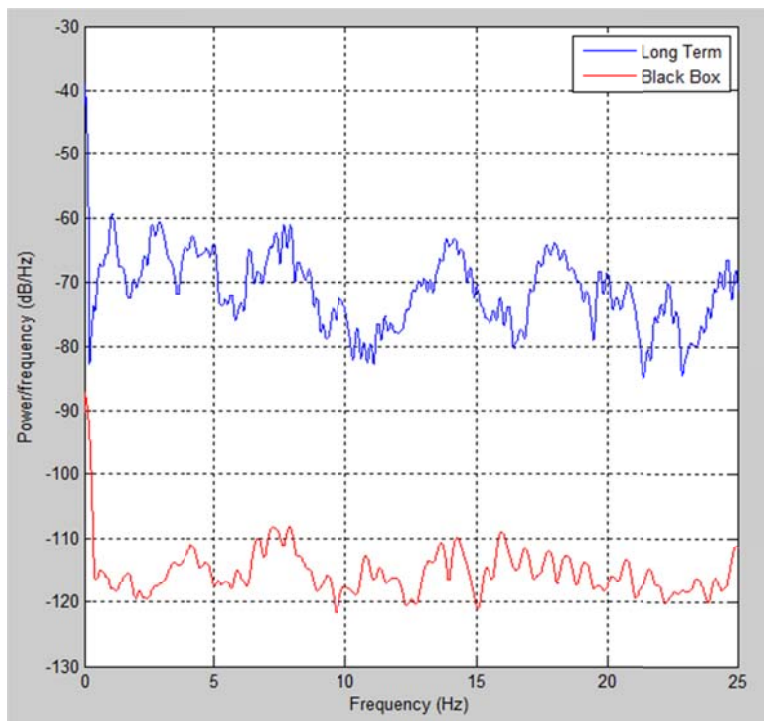


Figure 8.5 Comparison of bridge strain, ambient temperature, and bridge temperature

When comparing the accelerometer results to the long-term data results, a direct comparison could not be made because the long-term instrumentation includes velocity transducers, as opposed to accelerometers. Instead, a Welch’s power spectral density estimate was conducted in order to determine the frequencies of both the accelerometer and velocity transducer data. Though some of the data sets were too noisy to show a strong comparison

between the sensors, as shown in Figure 8.6, other data sets show a strong correlation between the sets of data, as shown in Figure 8.7. Most of the noise generated by the sensors was obtained when looking at the long-term instrumentation data which, when comparing to the black box data, makes the black box and its sensors look good.



*Figure 8.6 Welch power spectral density estimate of long-term and black box data*

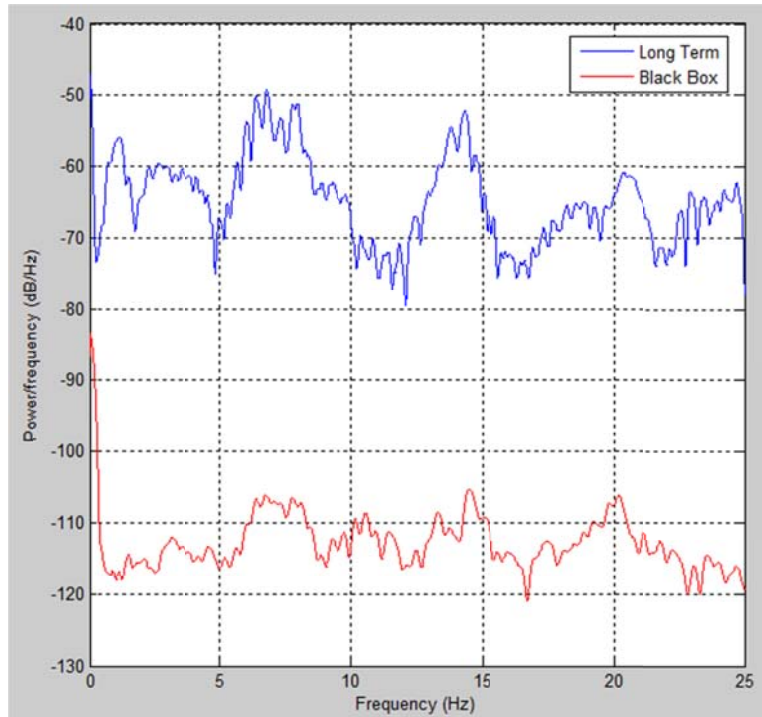


*Figure 8.7 Welch power spectral density estimate of long-term and black box data*

As part of the data analysis phase, a block of data was sent to researchers at Columbia University. The data was sampled over an eight day period with measurements being recorded for five minutes every three hours. During this recording period, the data was sampled at a frequency of 50 Hz. Initially the data was evaluated using a time history and power spectrum for each group of each day. Using this approach, natural frequencies could not be identified. Figure 8.8 shows a typical time history and power spectrum for the Group 1 data set taken on Day 1. This corresponds to the data being recorded starting at 5:00 in the morning. The figure shows the difficulty in clearly identifying the natural frequencies of the bridge.

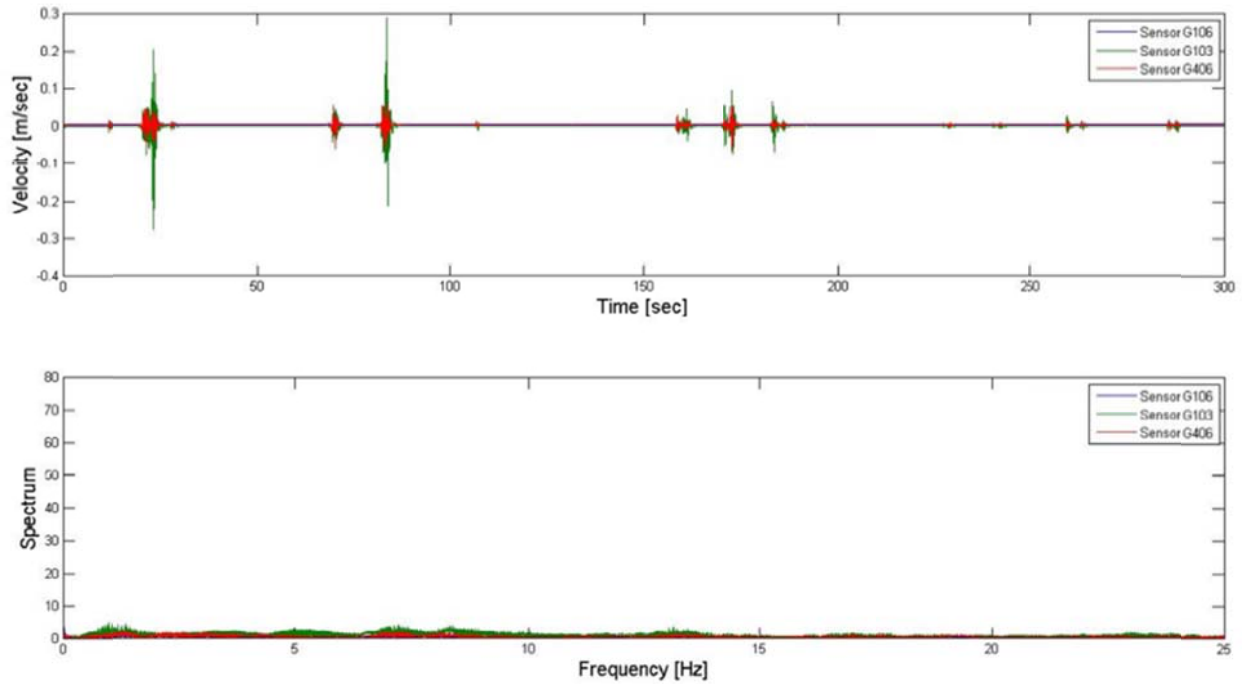


*Figure 8.8 Group 1 – Day 1, Raw Data*

The data was further analyzed by removing a potential linear trend from the data block. The detrending process was performed using a linear and constant approach. The linear approach removes a continuous, piecewise linear trend. The second approach removes just the mean value from the vector. Figure 8.9 shows the results using the linear approach and Figure 8.10 shows the results using the constant approach. Both figures show that there was no substantial difference between the constant and linear detrend.

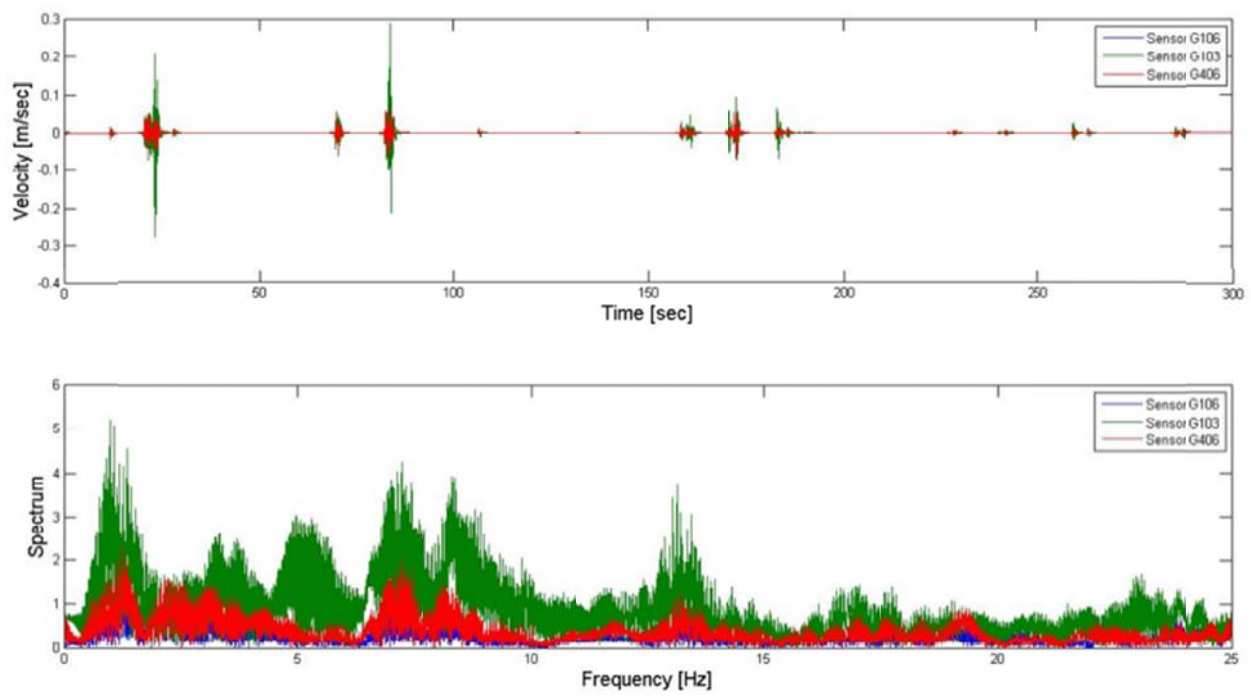


Figure 8.9 Group 1 – Day 1, Linear Detrend

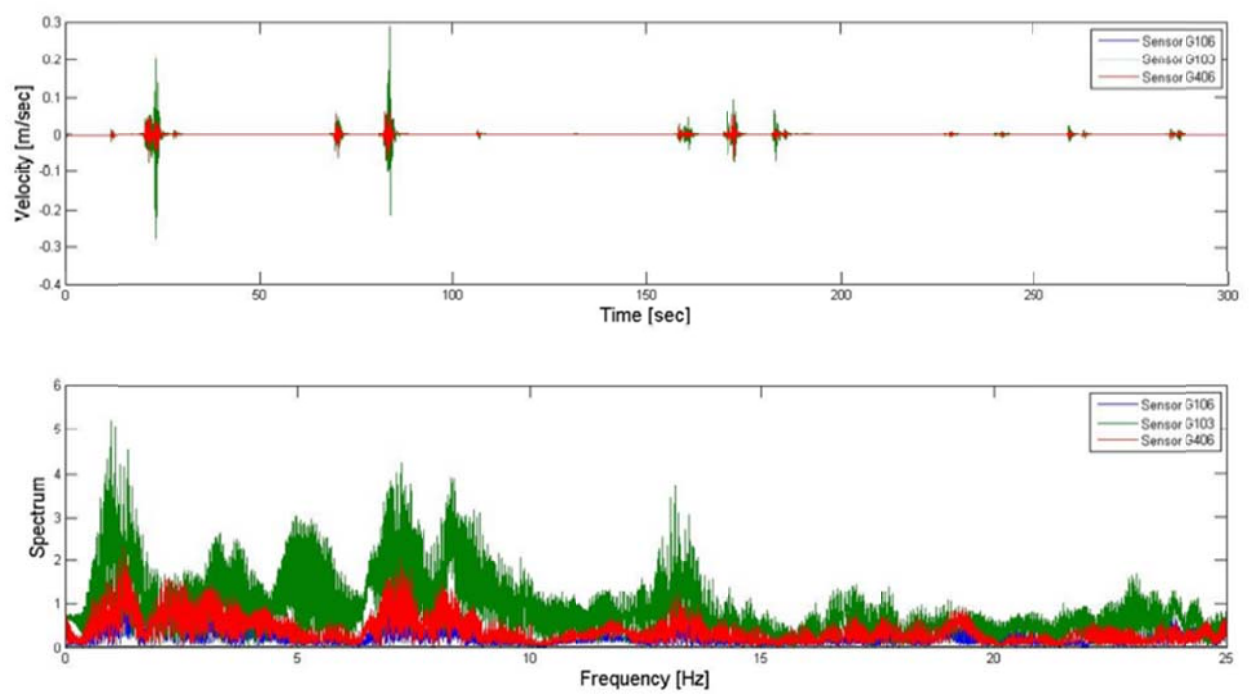


Figure 8.10 Group 1 – Day 1, Constant Detrend

A highpass Butterworth filter was applied to the detrended data. The cutoff frequency for this filter corresponds to half the sample rate. The order of the Butterworth filter was set at 5. The data was processed using the Observer Kalman/Filter Identification Algorithm. The results are shown in Table 8.1.

*Table 8.1 Frequency Overview*

	<b>F1</b>	<b>F2</b>	<b>F3</b>	<b>F4</b>	<b>F5</b>	<b>F6</b>
	<i>Hz</i>	<i>Hz</i>	<i>Hz</i>	<i>Hz</i>	<i>Hz</i>	<i>Hz</i>
<b>Maximum</b>	2,0266	7,9582	8,9735	9,9898	14,058	18,8041
<b>75th Percentile</b>	1,2571	7,5609	8,4752	9,8889	13,4716	17,6541
<b>Median</b>	1,1532	7,3003	8,3658	9,7295	13,3505	17,5418
<b>25th Percentile</b>	1,0873	7,1438	8,2259	9,6112	13,2456	17,3391
<b>Minimum</b>	1,0057	6,8729	8,0518	9,0143	12,9375	16,4939

Based on the results from Table 8.1, the researchers have concluded that the first frequency is associated with very high damping ratios and is not being considered as a structural frequency. This very high damping result also occurred with the second set of data and also using the ECA algorithm. The most consistent frequencies were found to be the third and fifth (F3 and F5). The mode shapes were also analyzed. It was noted that for the third and fifth frequencies, the second sensor always presented a negative value for the eigenvector. This occurred for both the OKID and ECCA algorithms.

## **Chapter 9: Research Conclusions**

In this study, a newly developed short-term data acquisition system was compared to a long-term instrumentation system over a two day period to determine whether or not the system could be trusted as a mobile alternative to a fully instrumented bridge. Through this study, it was determined that the black box provides comparable, if not less noisy data, than the long-term instrumentation. Whether this noise is due to the sensors being made from different companies, doesn't really make a difference. The goal of the black box is to be a system that can be taken to a bridge with no power, instrumented within a few hours, and then left for two weeks to collect accurate data. As compared to the long-term instrumentation, the data collected from the black box is believable. While there are some issues remaining to be worked out, such as the auto zero function which would prevent the drifting of the gauges due to temperature, as well as the sleep mode which would enable the system to be left on a bridge with no power for two weeks instead of four days, overall this system shows promise as a possible alternative to long-term instrumentation. USU and BDI are currently working on the various issues and the system is expected to be running optimally by this summer.

## **Chapter 10: Bridge Instrumentation & Diagnostics Using STS4 & STS Live Testing System**

### **Introduction**

Currently there are two types of bridge monitoring systems available at the structures and materials laboratory of Virginia Tech. The first is a system developed by Bridge Diagnostics Inc. (BDI), which is primarily a system developed for the short term instrumentation of bridges. This system is ideal for performing live load tests where the desired tests can be performed over the course of a day. The second is a system created by Campbell Scientific (CS), which are a set of data loggers that allow connection of various instruments. CS systems can be used for both short and long term monitoring, but can be difficult and complicated to program to achieve the desired data collection.

A new system that has been created by BDI, STS4, will allow for simple deployment for both a live load test and also long term monitoring. Its greatest advantage will allow the system to be placed on a structure for a period of a few weeks, be battery powered, and allow for simple user input for desired data collection. In this way, the system becomes a hybrid that will allow for one simple system to perform many structural instrumentation tasks.

The purpose of this project is to describe the uses of the new system and provide detailed instruction on its deployment in both a live load, and long term monitoring scenario. A proof of concept test on the Kerrs Creek Bridge was performed to ensure desired results could be obtained from the proposed system. A user's manual that will describe both hardware, and proper use of software for the STS4 system will be presented. Also, a system validation test will be completed by placing the new system with its instruments next to current monitoring

instrumentation to compare results. Finally, the Varina-Enon monitoring test will be presented as a practical application of the system.

The vision for the STS4 system is that it would have the following characteristics:

- A minimum of eight channels used to measure: strain, displacement, temperature, and acceleration.
- Simple deployment.
- No complex programming.
- Could withstand field conditions.
- Powered by a reasonable sized battery system for a period of two to three weeks.
- On-board data storage.
- Ability to perform both live load testing, and also long term monitoring.
- Ability to record data based from triggered events.

## **Proof of Concept Testing**

The proof of concept testing was a live load test performed using hardware and software developed by BDI. The hardware, STS-WiFi, is a data collection system consisting of battery powered nodes where up to four instruments are connected, and a base station that wirelessly collects the data from these nodes. A PC is wirelessly connected to the base station. The software used to run this system is WinSTS, also developed by BDI. WinSTS provides a simple user interface and allows for real time graphic/display of instrument response. The proof of concept test was completed before the STS4 system was ordered to insure the purpose of the STS4 was achievable. Also, the test was set up so that the researchers could investigate the type of information that could be gathered using the proposed STS4 system. In other words, the test was set up to mimic the STS4 system. More specifically, the purpose was to find if various traffic characteristics i.e. speed, lane position, load of vehicle, and number of axles could be determined from data obtained using the proposed system.

Also, the researchers were interested in comparing the joint displacement in an adjacent box girder bridge with a previous test done on the Aden Road Bridge. The Aden Road Bridge is similar to the bridge presented below. The presentation of the live load test will focus on the instruments used to reproduce the STS4 system and the investigation of traffic characteristics. The comparison of joint movement to that found in the Aden Road Bridge will be reported elsewhere.

## **Bridge Selection**

A concrete adjacent box girder bridge in good condition was needed to complete an appropriate comparison with the Aden Road Bridge. The Kerrs Creek Bridge, located on Route 60 one mile from Interstate 64 and near Lexington, VA., was selected based on VDOT inspections of these bridge types and corresponding ratings. The bridge allowed for an instrumentation setup that would be similar to and could be performed with the STS4 system. Upon visual inspection the bridge was selected for its ease of access and similarities to the Aden Road Bridge. The following criteria were required for the bridge:

- No skew
- Superstructure rating of at least 8, with ratings for deck and substructure being above 5.
- Bituminous wearing surface.
- Within 2.5 hour drive of Blacksburg.
- Easily accessible

The Kerrs Creek Bridge, Virginia structure number 1022 and federal structure number 15219, carries route 60 over Kerrs Creek. The bridge was completed in 1984 and has an annual daily traffic (ADT) of 1955 and average daily truck traffic (ADTT) of 39. The bridge has a single simple span of 58 ft., and is shown in Figure 10.1.



*Figure 10.1 Kerrs Creek Bridge*

The joints of the adjacent box girders showed little signs of leakage and very little reflective cracking in the surface of the asphalt overlay. Images of these features can be seen in Figure 10.2 and Figure 10.3 below. This gave the research team an overall impression that the joints were in good condition relative to the condition of the Aden Road Bridge, which was the primary focus of bridge selection.



*Figure 10.2 Underside of Kerrs Creek Bridge*



*Figure 10.3 Asphalt wearing surface of Kerrs Creek Bridge*

### **Instrumentation**

The purpose of the testing was to determine traffic characteristics and bridge behavior using the eight channels that would be available with STS4. Twelve gauges were used, eight of which were strain gauges which would be used in determining traffic characteristics, and four gauges were used to measure relative girder displacements for comparison to the Aden Road Bridge. The instrumentation layout can be seen in Figure 10.4.

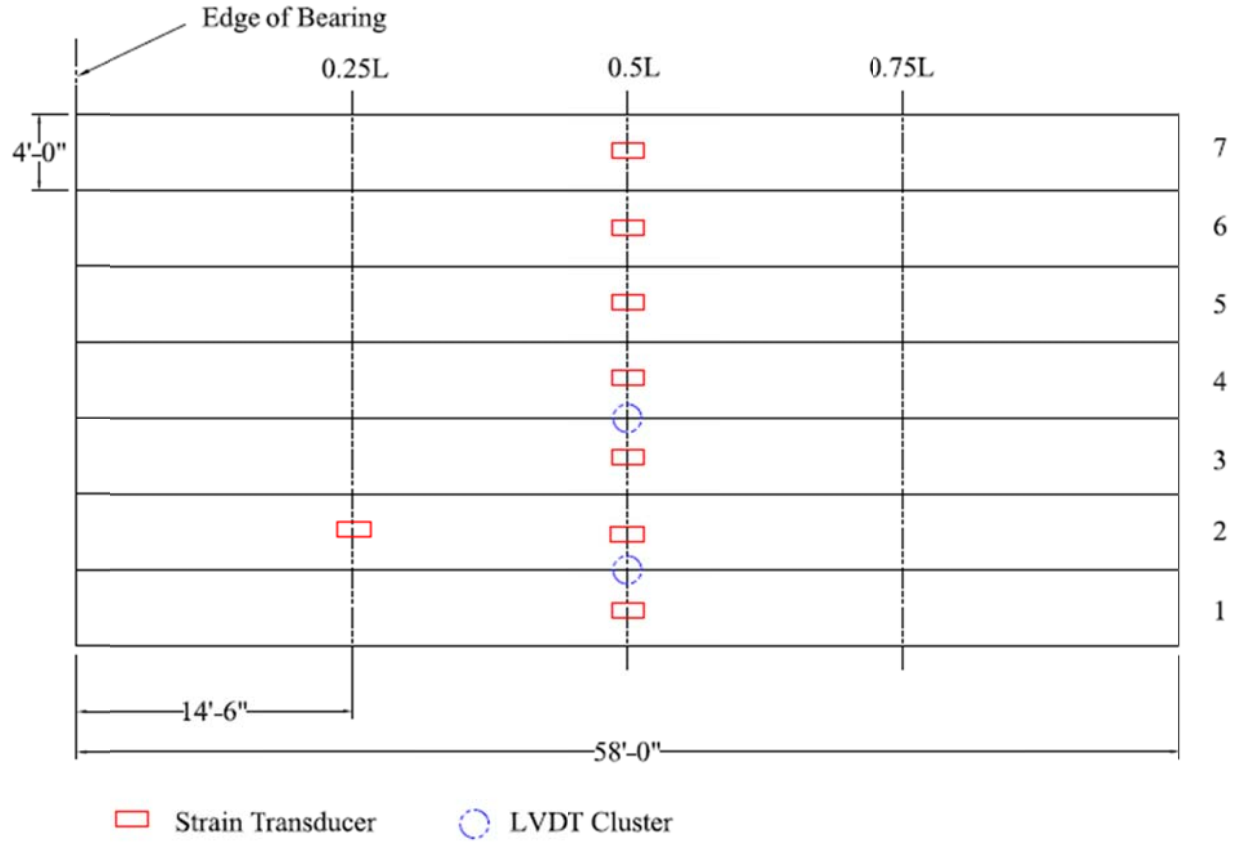
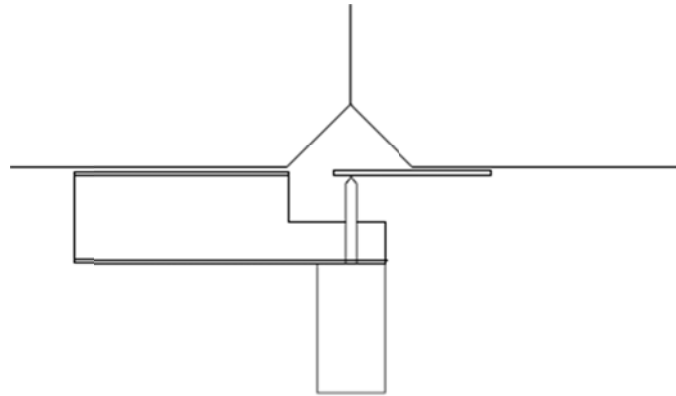
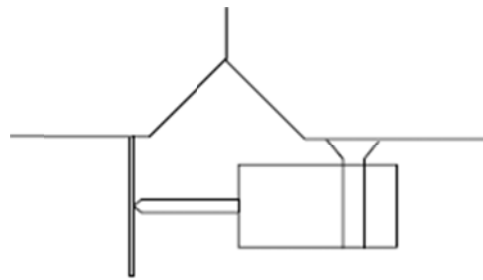


Figure 10.4 Instrumentation layout

Strain gauges were positioned to record mid-span, bottom flange strain in each girder. A strain gauge was also placed at 0.25L to allow for speed of vehicle estimation. LVDT's were placed to record horizontal and vertical deflection at the joints between Girders 1, 2 and also between Girders 3, 4 as shown in Figure 10.5 and Figure 10.6. These two instruments were placed next to each other to form what is labeled the LVDT cluster. This was done to provide data on the relative displacements of the girders that are in the wheel path of ambient traffic.



*Figure 10.5 Placement of LVDT to measure vertical joint movement*



*Figure 10.6 Placement of LVDT to measure horizontal joint movement*

The instruments used for representation of the STS4 system and those used for the Aden Road bridge joint comparison are listed in Table 10.1. All of the instruments used for STS4 representation were strain transducers manufactured by BDI shown in Figure 10.7. The transducers contain a full Wheatstone bridge, and measure a voltage that is linearly converted to strain. Because the test was performed on a concrete structure that typically experience small values of strain, it is important to have a high level of accuracy. The strain transducer is placed on the structure by attaching two tabs 3 inches apart directly to the structure using an adhesive. The instrument is then attached to the tabs.

*Table 10.1 Location and purpose of instruments used in bridge test*

<b>Instrument</b>	<b>Location</b>	<b>Purpose</b>	<b>Instrument</b>	<b>Location</b>	<b>Purpose</b>
ST1997	Girder 1 0.5L	STS4	ST2108	Girder 7 0.5L	STS4
ST2001	Girder 2 0.5L	STS4	ST1996	Girder 2 0.25L	STS4
ST2005	Girder 3 0.5L	STS4	LVDT4	Joint 1 0.5L	Aden Road
ST2002	Girder 4 0.5L	STS4	LVDT6	Joint 1 0.5L	Aden Road
ST3431	Girder 5 0.5L	STS4	LVDT2	Joint 3 0.5L	Aden Road
ST3199	Girder 6 0.5L	STS4	LVDT1	Joint 3 0.5L	Aden Road



*Figure 10.7 BDI Strain Transducer*

These instruments are well suited for field testing, since the strain gauges are encased in a waterproof aluminum housing. They can also operate at wide range of temperatures, from  $-58^{\circ}\text{F}$  to  $185^{\circ}\text{F}$ .

## **Test Procedure**

The Virginia Department of Transportation (VDOT) provided a two axle dump truck loaded to a gross weight of 30,400 lbs. The dimensions for the truck axles are shown in Figure 10.8 and associated load distribution in Table 10.2. This truck provided several highway-speed crossings of the bridge in order to determine strains and movements under a known load. The

truck was driven across the bridge in two different locations at three speeds: 5 mph, 25 mph, and 45mph. . Also, data was collected while twelve ambient trucks crossed the bridge.

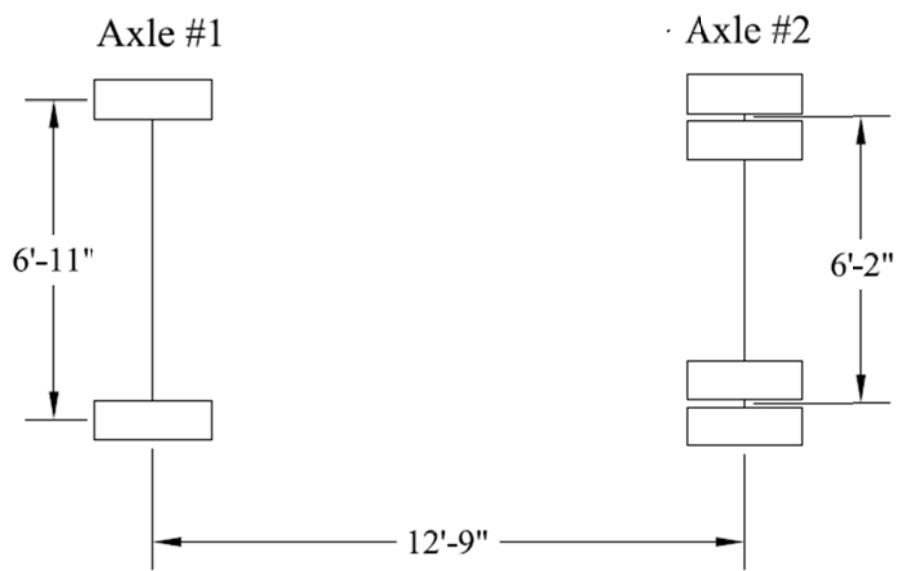


Figure 10.8 Test Truck Dimensions

Table 10.2 Axle load distribution

Axle	Axle #1	Axle #2
Weight (kip)	9.3	21.1

All dynamic data was recorded at 100 Hz per channel. Pseudo-static testing was recorded at 40 Hz per channel. The ambient traffic was recorded using 100 Hz per channel.

The live load testing of the bridge with the control truck was performed on June 12, 2013. A list of the runs that were recorded with the control truck is provided in Table 10.3. The truck provided runs in both lanes of travel, shown in Figure 10.9 and Figure 10.10, and at varying speeds.

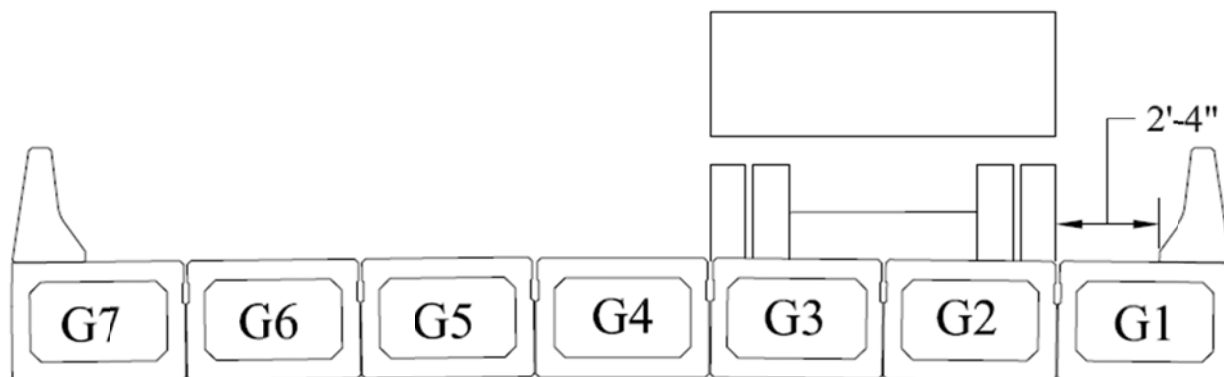


Figure 10.9 Control truck positioning on North runs

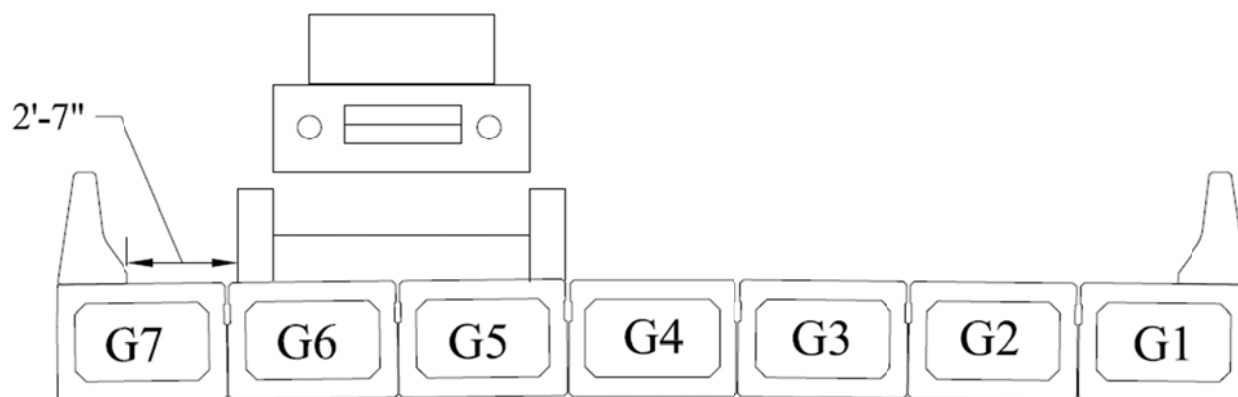


Figure 10.10 Control truck positioning on South runs

Table 10.3 Control truck testing information

Run #	Truck Direction	Communicated Speed (mph)
1	South	45
2	North	45
3	South	45
4	North	45
5	South	25
6	North	25
7	South	Pseudo-static
8	South	Pseudo-static
9	South	Pseudo-static
10	South	Pseudo-static

After the control truck had finished the desired bridge loadings, the instrumentation was left in place to allow for bridge testing of ambient traffic. Ambient traffic data was recorded to allow comparisons of the ambient traffic to the control truck for calculations of load and speed. Table 10.4 contains the ambient runs.

*Table 10.4 Ambient traffic testing information*

Run #	Direction	Assumed Speed (mph)	Run #	Direction	Assumed Speed (mph)
1	South	45	7	North	45
2	South	45	8	North	45
3	South	45	9	South	45
4	South	45	10	South	45
5	North	45	11	North	45
6	South	45	12	South	45

## Data Organization

All data was recorded and stored as a text data file. These files were then downloaded and imported into Microsoft Excel for analysis purposes. Each set of data was first zeroed by subtracting the first data point from subsequent data points. The data was also smoothed. Smoothing of data is necessary due to the nature of both dynamic loading and the inherent noise associated with strain transducers. An average smoothing was performed using Equation 1.

$$V_i = \frac{\sum_{z=0}^{2 \cdot n} D_{i-n+z}}{2n+1} \quad (1)$$

$V_i$  = New data point in place of replaced data point  $D_i$

$n$  = Number of data points before and after raw data point to average

An example of smoothed data is shown below in Figure 10.11. In this example a  $n$  value of 3 was used to obtain the smoothed data value, and this  $n$  value is used throughout the data analysis, except in speed calculations as shown in Table 10.5.\*\*\*

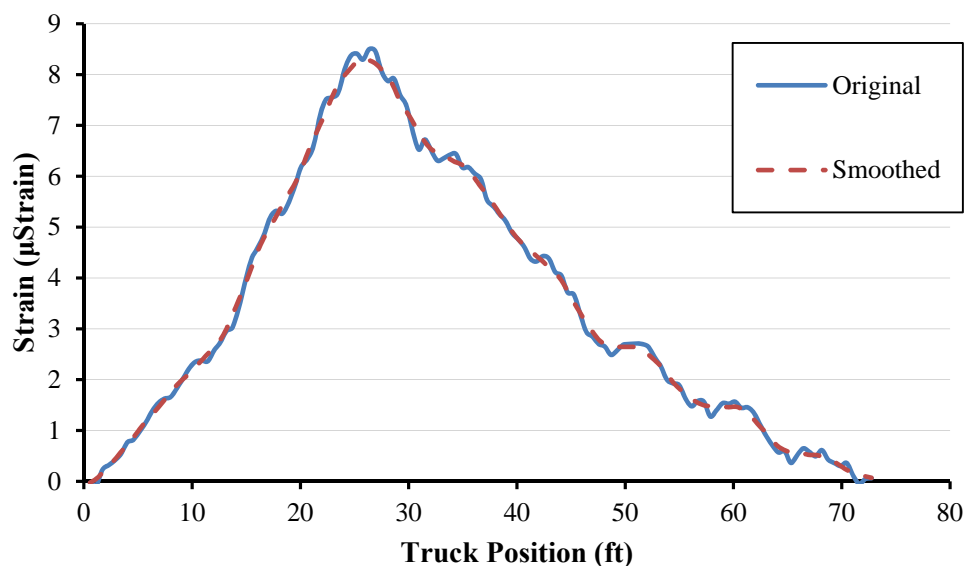


Figure 10.11 Example of smoothed data

## Results

The stated interest in the live load test was to see if the proposed STS4 system could be used to define traffic characteristics and general bridge behavior. The data is presented for transverse strain distribution in the bridge and the desired traffic characteristics (speed and truck location).

### *Transverse Strain Distribution*

One of the desired results from the test setup was to determine the transverse bottom flange strain distribution at midspan of the bridge. The transverse strain distribution is shown in relation to the front tire position of the control truck for Run #7 in Figure 10.12. The lengths shown in the x-axis are longer than the bridge length (61'4") since, when the front tire is off the

bridge, the bridge is still being loaded by the rear axle. The origin for the following graphics is when the front tire comes on to the bridge. The strain values are larger in the girders that are directly under the load of the truck. This is expected, but also shows the bridge is not acting as a single unit, as would be ideal.

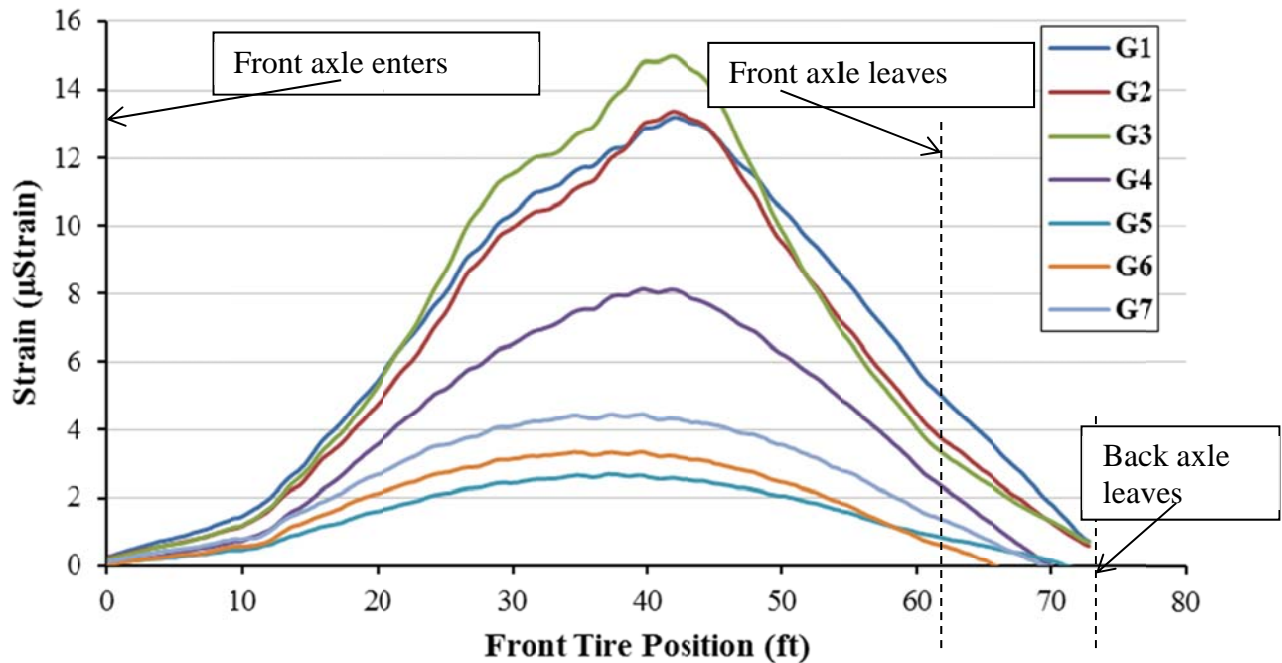


Figure 10.12 Influence of line diagram for 0.5L Run #7

Expected strains were also calculated. These strains were calculated assuming the end conditions of the bridge are simple (pin-roller). A comparison of expected strains to actual strains measured is presented in Figure 10.13. The maximum strain influence line was calculated with the girders acting alone, meaning the asphalt topping and the parapets do not contribute to the stiffness of the bridge. The minimum strain expected influence line was calculated with the topping and parapets acting compositely with the bridge girders. Both expected strain influence lines were calculated assuming that Girder 2 has a distribution factor of 0.18. This distribution factor was calculated based on the northbound runs. The data shows that the parapets and bridge

deck participate in the overall stiffness and load distribution of the bridge. Also, by bracketing the measured results, it is shown that the measured results are reasonable.

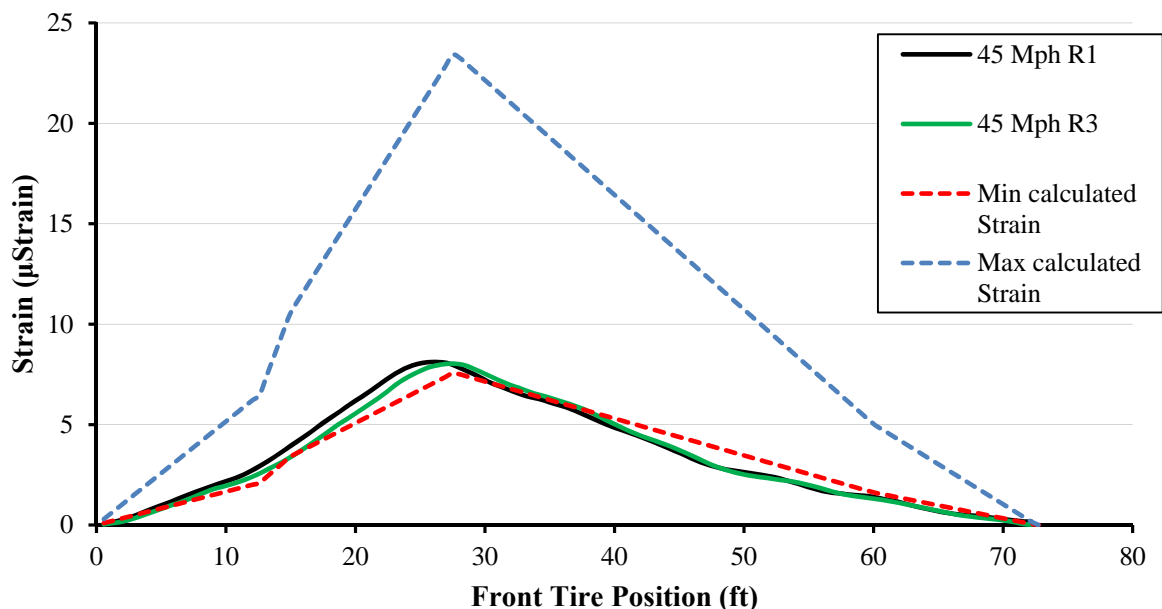


Figure 10.13 Comparison of expected strains to actual strains at 0.25L for Girder 2

### ***Traffic Characteristics***

One of the objectives of this paper is to determine the plausibility of using a small number of instruments that would be available in the STS4 system to estimate various traffic characteristics. The items considered were speed of travel, direction and lane of travel, load of vehicle, and number of axles. Each of these were investigated using the data obtained and are presented below.

### ***Speed***

In order to estimate the possible speed of traffic, the data was first smoothed using Equation 1 using various  $n$  values. Using the strain influence diagram for the strain gauges on girder 2, with one gauge placed at 0.5L and the other placed at 0.25L, a simple calculation to find

the speed was performed (algorithm used presented in Appendix). By finding the maximum strain in each gauge, the time at which the maximum occurred, and knowing the distance between the two gauges, the speed was calculated for each run. The smoothed influence line diagram for a 45 mph run in the South direction (Run #1) is shown in Figure 10.14.

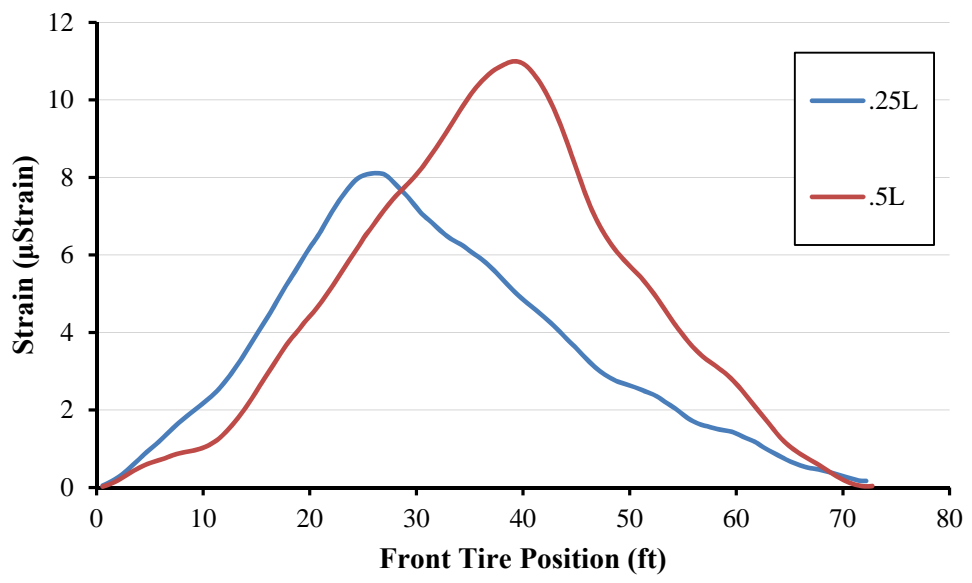


Figure 10.14 Influence line diagram of 0.25L and 0.5L for Run #1

The issue that arises in this type of calculation is how to smooth the data. This is because the maximum values, and when the maximum values occur, are highly dependent on how the data is smoothed. Presented in Table 10.5 are the speed calculation results from the algorithm based on the *n* value used in smoothing of the data.

*Table 10.5 Results from speed calculation algorithm with respect to smoothing value  $n$*

Run	Direction of Travel	Speed (mph)	Calculated Speed (mph)					
			$n=3$	% error	$n=5$	% error	$n=7$	% error
1	S	45	45.5	1.2	43.6	-3.0	43.6	-3.0%
2	N	45	87.3	93.9	74.8	66.2	104.7	133
3	S	45	40.3	-10.5	44.6	-0.9	45.5	1.2%
4	N	45	80.6	79.0	99.7	121.6	209.4	365
5	S	25	23.3	-6.9	23.8	-4.8	24.4	-2.6
6	N	25	80.6	222	95.2	281	99.7	299

The error values presented are not only based on the calculated speeds but also depend on the accuracy of the truck's speedometer. Assuming that a vehicle speedometer is not precisely accurate, the error values shown for northbound runs are not statistically different from the actual speed of the vehicle. More runs would be required to provide a more thorough statistical analysis of the accuracy of the calculation.

It can be seen that speed cannot be accurately determined for runs where the vehicle is not traveling over the strain gauge at  $0.25L$ . Each of the calculations with significant error is when the control vehicle was traveling north and the strain gauge at  $0.25L$  was placed under the north lane of travel. For accurate predictions of vehicles traveling both directions, strain gauges need to be placed in line in two locations longitudinally.

Figure 10.15 shows graphically the relation of the  $n$  value used and the accuracy of the speed calculation. It can be observed that as more points are averaged in the smoothing function the better prediction of speed obtained. This is true up to an  $n$  value of eight at which point the calculation becomes less accurate. Large values of  $n$  (values greater than eight) begin to eliminate the effect of a local maximum and therefore the speed cannot be accurately determined.

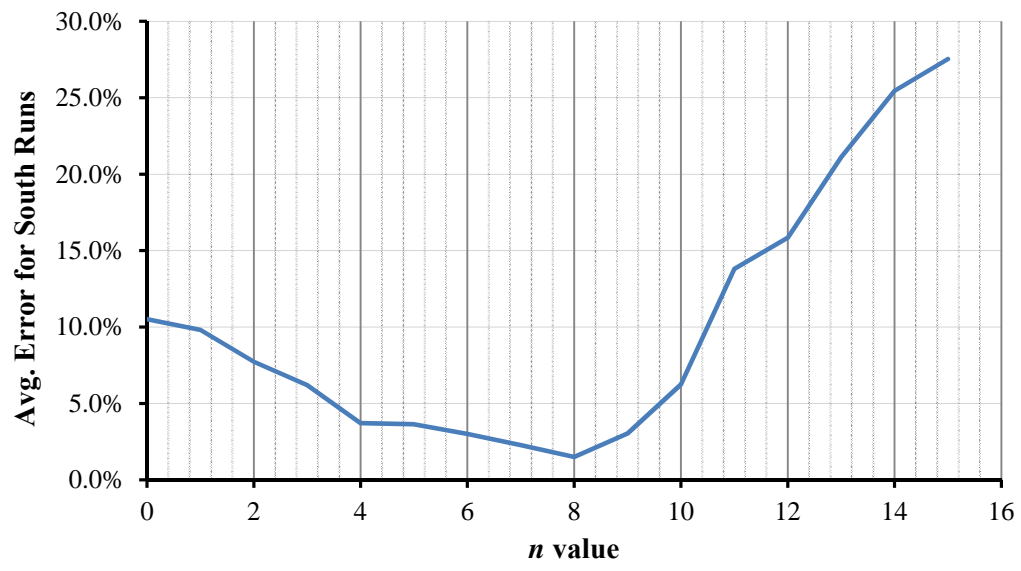


Figure 10.15 Accuracy of speed calculations based on increasing n values

### Vehicle Weight

The possibility of identifying the weight of a vehicle due to strains produced in the girders was also considered. The maximum strains at midspan produced by the control truck in each direction were recorded. These same strains were then recorded for an ambient vehicle.

The comparison of the strains is shown in Figure 10.16.

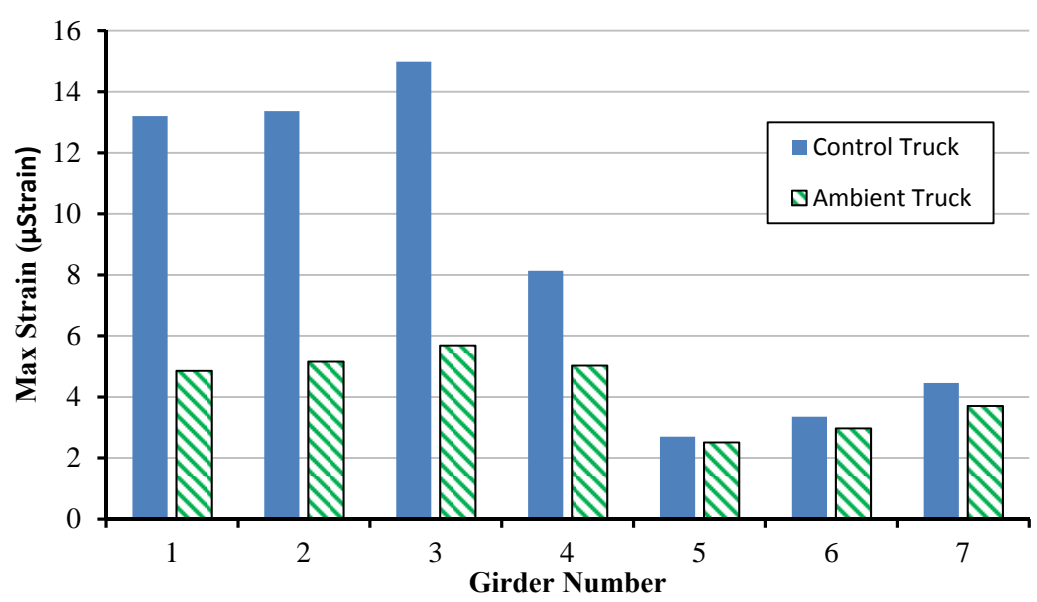


Figure 10.16 Control Truck Strains compared to Ambient Truck strains

The total gross weight of the Control Truck was 30.4 kips, which was used to obtain the weight of the ambient truck. Using the strain in the girders under the lane of travel, an estimated weight of the ambient vehicle can be calculated. Table 10.6 shows the maximum strain produced in each girder for both vehicles. In order to find the ambient vehicle weight the difference in strain from the two events was used. It can be seen that the percent differences of strain in girders 1 through 3 are very similar. By taking the average percentage of strain over girders 1 through 3 and multiplying by the control truck weight (30.4 kips), the estimated weight of the ambient truck presented in Table 10.6 is 11.5 kips. The other girders were not used because of the small readings of strain.

*Table 10.6 Calculation of approximate ambient vehicle gross weight*

<b>Girder #</b>	<b>1</b>	<b>2</b>	<b>3</b>	<b>4</b>	<b>5</b>	<b>6</b>	<b>7</b>
<b>Control Truck (<math>\mu\epsilon</math>)</b>	13.2	13.4	15.0	8.1	2.7	3.4	4.5
<b>Ambient Vehicle (<math>\mu\epsilon</math>)</b>	4.9	5.2	5.7	5.0	2.5	3.0	3.7
<b>Difference in Strain (%)</b>	36.8	38.6	37.9	61.8	93.1	88.5	83.1
<b>Calculated Load (kip)</b>	11.2	11.7	11.5	18.8	28.3	26.9	24.3

### *Lane Placement*

It can easily be discovered from the maximum strain produced in each girder the lane of travel for the vehicle. Since the bridge does not act perfectly compositely, the amount of strain varies across the cross section of the bridge. There is then associated a larger strain with the path of the vehicle. This is shown graphically in Figure 10.17 and Figure 10.18. These figures represent a vehicle traveling North and South respectively.

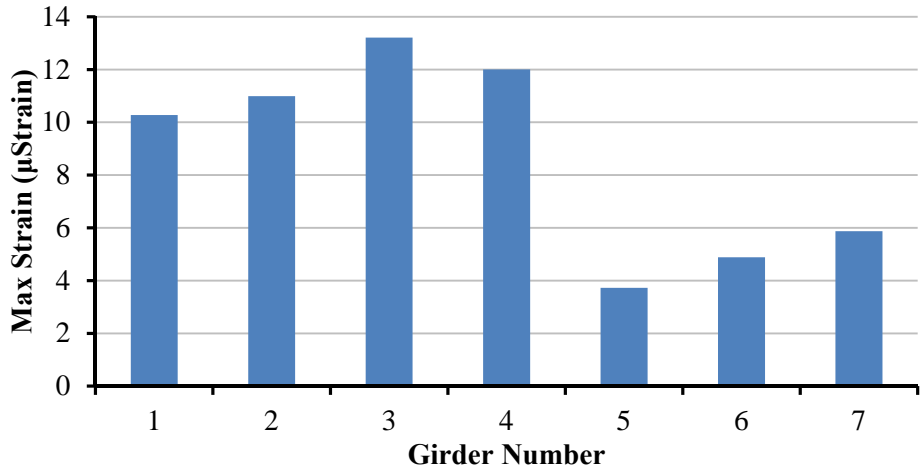


Figure 10.17 Maximum strain in each girder corresponding to Run #1

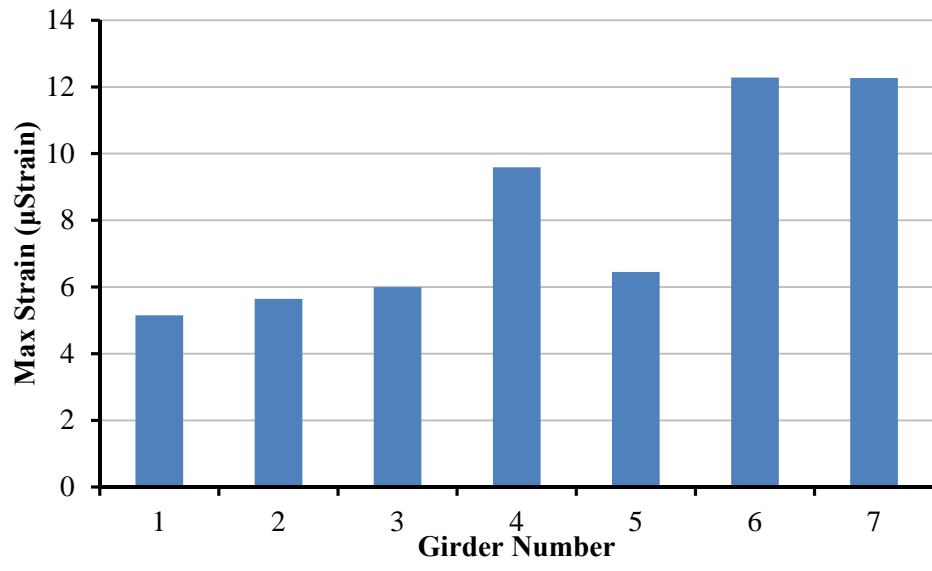
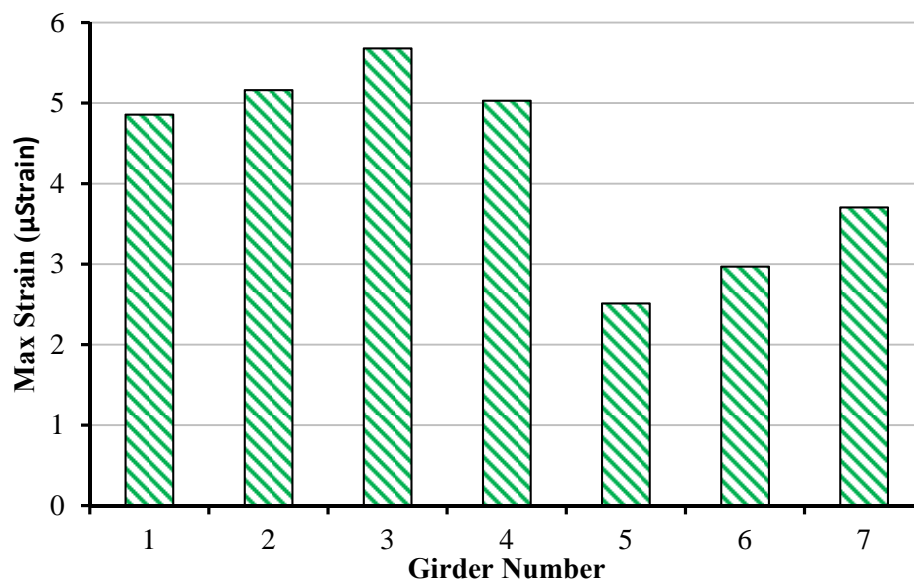


Figure 10.18 Maximum strain in each girder associated with Run #2

The same type of results can also be easily seen from an ambient truck. Figure 10.19 shows the maximum strain in each girder for an ambient truck. The truck was traveling north.



*Figure 10.19 Maximum strain due to ambient truck*

Observation of lane of travel seems to work well, but problems could arise when we have multiple vehicles on the bridge at the same time. Having trucks pass each other while on the bridge traveling in opposite directions would not allow for accurate records of load, lane placement, or speed.

### *Summary of Test*

The proof of concept live load test showed that the proposed system could provide useful information about bridge behavior and traffic characteristics with a limited number of instruments. Speed and lane placement were discovered simply and quite effectively. Also the strain distribution allows for insight into the condition and behavior of the bridge.

There are ways in which the test could be better performed to allow for more accurate calculations and the elimination of assumptions. In order to determine the speed of vehicles, two strain gauges must be placed in line longitudinally in each direction of travel. To determine the ambient vehicle weight it is recommended to use two control trucks of different weight. This

will allow for an accurate scaling of the strains which can then be applied to the ambient traffic. It was not possible with the acquired data to determine the number of axles, or even groups of tandem axles for that matter. This is because the noise in the strain gauges was large compared to the overall strain. In a bridge where large strains are experienced, it could be possible to discover local effects like number of axles.

## **User Operation of STS4**

The STS4 structural testing system was designed to provide easy operation and deployment. Through proper understanding of the hardware utilized and the software developed, simple and effective data collection can be achieved. Figure 10.20 shows the two major physical components of the system. The gray box contains all of the computing hardware. The STS4 nodes are the link between the instruments and the gray box.



*Figure 10.20 The STS4 testing system*

## System Hardware

The hardware of the system, besides the nodes, is incased in a weather-proof box. The contents of the box along with some basic descriptions as to their purpose are shown in Figure 10.21 and Table 10.7. This is not an inclusive listing, but should provide the user with enough information to understand the contents, and begin using the system.

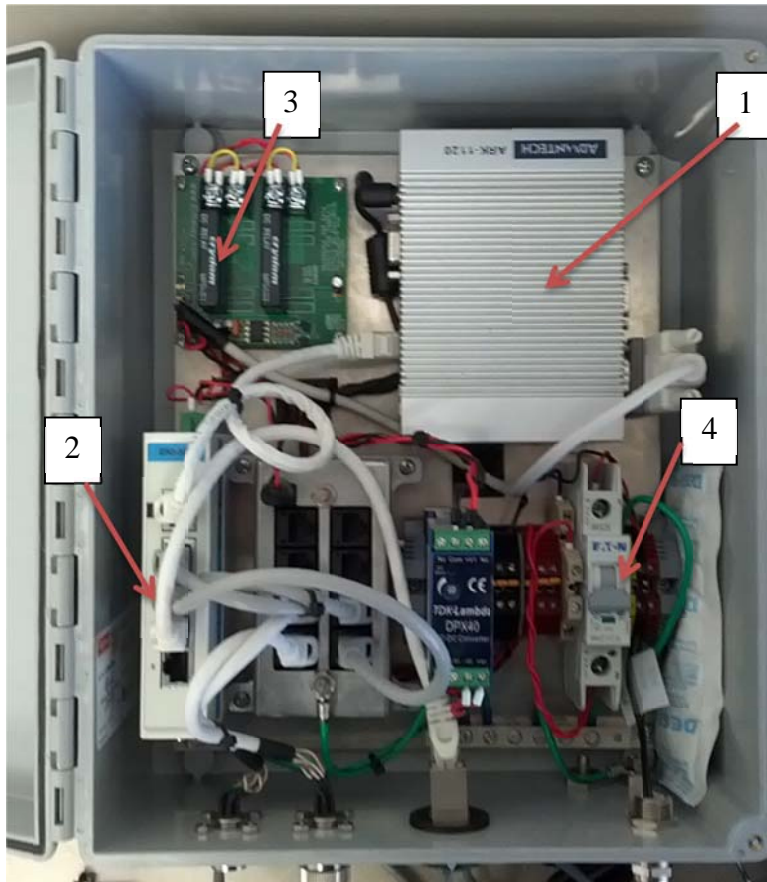


*Figure 10.21 Hardware in box of STS4*

Table 10.7 List and Description of Hardware

Item no.	Device	Description
1	ARK-1120L Remote Core	<ul style="list-style-type: none"> <li>• This is the computer of the system.</li> <li>• 2.0 GB memory</li> <li>• Low power consumption, &lt;10W</li> <li>• 2 RS-232 &amp; 4 USB Ports</li> <li>• Runs a Windows operating system</li> </ul>
2	EKI-3525 Ethernet Switch	<ul style="list-style-type: none"> <li>• Energy efficient. Automatically powers down ports not being utilized.</li> <li>• Manages data transfer</li> </ul>
3	SSR 2x Solid State Relay	<ul style="list-style-type: none"> <li>• Turns power on and off by an electrical current instead of a using physical switch.</li> </ul>
4	Electrical Switch	<ul style="list-style-type: none"> <li>• In order to deliver power to the rest of the components in the box, this switch must be in the on position. (Shown in Figure 10.21 in the off position).</li> </ul>

The nodes are connected to the gray box via Ethernet cable. Each Ethernet cable is 200ft and is industrial shielded with military style connectors at each end. This allows for the gray box to be placed at a convenient location, several hundred feet from the location of the instruments. The gray box has connections available for two Ethernet cords. This allows for the connection of two nodes, or a capacity of 8 channels.

Once the desired instruments have been attached to the nodes, nodes are connected to the gray box, and power is supplied to the box, the system is ready to be turned on and operated. To turn the system on simply switch the Electrical switch so that it displays the color red. Power lights should be illuminated on the Ethernet switch and the core computer should show an orange light. This orange light signifies that there is power to the computer, but it is not on. To turn the core computer on, press the button emitting the orange light on the core computer. The light should turn green. At this point a faint power light should also be seen on each of the nodes. The hardware is now ready for operation.

## System Software – STS Live

STS Live is the software developed to control the core computer and the instruments connected to each of the nodes. In order for the software to work with the hardware a connection needs to be made from the personal computer (PC) to the instruments. (Note: The PC must run a windows operating system. Windows XP or later version is recommended.) This is done by connecting an Ethernet cord from the PC's Ethernet port to the Ethernet port on the outside of the gray box (see Figure 10.22).

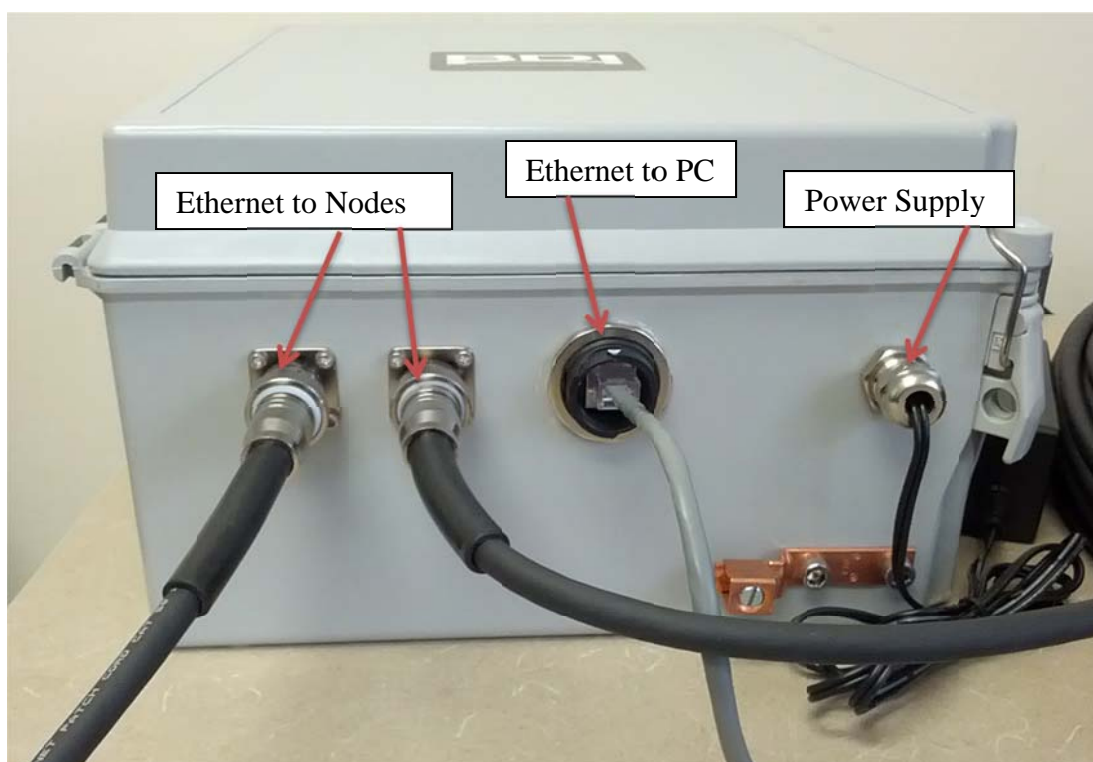


*Figure 10.22 Inputs into gray box*

### ***Core Options***

When first opening STS Live a splash screen is presented. This is where the user must first make a choice about how to run the hardware. The nodes, and thereby the instruments, can be programmed and operated through either the Core\_local (referred to as Local Core) or the CoreRemote\_1 (referred to as Remote Core). The difference between the two is in which

computer controls the nodes. Running on the Local Core basically bypasses the computer hardware in the gray box and allows the local computer (PC) to serve as the “core” of the test operation. This means that all data obtained through running the test will be stored directly on to the PC and will not be stored on the computer located in the gray box. The only practical application where this may be useful is in running a live load test where a PC can be continuously connected to the system. It can also be used when there is some issue with the remote computer located in the gray box.

In order to utilize the true capabilities of the system, the Remote Core option should be selected. This essentially makes the computer inside the box active. When running STS4 from the Remote Core, all information, i.e. groups, triggers, calendar features, is stored in the core computer. Once the connection has been removed from the PC to the box, the Remote Core continues to run and collects the desired data. The remote core can store up to 2GB of data and can therefore be used for the entirety of the test duration. The system should be run on the Remote Core for nearly all applications of STS4.

### *Connecting to the Local Core*

In order to run off the local core, settings on the PC need to be adjusted. This has to do with the IP address of the connection to allow for communication of the nodes to the PC. The nodes communicate to an IP address of 192.168.10.2. In order to make the connection from the PC to the nodes, the LAN network settings need to be set accordingly. The following steps on a windows operating system need to be performed.

- Control Panel > Network and Internet > Network and Sharing Center > Change adapter settings > Network LAN/Ethernet
- Under the network tab, highlight internet protocol Version 4 (TCP/IPv4).
- Select properties

- Select the radio button titled “Use the following IP address”.
- In the IP Address enter 192.168.10.2. The subnet mask should be set to 255.255.255.0

These settings will allow the PC to communicate with the nodes. Data from the nodes will be directly stored on the PC. Before running the software, the gray box needs to be opened and the Ethernet cord going into the core computer needs to be unplugged. This is because both computers, the PC and the core computer, have now been assigned the same IP address. Windows will show an error, and connection to the nodes is not possible. After the cord is removed, you are ready to run STS Live.

### *Connecting to the Remote Core*

In order to connect to the remote core over Ethernet the preceding section needs to be repeated. However, in this case the IP address needs to end in a value greater than 2, i.e. 192.168.10.4 as shown in Figure 10.23. The user needs to make sure the Ethernet cord is placed into the core computer. This will allow the nodes to communicate directly to the remote core, which is assigned the IP address of 192.168.10.2. This is the preferred method of running the system and allows it to use all of its intended functionality.

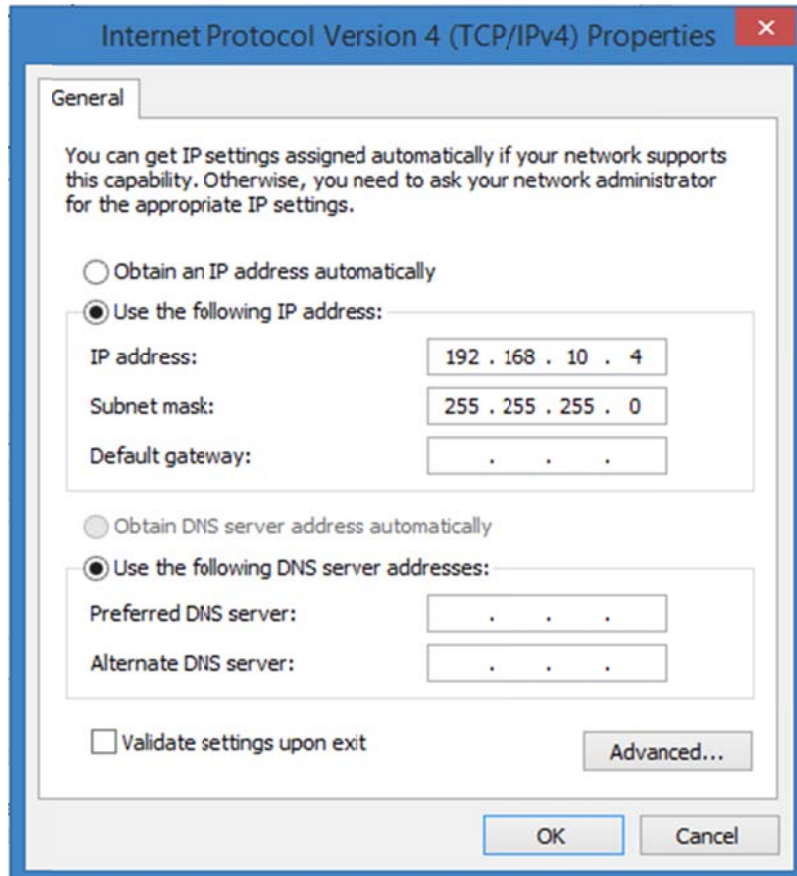
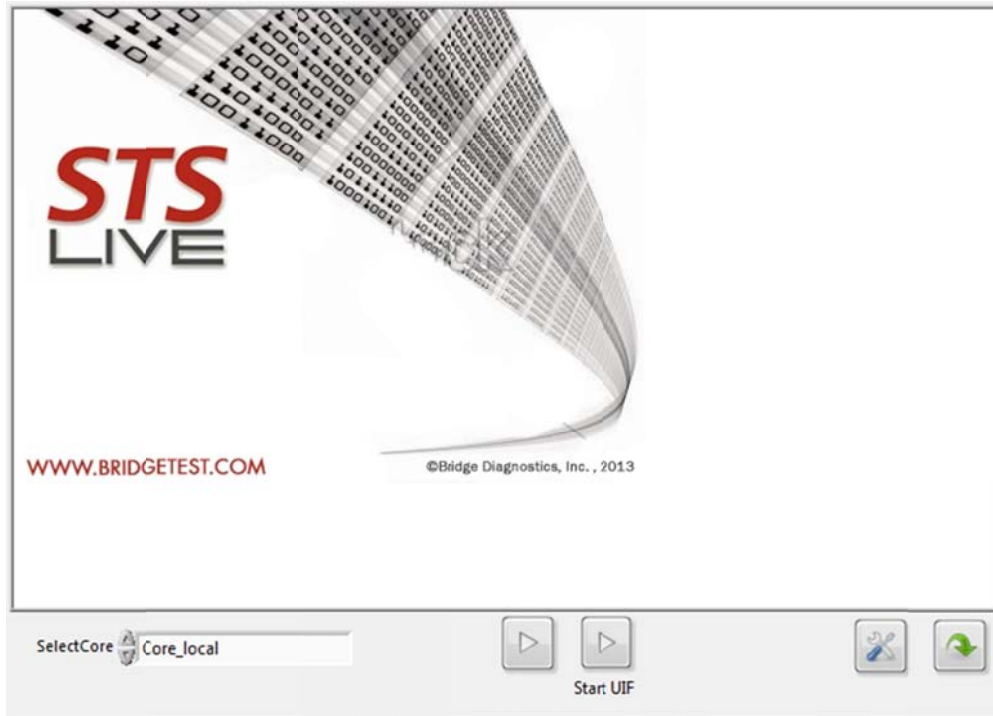


Figure 10.23 LAN (TCP/IPv4) setting to run on remote core

### ***Preparing a Test in the User Interface***

One of the main advantages of the STS4 system is the software user interface. STS Live was created by developers at BDI using National Instrument's LabVIEW. This provides simple and effective software for data collection and monitoring that can be integrated with many types of hardware. When first opening STS Live a splash screen is displayed, shown in Figure 10.24.



*Figure 10.24 Splash screen for STS Live*

Here the user must select from the pull down which of the Core computers the test should be run from. To connect to the selected core, press the first play button from the left. A box will appear showing your connectivity based on color. Within a relatively short period of time, the box should turn green to indicate that you are connected (see Figure 10.25). If the box does not turn green a connection has not been established and the user will need to troubleshoot the connection. Once the user is connected the “Start UIF” play button can be selected to enter the user interface.

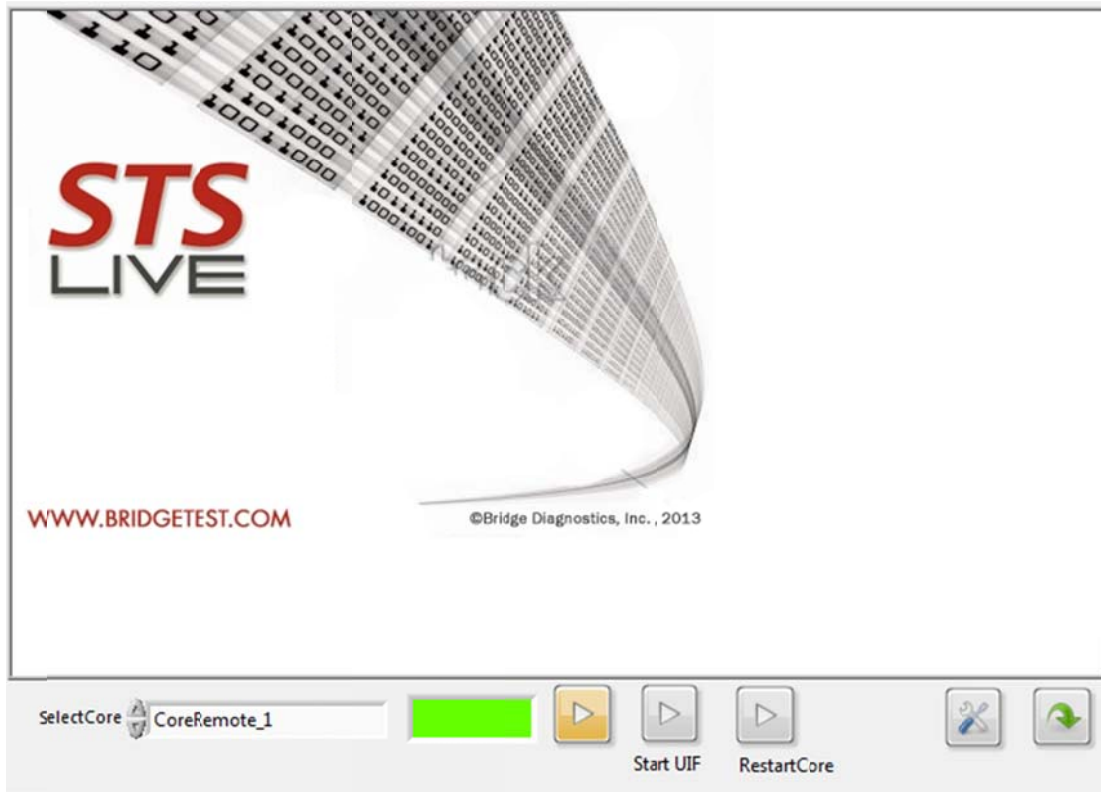


*Figure 10.25 Splash screen after connecting to core*

When entering the user interface, the user is presented with a display that lists each of the nodes connected including the sensors. Figure 10.26 shows the initial screen seen upon opening. There are three main tabs that the user will need to be familiar with. The first is the Configuration tab (picture of a node). In this tab the user inputs settings for sensors such as calibration factors and offsets. The second is the graphing tab (picture of graphs). The graphing tab will show the current response of the instruments. The third is the processing tab. This is where the user will input and manage the grouping and set up of data collection for the sensors. The other tabs shown have no use to the user and will be eliminated from the program in future updates. The following sections provide a description of how to set up and run a test using STS Live.

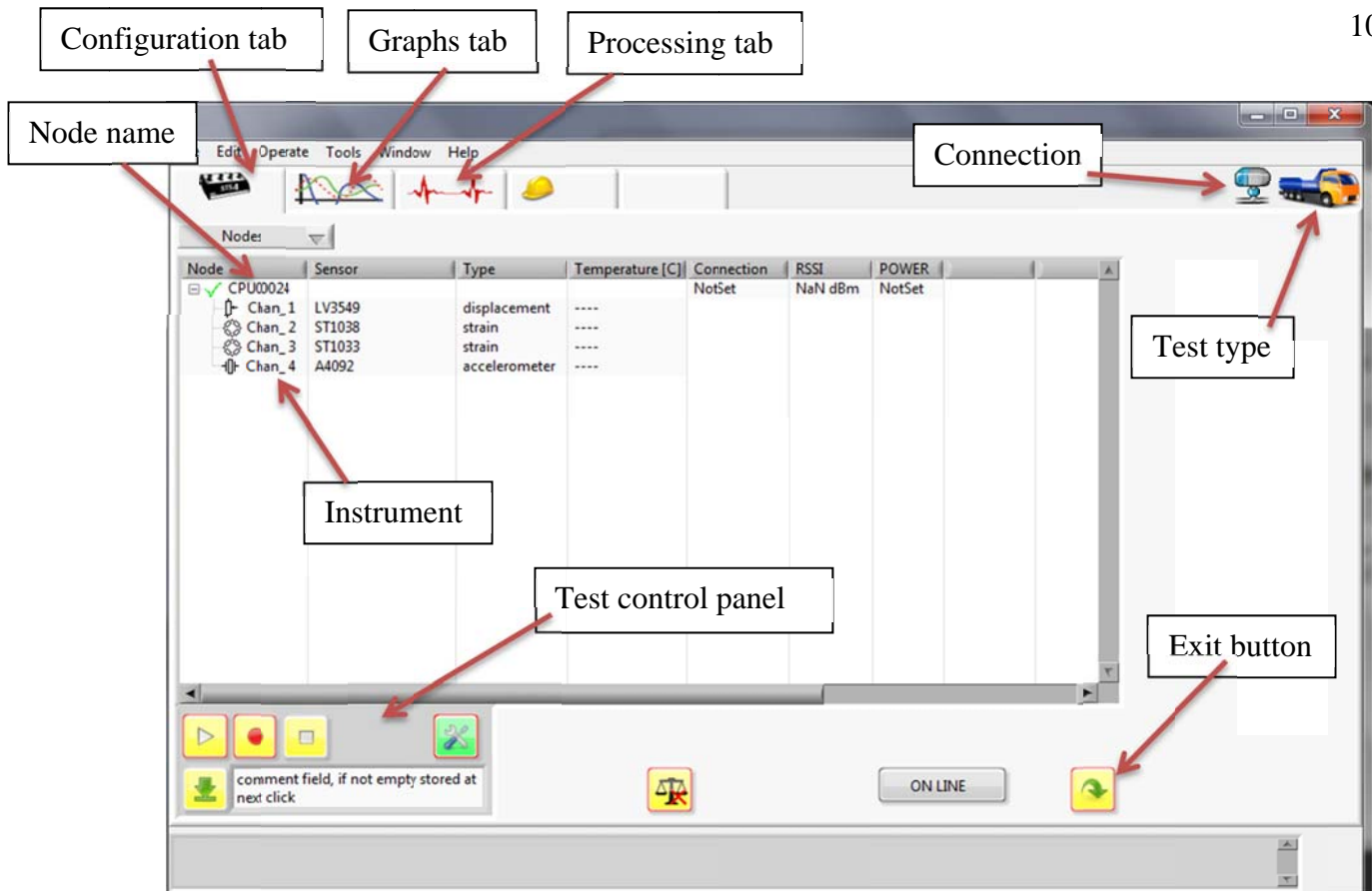
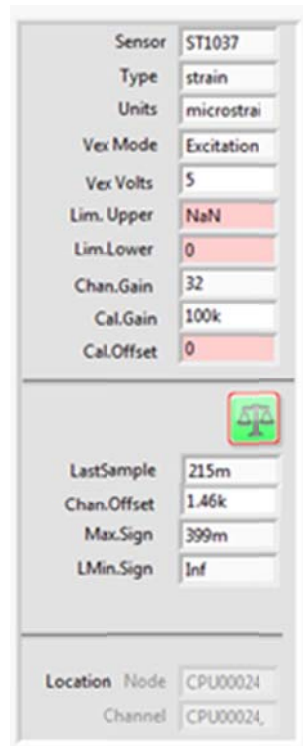


Figure 10.26 Navigation of Configuration tab

### Step 1. Setting up the sensors

In order to obtain accurate and reliable data the sensors need to be properly set up using the user interface. Each sensor has a several inputs that need to be configured. On the configuration tab the user can select an instrument. On the right side of the screen information regarding that sensor will be displayed as shown in Figure 10.27. The type of instrument should be selected along with the appropriate units. The other two major inputs are the “Chan. Gain” and “Cal. Gain”. The “Chan. Gain” should be 32 for strain gauges and a value of 1 for LVDT’s. The “Cal. Gain” is the appropriate calibration factor for the instrument selected. This value can be obtained by using the calibration factor given by BDI. The value provided should be multiplied by 200. For example, ST1034 is a BDI strain gauge that has a calibration factor of 496  $\mu\text{V}$  on its calibration sheet. This number would be multiplied by 200 to become 99200. This

is the value placed in the “Cal Gain” box. The name of the sensor can be changed, and will be stored in the sensor so it will not need to be assigned each time. In order to properly balance the gauge the balance button should be selected and show the color green.



*Figure 10.27 Sensor set-up and configuration*

## *Step 2. File and Data Setup*

The next step in running a test is to set up the data collection and general test settings. This is done by selecting the setup button  in the test control panel. A new window will pop up with three different tabs as shown in Figure 10.28.

The project info tab is for general test setup. Here the user will specify where to save the data and any necessary descriptions of the test. This will be stored as part of the data output file. This is also where the user will specify the sample frequency (in units of samples/sec) for the instruments (Fs). The duration of test can be specified from a list of predetermined times. Also the test mode is chosen as either “LiveLoad” or “Monitor”. “LiveLoad” mode is the simplest of

the tests. It will simply record data at the frequency specified and for the duration selected for every instrument. Triggers, Decimation, and other tools are not available in “LiveLoad” mode. “Monitor” mode should be used in most cases as it allows for the most customization, but if you simply want the recording of every instrument “LiveLoad” is a good option. The user will also see the “Continue” and “Balance” radio buttons. If the continue button is selected, the test will run until it is stopped manually. The test duration time does not apply. The balance button is not operational at this point.

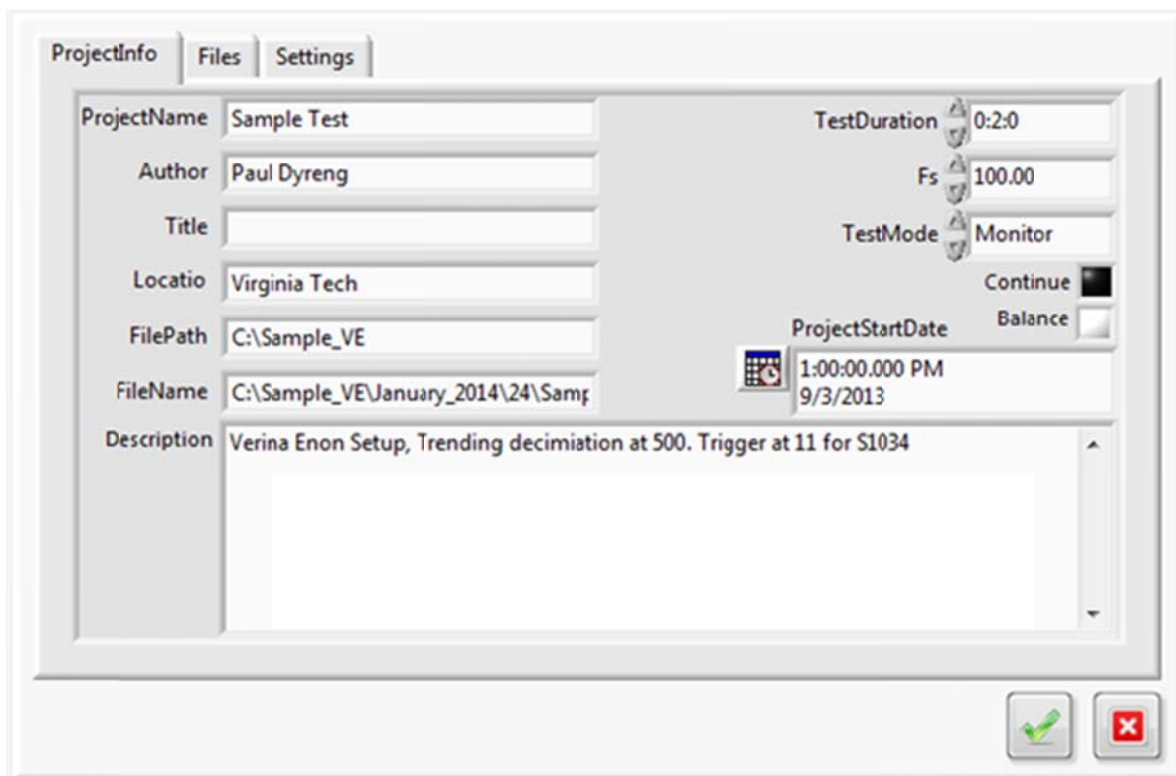


*Figure 10.28 Set-up window*

The “Files” tab is used for data collection once the test is complete and will be discussed later. The “Settings” tab allows the user to make a few minor adjustments to how the instruments are viewed during a monitor type scenario, and allow for setup of sleep mode of the remote core. The core will sleep for the amount of time specified, wake up and collect data from the nodes,

and then go back to sleep. The default setting is 100. This default has been set by BDI as a safe amount of time to allow the core to sleep to ensure that no data is lost. This is because the nodes can only store so much data and 100 seconds will allow the safe transfer of this data to the core. This value will eventually be automated to account for test settings and to ensure minimum power consumption. When the system is not on battery power, there is no reason to enable the sleep mode. This is also where the user needs to select if the calendar option will be used, which will be discussed in succeeding sections.

### *Step 3. Monitor and balance the sensors*

The next step is to balance the sensors and to ensure that they are reading properly. It should be noted that for a test, the instruments should be in place on the structure at this point. Balancing of the sensors can be accomplished by selecting the graphing tab. Once on the graphing tab the play button on the Test Control Panel should be selected. This allows the user to see the current reading of all the instruments running. The viewing rate in this “monitoring mode” is set to a default of 5 Hz. Smaller viewing rates can be selected, but not larger. By selecting the radio buttons next to each sensor name, the user can toggle to show or hide a particular instrument. At this point the user should balance the sensors. This is done by selecting the balance button that has appeared in the Test Control Panel. The sensors should all go to zero position. This balancing stores an offset and saves it to each respective instrument. The value of this offset can be seen on the configuration tab. At any point the monitor can be stopped by pressing the stop button. 

### *Step 4. Group and Test Setup*

The ability to set up groups is one of the STS4 systems most useful features, and every monitor test must include groups. Groups are defined as a collection of instruments for which a unique type of sampling is performed. The user can define as many groups as they would like, and a sensor can go into as many groups as is needed. Groups are not utilized in the live load test mode, and are only available during monitor mode. If the user desires to use groups during a live load test, simply use the monitor mode with a set amount of time.

Groups are set up in the processing tab. By selecting the dashed lines in the window, the group setup window is presented. The user is then presented with three areas of entry. The first is the name. Each group needs to be assigned a unique name. This is critical, as using the same name twice will cause issues with the program and data collection. The second is sample mode. There are three options presented; normal, decimated, ontime. Each option is presented in Table 10.8.

*Table 10.8 Group options for sampling*

Normal	TriggerMode	Off	No triggers set. All instruments in group will record for the duration of test at frequency specified in test settings.
		Pre_Trigger	Allows for an input of amount of time for data output before and after the trigger event. Also a time input for the amount of time the trigger must be active.
		Pre_Add_post	This is still under development and should not be selected.
Decimated	Decimation	MinMax	Find the min and max value over the set of decimation and outputs these two values.
		Average	Returns the average reading over the number of samples entered in the decimation.
ONTIME	On Time	EachDayAt	Collect reading at one time each day.

Once the group settings are included, the add button appears and can be selected. At this point a list of sensors is displayed and the desired sensors can be added to the group. When all sensors have been added to the group, the finish button can be selected. If TriggerMode is used, the actual trigger level can now be assigned. Double clicking on the sensor now listed in the group tree will allow for entry of the trigger level. The trigger value is entered in PreTriggerLevel, and is in the units specified for the sensor. The polarity is used if you want the trigger to happen on the positive or negative slope of the reading. Only one of the sensors in the group can be a trigger. The others should be selected and the Polarity tab should be set to off.

Sensors can also be set to AutoZero. This is especially important with the BDI strain gauges as they are subject to drift. The AutoZero function ensures that the gauge is always balanced at zero and so the accurate trigger can be obtained for each event. How this AutoZero function works is explained in the Appendix. It should also be noted that AutoZero cannot be used for the same instrument in different groups.

It is at this point the user would also set up the calendar feature if desired. The calendar feature allows the user to set up days and times during a week in which to run a certain group(s). This is another power saving feature of STS4 and will allow for further customization of data collection.

The test is now ready to run. To run the test and record the data the record button on the Test Control Panel should be selected. The test has now begun and data is being recorded. If the test is set to continue, the test will now run until it is stopped by the user. The user can now exit the program and disconnect the PC from the remote core. When desiring to end the test the user should reconnect to the core, and press the stop button on the TCP.

### *Step 5- Data Download from Remote Core*

Once the test is stopped the data can then be downloaded from the Remote Core. This is done by selecting the settings button on the TCP. Under the “files” tab the user will find a file tree. All of the data is placed in folders by the month and day of when the test was started. The files are named by time of the start of the test. The user should select the desired folder or file they wish to download, select a destination folder, and then press the download button.

The file produced is a TDMS file. This type of file is meant to be used with Microsoft Excel. A simple add-in is available from the National Instruments website for download. This type of file makes for easy and simple data analysis, and requires less post-processing of data.

### **Attempted System Validation**

The Varina-Enon Bridge (VEB) near Richmond Virginia currently has a long term monitoring system set up in one of the approach spans. The data collection system currently being used is a Campbell Scientific (CS) system using CR1000 dataloggers. This system has been in place since August 2012 and the data that is being gathered is reliable and accurate. In order to validate the STS4 system for accuracy and reliability, it will be compared to the CS system.

### **Current Test Setup**

During a routine inspection of the Varina-Enon Bridge, a joint in the 6<sup>th</sup> span of the approach structure was observed to visibly open under live load. This effect seemed to be caused by large temperature gradient. The joint of interest is shown in Figure 10.29 as Joint E. Virginia Tech was tasked with instrumenting the bridge to understand the behavior of the joint over a period of time.

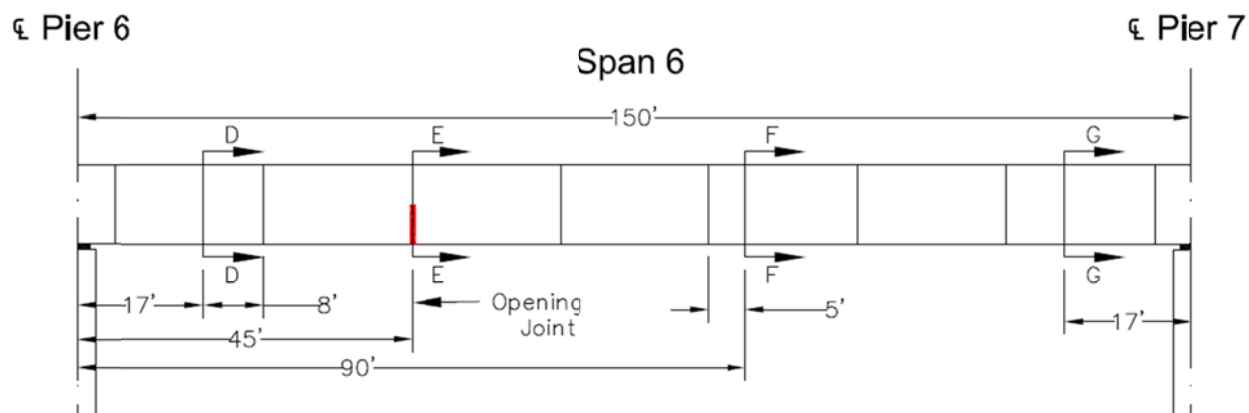


*Figure 10.29 Elevation view of Span 6, traffic in direction of cross sections*

To monitor the joints' behavior over a long term, several types of instruments have been placed on the structure. Currently two linear variable differential transducers (LVDTs), two BDI strain transducers, 12 vibrating wire strain gauges (VWGSs), and 24 thermocouples are in place at various locations on the bridge.

The current test has a BDI strain transducer (BDI(1)) placed on the bottom web in the center at section F (see Figure 10.30). This is approximately the location of expected maximum moment due to live load. This instrument is set as a trigger at a value of 11 microstrain. Once this value is reached, the dataloggers record the history of this gauge along with the LVDTs (labeled LVDT(1) and LVDT(2)) and the BDI strain transducer (BDI(2)) at section E (see Figure 10.31) approximately two seconds before and after the trigger occurrence. All other instruments, the VWGSs and thermocouples, take a reading every 2 minutes.

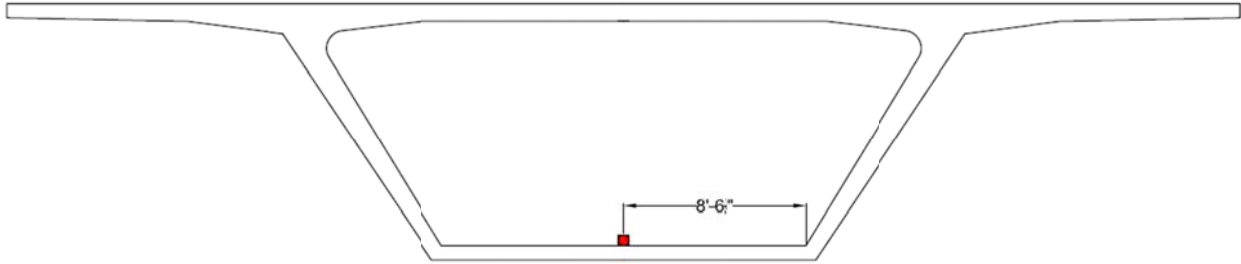


*Figure 10.30 Section F instrument locations*

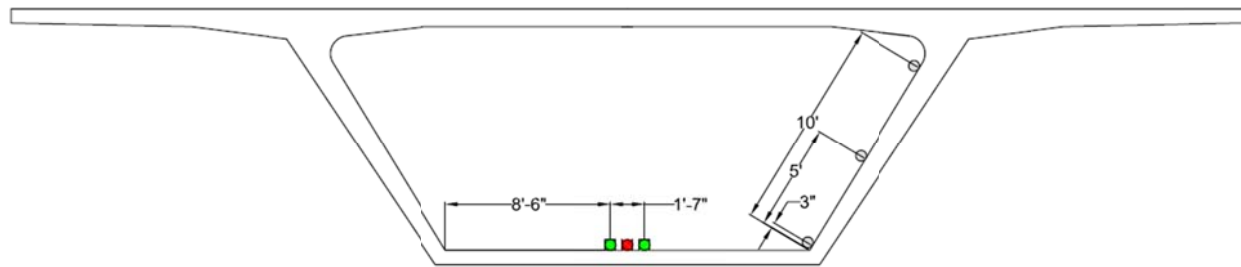


*Figure 10.31 Section E instrument locations*

### **Deployment of STS4 for comparison**

The STS testing system was deployed next to the instruments shown above. Two LVDTs, LV3550 and LV3549, were placed next LVDT(1) and LVDT(2) respectively. They were positioned as near as was reasonable taking into account the nature of the surface the instruments were attached to. Two BDI strain gauges, ST1034 and ST1035, were also placed next to BDI(1) and BDI(2) respectively. Each of the instruments was connected to the same node. The setup as described is shown in Figure 10.32 and Figure 10.33.

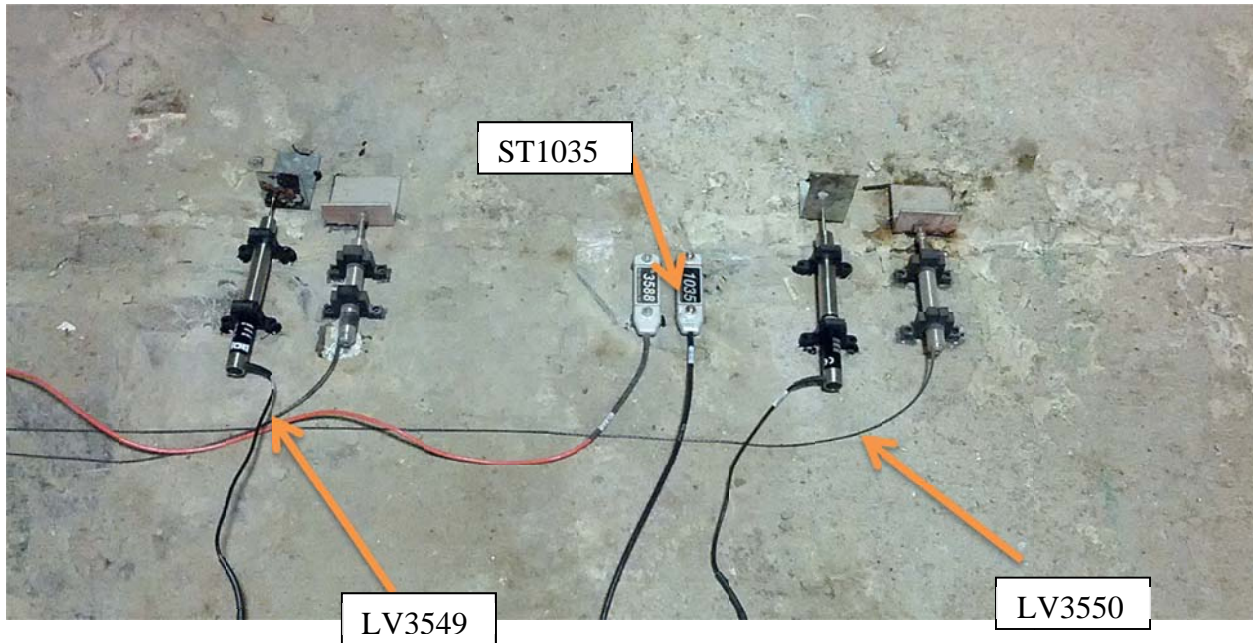


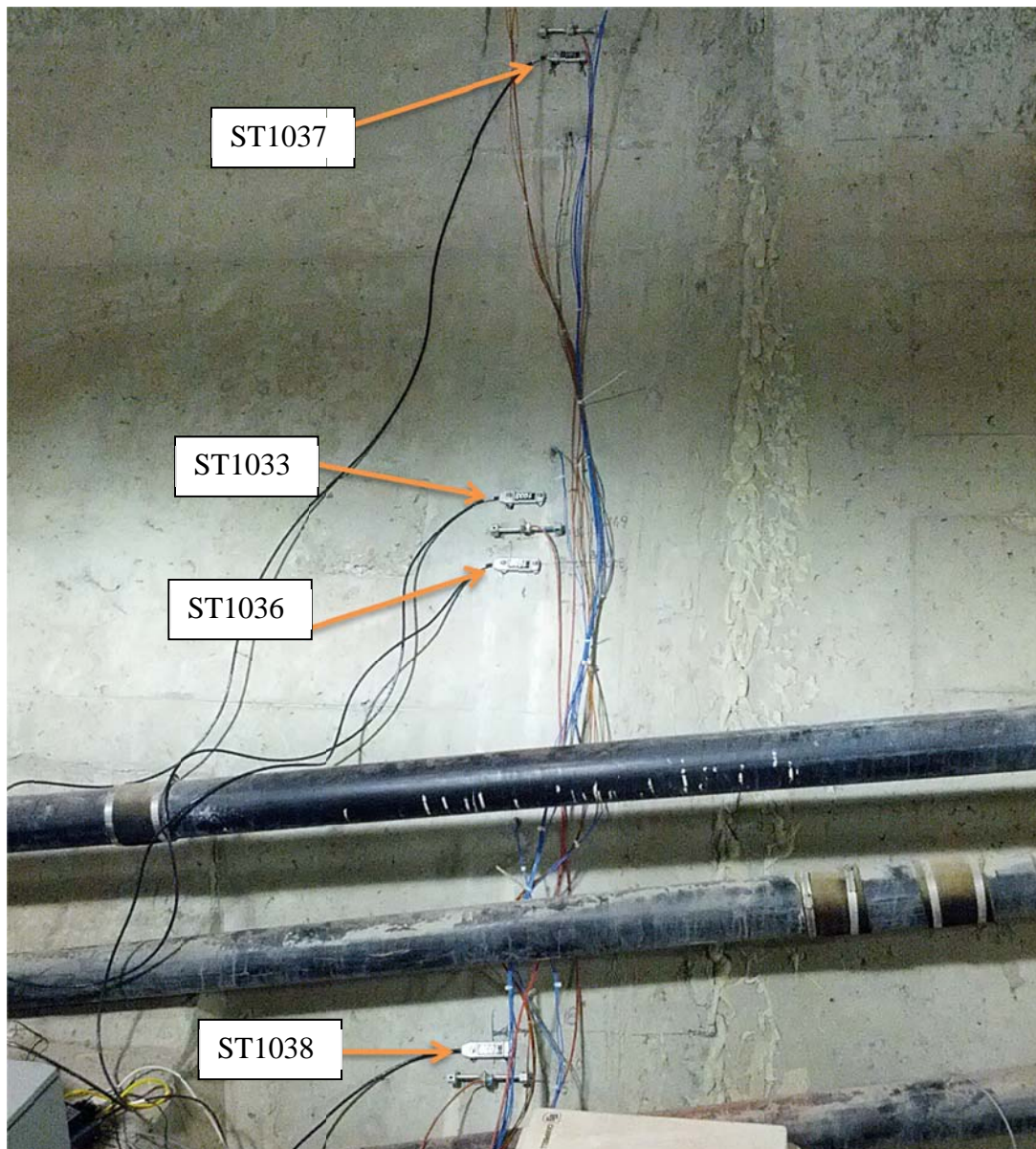
Figure 10.32 Set-up of instruments next to existing instruments at Section E



Figure 10.33 Set-up of strain gauge next to existing at Section F, this is the trigger gauge

The other four instruments used were BDI strain gauges. These gauges were placed near to the VWSGs at Section E. The placement of these instruments is shown in Figure 10.34. The layout of the STS4 instruments therefore is nearly identical to that shown in Figure 10.30 and

Figure 10.31. This setup could then provide an accurate comparison of STS4 with the CS system already in place.



*Figure 10.34 Instruments placed next to VWSGs at Section E*

Two groups were used in the testing setup. The first group contained the four BDI strain gauges that were placed next to the VWSGs. These gauges sampled at 100 Hz and the output

was a decimation of an average of 1000 points. So these instruments gave one recording every ten seconds.

The other group was setup as a trigger group. The instrument to be set as the trigger was ST1034. The value of the trigger was set to 11 microstrain. This trigger would give recordings of ST1034, ST1035, and the two LVDTs of 2.5 seconds before and 2.5 seconds after the trigger occurrence. Both of the strain gauges were set to AutoZero, so that theoretically the trigger value would work regardless of the drift of the instrument.

## **Results**

The test was started on January 30<sup>th</sup> at 1:21 pm and the data was retrieved on February 4 at 11:30 am. Although a few recordings were obtained that seemed to show results that were expected, upon closer examination much of the data obtained was not accurate or complete.

### ***Overall System Behavior***

STS Live recorded 19 triggered events over the duration of the test. During the same time period the CS system only recorded three events. This was the first indication that STS4 did not give the desired results. Figure 10.35 shows the maximum and minimum values that were obtained from the trigger gauge (ST1034) for each event. A good triggered event would show a minimum value around zero. This value could be larger or smaller based on what type of live load event is occurring, but should be within a few microstrain of zero. The maximum value should be greater than or equal to 11  $\mu\epsilon$  in all situations.

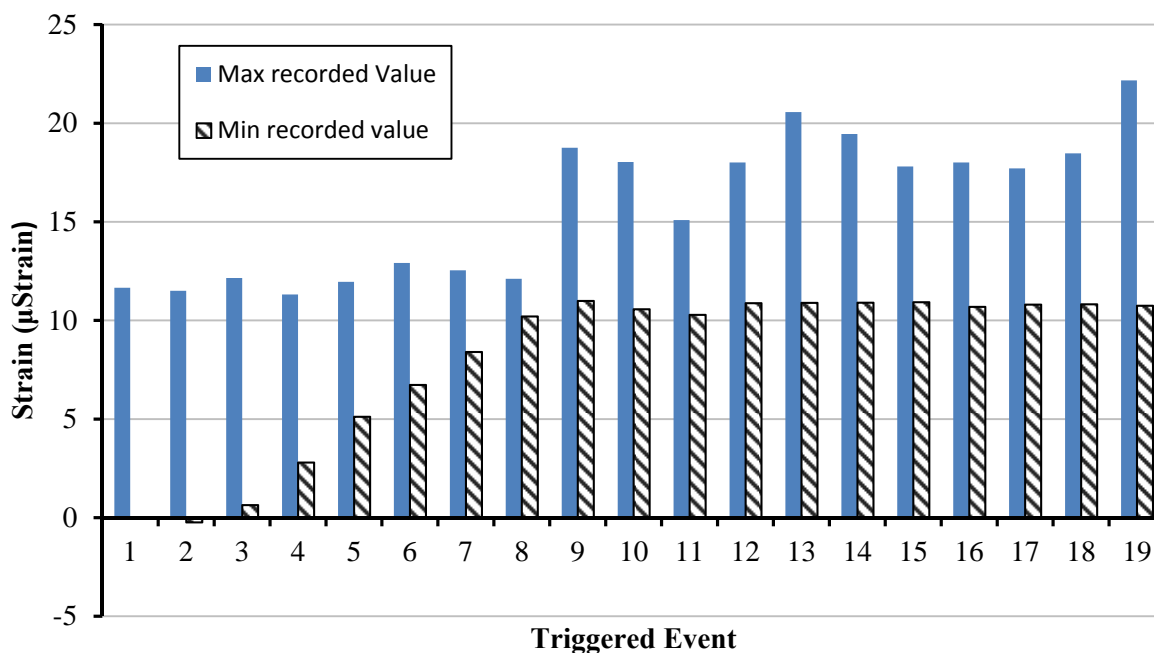


*Figure 10.35 Maximum and minimum strain for the trigger strain gauge*

It can be seen that the first three records gave reasonable results. The trend of the minimum recorded value increasing can also be observed. This shows that the gauge was experiencing some type of drift and was not being set to zero after triggered events. Drift of this nature does not provide the desired results because the trigger is set at  $11\mu\epsilon$ , and therefore a live load event where the gauge experiences less than  $11\mu\epsilon$  will cause the trigger to be set. It can be seen that the minimum never reaches above  $11\mu\epsilon$ . This can be explained by noting that once the gauge drifts above  $11\mu\epsilon$  the trigger will never occur and therefore no more events are recorded.

The timing of these events is also of interest. Figure 10.36 shows the same maximum and minimum values for the trigger gauge as displayed in Figure 10.35 but this time they are plotted with respect to time. It can be seen that during the first recordings the gauge is producing minimum values that are zeroed properly. The gauge then begins to drift rapidly. The minimum recorded value shows a large amount of the drift occurred at the same period of time, about 11

hours after the system was deployed. The gauge then seems to have not experienced much drift over the course of the next 70 hours. The recordings cease at just less than 80 hours even though the system was deployed for a total of 118 hrs. This is another indication that the system drifted out of the range of the trigger.

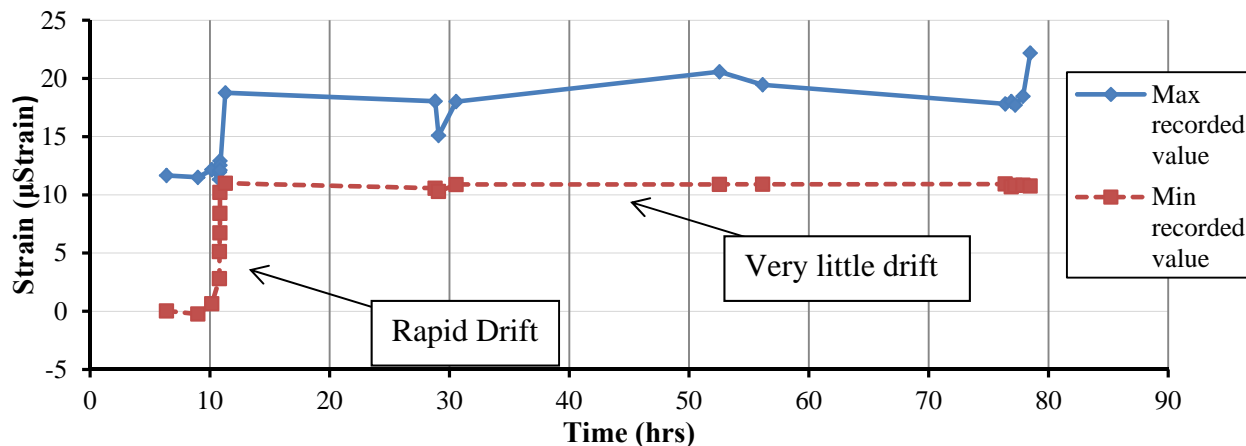


Figure 10.36 Maximum and minimum recorded value for trigger vs. Time

### Triggered Strains

The strain recordings obtained from the STS4 system were compared to those produced by the Campbell Scientific dataloggers. The recordings that are of use from the STS4 system are those where the difference in maximum and minimum strain recorded by the trigger gauge are larger than 10. These will be compared to the three recordings obtained using the CS equipment. All plots from the STS4 recordings have been smoothed using a 10 point running average. The CS data did not require as large a running average for smoothing because a sample rate of 33 Hz was used. Therefore, a five point running average was used to smooth the CS strain data.

Figure 10.37 shows the strain recordings for the first triggered event recorded by STS4. Already it can be seen that the instruments have begun to drift. The reading begins at about 2-3  $\mu\epsilon$  and then shows a dip in the strain due to the concrete being in compression. The bottom

bridge flange then experiences tension to increase the strain at Section F to a value where ST1034 triggers at a value of  $11\mu\epsilon$ .

It would be expected that the instruments located at Section E and Section F would record their peak readings at a slightly different time because of their different location longitudinally along the bottom bridge flange. Figure 10.37 shows this result and gives good confidence in the timely response of the system.

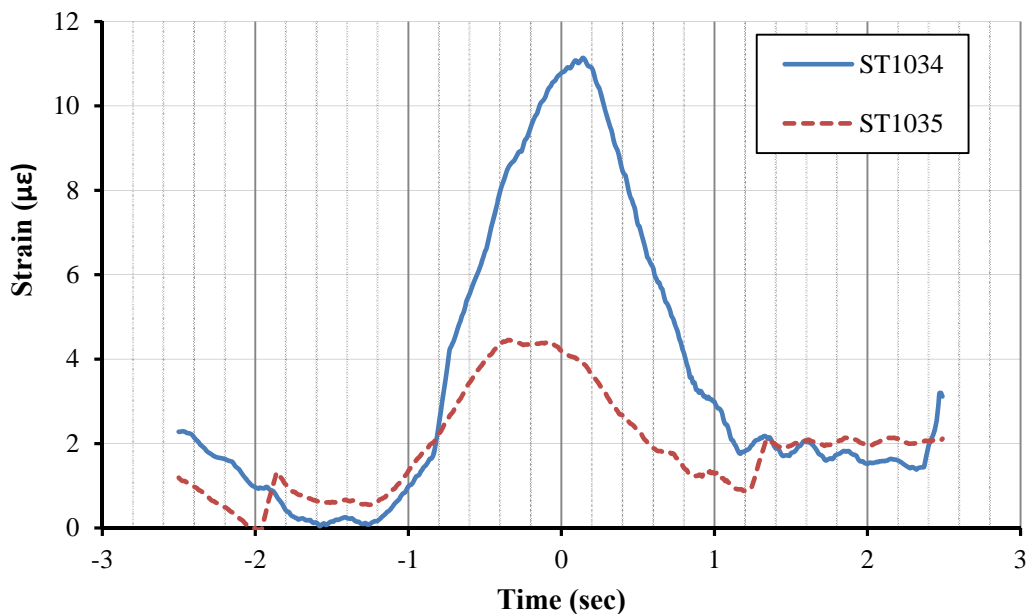


*Figure 10.37 Typical strain recordings for ST1034 and ST1035 from STS4*

An example of a strain recording for the CS system is shown in Figure 10.38. The same type of behavior is exhibited as was recorded using the STS4 system. We clearly see the trigger occurring at 11 microstrain, the dip showing compression, and the peaks of the two gauges being at different times.

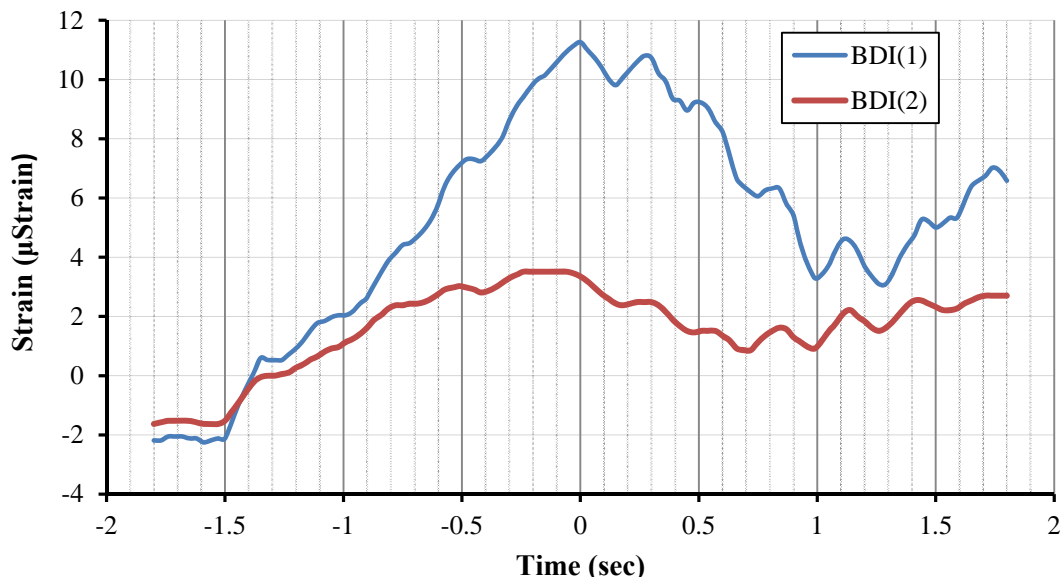


Figure 10.38 Strain recordings for DBI(1) and BDI(2) from CS

It is difficult to compare in detail the two systems because at no point did a trigger from the CS system occur at the same time as the STS4 system. This is mostly associated with the drift in the trigger gauge. At the time of the first recorded event of the CS system the STS4 instruments had drifted beyond a reasonable minimum starting point.

Table 10.9 shows a comparison in the average recording of both the STS4 and CS strain gauges. The values corresponding to the CS instruments are an average of the three events that occurred during the STS4 deployments. The values corresponding to the STS4 instruments are the average of the four significant events that were recorded.

The CS records are triggered at the same value, but it is clear to see that it took a much larger event to set the trigger. This shows a proper zeroing effect of the CS system. However, the differences between the recordings at Section E and F for both systems are quite well proportioned. The CS events at Section F are 3.62 times greater than at Section E. The STS4 are 3.08 times greater for the same instruments. For a small sample size, this shows that reasonable strain values were recorded by the STS4 system.

Table 10.9 Average reading of strain gauges

System	Instrument	Max	Min	Range (Max-Min)
CS	BDI(1) ( $\mu\epsilon$ )	11.11	-1.99	13.10
	BDI(2) ( $\mu\epsilon$ )	2.31	-1.30	3.61
STS4	ST1034 ( $\mu\epsilon$ )	16.97	8.31	8.66
	ST1035 ( $\mu\epsilon$ )	45.44	42.63	2.81

It is also worth noting that the strain gauges associated with the STS4 system experienced jumps in the recordings. This jump occurred at random times within each triggered event. During some events there would be no jump and in others there would be more than one. A typical jump in the readings was around 1-3 $\mu\epsilon$ . The jumps are best seen in the raw data as presented in Figure 10.39 and Figure 10.40. BDI has been made aware of the strain jumping and is troubleshooting the issue.

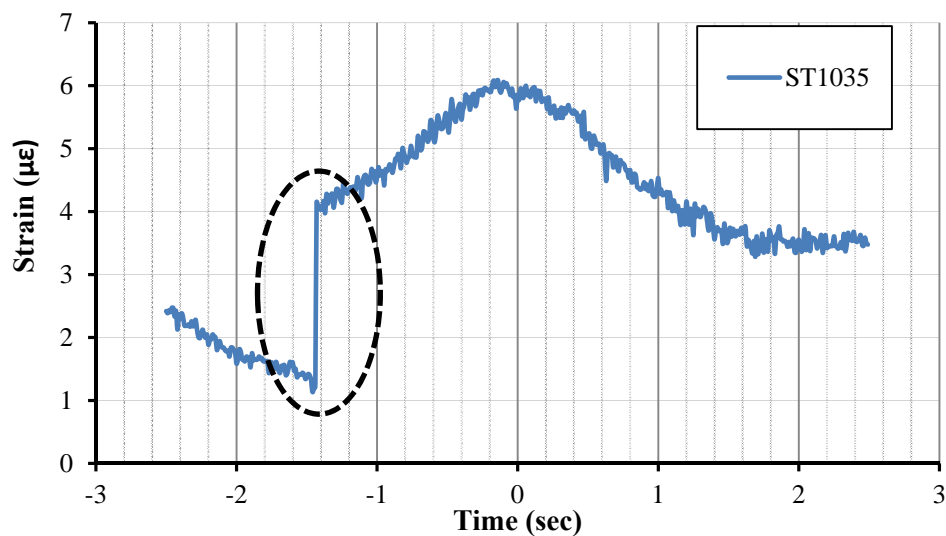
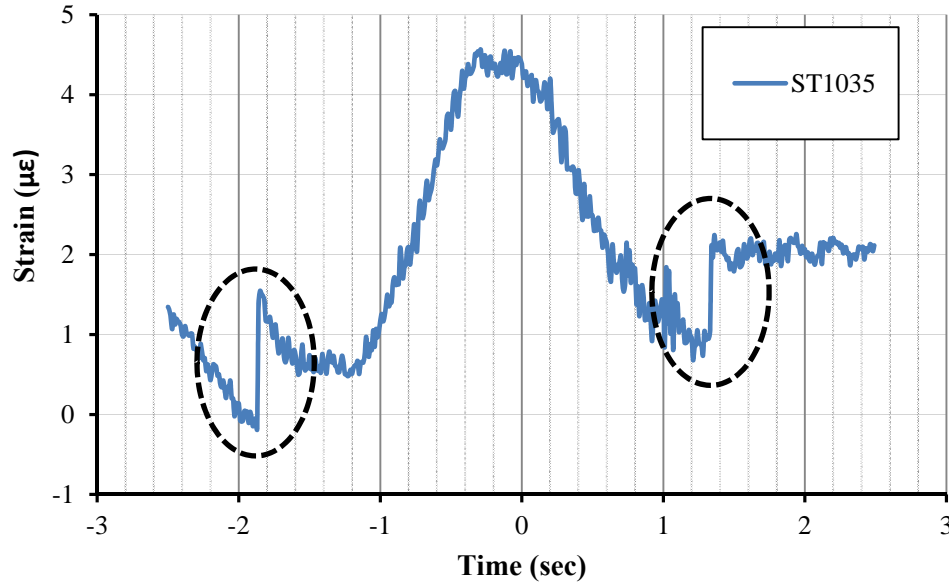


Figure 10.39 Strain jumping as observed in STS4 instruments



*Figure 10.40 Strain jumping as observed in STS4 instruments*

### ***LVDT Results and Joint behavior***

As mentioned in the test setup, LVDTs were positioned over the joint at Section E and were placed as close as was reasonable to the LVDTs already in place. The LVDTs were programmed to the same trigger as the strain gauges so as to be able to note the opening of the joint during significant live load activity.

The initial observation of the LVDTs used for the STS4 system showed a very large amount of noise in the data. Figure 10.41 shows a reading for a LV3550 during a live load event. The noise of the gauge covers 0.0004 in. This is significant when the event has a total range less than 0.0008 in.

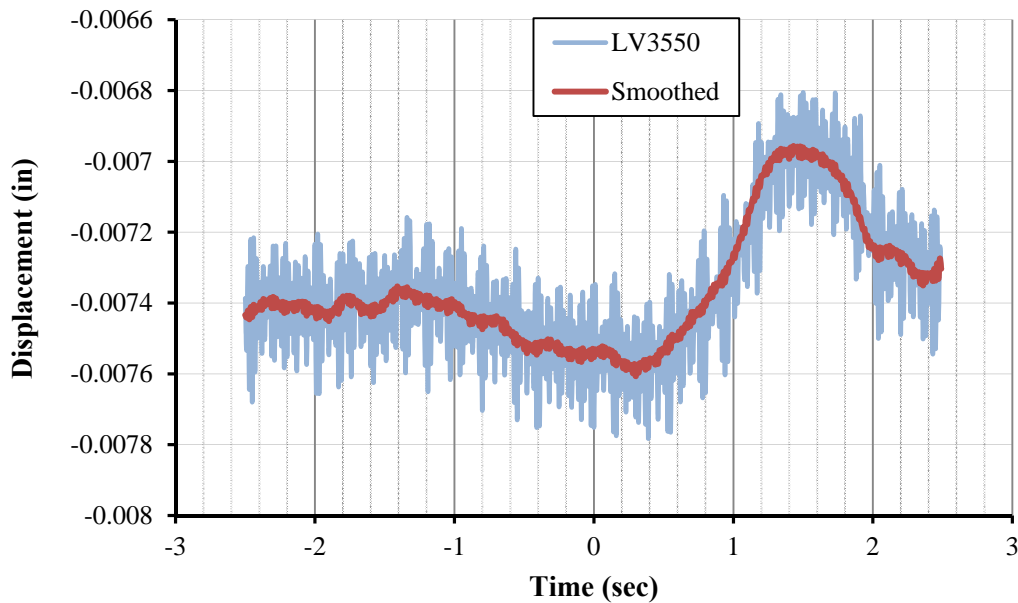


*Figure 10.41 LVDT record from STS4, raw and smoothed data*

LVDT(1), which was next to LV3550, and recorded by the CS system, shows very little noise in comparison to LV3550 as is shown in Figure 10.42. Upon further communication with Bridge Diagnostics it has been determined that the intelliducers (plug placed into node) on the STS4 LVDTs are the source of the noise in the system. This can be fixed and should not be an issue for future uses of the system.

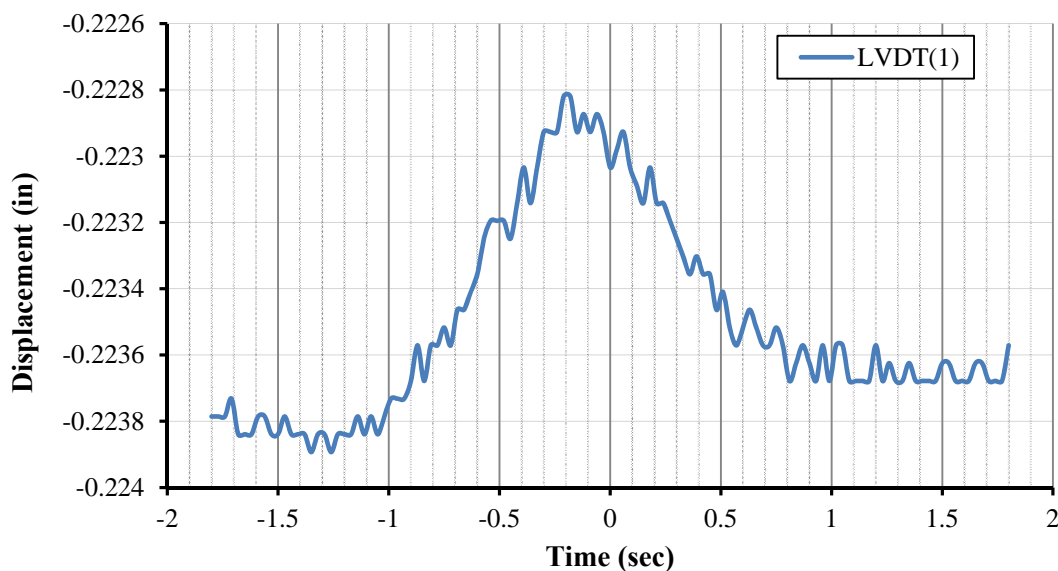


Figure 10.42 LVDT record from CS without smoothing

After smoothing of the results a more accurate comparison could be made in regards to the opening of the joint. Again the three records from CS will be considered along with the four significant events recorded by STS4. The smoothing for the STS4 LVDTs was a 10 point running average and the CS LVDTs were smoothed with a three point running average.

Table 10.10 Comparison of average LVDT readings at joint at Section E

System	Instrument	Max	Min	Range
STS4	LV3550 (in)	-0.00572	-0.00627	0.00054
	LV3549 (in)	-0.00858	-0.00886	0.00029
CS	LVDT(1) (in)	-0.22350	-0.22406	0.00056
	LVDT(2) (in)	-0.23752	-0.23788	0.00036

Table 10.10 shows that the LVDTs accurately captured the opening behavior of the joint. The difference in opening values for LV3550 and LVDT(1) is only 3%. LV3549 and LVDT(2)

show a difference of 24%. The reason the difference is greater between the latter LVDTs is because at smaller readings the noise and smoothing has a larger effect.

## **Conclusions and Recommendations**

It has been shown that the STS4 system has many applications and uses. The system can be used for simple monitoring of traffic characteristics, joint behavior, general bridge behavior, and other things of interest to the bridge and structure monitoring community. The ability for rapid deployment, ease of use, and battery powered operation make the system of interest for both private structure monitoring firms and government agencies such as a state department of transportation.

Although a very useful system as is, there are many improvements that could be made on the system after testing its use. Battery powered operation must be improved. Currently the system will require four large marine batteries to power the system for a period of two weeks and a special adapter. The developers are working on ways to allow for more power saving operations in the system.

The user interface has room for improvement as well. The following things need to be addressed to fully utilize the system.

- The software should flow naturally from the logical steps of a bridge test. Sensor information- sensor setup- test variables and conditions- run and monitor- data collection. The user needs to go back and forth from one tab to another to successfully complete a test. It is not made evident where the necessary components that need to be setup are.
- It should not allow for the beginning of a test until all the inputs have been placed and verified.

- The data is currently stored in a TDMS file format. This is a good feature; however in many situations a text file is useful for data analysis using various programs.

There are clearly issues with current system as was shown in the Varina-Enon comparison. As of the writing of this report the following items are still being worked on or developed:

- The spontaneous jumping of strain gauges.
- The drift of instruments that are set to AutoZero. These first two issues are the most critical errors and must be fixed before further deployment in the field.
- A calendar feature is part of the program and allows the user to run groups only during certain times of the day. According to BDI this feature is not yet ready for full implementation. The feature has not been tested in the field, and further investigation into its functionality needs to be explored.
- Proper elimination of noise in LVDTs

The STS4 system will become a successful tool to be used in the monitoring of structures. However, the product just needs more time for the issues with software and hardware to be properly worked through.

## **Appendix**

### **Speed Calculation Algorithm**

The routine is a function of the Data “D” and the distance between the two gauges “dist” in inches. The first line finds the maximum value for the strain gauge at 0.25L, and then saves the point at where that value occurs. The second line does the same for the strain gauge at 0.5L. The third line takes the difference in the record points and divides them by the sample rate. This

gives you the time between the two maximums events. The fourth row divides the distance by the time and is multiplied by a conversion factor to output MPH. Note: The data should be smoothed prior to running the algorithm.

$$\text{Speed}(D, \text{dist}) := \left\{ \begin{array}{l} n \leftarrow \text{match}(\max(p), p) \\ m \leftarrow \text{match}(\max(q), q) \\ k \leftarrow \frac{(n - m)}{100.16} \\ \text{Mph} \leftarrow \frac{\text{dist}}{k} \cdot 0.05681818 \\ \text{Mph} \end{array} \right.$$

### **AutoZero Function Algorithm (Developed by Rene Hamer of Bridge Diagnostics Inc.)**

The AutoZero mode is intended to slowly compensate initial offsets and drifts to zero level. The speed of the AutoZero mode, or how aggressive the routine compensates to zero, is controlled by a time constant that the user can enter. The lower the value of the time constant the more aggressive the zero will be. The routine is as follows:

$$\text{ValueOut}(n) = \text{ValueIn}(n) - \text{Error}(n - 1)$$

$$\text{Error}(n) = \text{Error}(n - 1) + k * (f(\text{ValueOut}(n - 1)) / (\tau * s))$$

Where:

$f(x)$  is defined as:

$$\begin{array}{ll} \text{if } ABS(x) < 0.1 & f(x) = x \\ \text{if } ABS(x) \geq 0.1 & f(x) = 0.1 * \text{sign of } x \end{array}$$

In other words  $f(x)$  is limited to +/- 0.1

$n$  = sample number

$\tau$  = time constant entered by user (sec)

$s$  = sample rate (hz)

$k = 100$  this is a gain factor

When triggered the compensation is on hold.

$f(x)$  limits the rate of the compensation heavily. Before running a test, the user should still balance the sensors.

### Calculation for Expected Strains in Kerrs Creek Bridge

The properties for the bridge, assuming each girder and parapet act compositely as a single whole:

$$I = 2670894 \text{ in}^4 \quad y_{bar} = 17.34 \text{ in}$$

The properties for the bridge, assuming each girder acts compositely as a single whole, without parapets.

$$I = 798153 \text{ in}^4 \quad y_{bar} = 16.95 \text{ in}$$

The strain experienced by the cross section due to load can be represented by:

$$\varepsilon = (M * y)/(I * E)$$

Where:

$$E = 4030.5 \text{ ksi} \quad \text{for Concrete} \quad E = 29,000 \text{ ksi} \quad \text{for Steel}$$

$$M = 0.75x \quad \text{from 0 to 180 inches. Where } x \text{ is inches}$$

$$M = -0.25x + 180 \quad \text{from 180 to 720 inches}$$

Therefore the lower bound, or minimum expected strain becomes:

$$\varepsilon = 1.2081 * 10^{-9}x \quad \text{Strain per 1 kip of load. } x \text{ from 0 to 180 inches}$$

$$\varepsilon = -4.027 * 10^{-10}x + 2.90 * 10^{-7} \quad \text{Strain per 1 kip of load. } x \text{ from 180 to 720 in.}$$

Maximum expected strain, assuming parapets do not act compositely:

$$\varepsilon = 3.73 * 10^{-9}x \quad \text{Strain per 1 kip of load. } x \text{ from 1 to 180 inches}$$

$$\varepsilon = -1.248 * 10^{-9}x + 8.984 * 10^{-7} \quad \text{Strain per 1 kip of load. } x \text{ from 180 to 720 in.}$$

## **Instructions for Using TDMS Files in Excel**

Excel as it comes regularly installed cannot open the TDMS file produced by STS Live. A TDMS importer is required. The TDMS importer is a Excel “Add-in” and can be downloaded from the National Instruments website: <http://www.ni.com/example/27944/en/>.

Once this is downloaded, a TDM importer will appear in the “Add-ins” tab of Microsoft Excel. Clicking on this icon will open a file explorer, where a TDMS file can be selected and opened in Microsoft Excel. The file can then be saved as a regular excel file.

## **Updating STS Live and the Remote Core**

Because STS Live is a new product and still under development, there will be several updates required by the users. Up to this point, updates have come via email from Rene Hamer at BDI. Two files are included in each update, one to update STS Live on the PC and the other to update the Remote Core computer. These files are sent with a file type .ex\_. Once the user downloads the updates these files need to be changed to .exe. Once the STS Live file extension has been changed it can be run and the previous version of STS Live can be deleted. The remote core usually comes as Core\_XXX.ex\_. Again, the extension needs to be changed to .exe. This file then need to be copied into destination C:STS\_Live/STS\_APP. Open STS Live, connect to the core computer and open Settings. On the settings tab, the user will be able to see the version of the core currently running, and a box can be selected to upload the new the Core version. After this is complete, the user should exit STS Live and restart the core using the “Restart Core” play button on the splash screen. The core is now updated.

## Statistical Difference of Calculated vs. Observed speeds

A simple paired t test was used to test the statistical significance of the results the speed calculation results when smoothed using an  $n$  value of 7.

$$\hat{X}_i = (X_i - \bar{X}) \text{ and } \hat{Y}_i = (Y_i - \bar{Y})$$

Where  $X_i$  represents each sample and  $\bar{X}$  represents the mean. Same for  $Y$

Then:

$$t = (\bar{X} - \bar{Y}) \sqrt{\frac{n(n-1)}{\sum_{i=1}^n (\hat{X}_i - \hat{Y}_i)^2}}$$

Where  $n$  represents the number of samples. In this case 3.

Using the calculated speed heading south we get:

$$t = (38.33 - 37.83) \sqrt{\frac{3(3-1)}{(6.67 - 5.57)^2 + (6.67 - 7.67)^2 + (-13.33 + 13.43)^2}}$$

$$t = 0.9078$$

This  $t$  value corresponds to a P value of 0.4598.

By conventional criteria the difference is not considered statistically significant.

See <http://www.graphpad.com/quickcalcs/ttest1/>.

## Chapter 11: References

AASHTO. (2010). *AASHTO LRFD bridge design specifications*, 5<sup>th</sup> Ed., American Association of State Highway and Transportation Officials, Washington, D.C.

Barr, P., Eberhard, M., and Stanton, J. (2001). "Live-load distribution factors in prestressed concrete girder bridges." *J. Bridge Eng.*, 6(5), 298-306.

Burke, M. (2009). "Integral bridges." *Integral and semi-integral bridges*. Wiley-Blackwell, U.K., 1-19.

Dicleli, M. and Erhan, S. (2009). "Live load distribution formulas for single-span prestressed concrete integral abutment bridge girders." *J. Bridge Eng.*, 14(6), 472-486.

Hodson, D., Barr, P., and Halling, M. (2012). "Live-load analysis of posttensioned box-girder bridges." *J. Bridge Eng.*, 17(4), 644-651.

Kalayci, E., Civjan, S., Brena, S., and Allen, C. (2011). "Load testing and modeling of two integral abutments bridges in Vermont, US." *Structural Engineering International.*, 21(2), 181-188.

Lahovich, A. (2012). "New technologies in short span bridges: a study of three innovative systems." M.S. thesis, Univ. of Massachusetts Amherst., Amherst, Mass.

Mourad, S. and Tabsh, S. (1999). "Deck slab stresses in integral abutment bridges." *J. Bridge Eng.*, 4(2), 125-130.